UNIVERSIDADE DE LISBOA
FACULDADE DE CIÊNCIAS
DEPARTAMENTO DE FÍSICA

Development of magnetic responsive nanocomposite scaffolds for tendon tissue engineering

Ana Rita Soares Tomás

Mestrado Integrado em Engenharia Biomédica e Biofísica
Perfil em Engenharia Clínica e Instrumentação Médica

Dissertação orientada por:
Prof. Dra. Manuela Gomes
Prof. Dr. Hugo Ferreira

2018

Acknowledgments

Let it be known that whosoever ventures in Science, specifically in Research, does not venture alone. That said, all the work developed under the scope of this project is the result of the joint efforts of a group of people who worked very hard to see it through.

I start by thanking Professor Rui Reis for the opportunity of developing my Master Thesis in the 3B's Research Group from the University of Minho which allowed me to make a small contribution to the research developed in his institute. I thank my supervisor Professor Manuela Gomes for accepting me as her student, making me a part of her research group; for closely following my work and for always being available. I also thank my other supervisor, Professor Hugo Ferreira, for overseeing my thesis and for the much-needed advice, especially during the final period of its development.

To the people with whom I have worked directly, I appreciate all the time that you took to teach me and to help me to whatever extent I needed at that moment. I thank my mentor, Rui Domingues, mostly for the knowledge, and the guidance, and the patience; for it was him directing from behind the curtain and, even though I had a big part to play, it was truly his vision that made this project happen. I also thank Ana Gonçalves for her help with everything involving cells, for always being available and for being a major player in seeing this project through. I thank Sandra Araújo for taking her time to teach me everything when I first started to work in the lab, for all the advice and patience when I was just a newbie. Finally, I thank Mariana Laranjeira for teaching me the ways around electrospinning before I could do anything else.

To the people that have not worked on this project but were somehow important for its outcome, I appreciate, most of all, the time and the energy spent on me. I thank Mahwish Bakht for being the less stress-inducing house mate in the history of house mates, for going out for waffles in the Winter and calling for pizzas in the Spring. I thank all the people who have come through our library in 3Bs, for the Library Crew (it's what we call ourselves) has made it the most joyful place I could ever hope to sit at and is also a big part of what made last year so fun. I want to acknowledge Helena Almeida, Ana Luísa Silva, Rafael Lemos, Sara Moura, Sofia Oliveira and Vera Barros because they deserve the world and all the good that comes with it, after the countless times waiting for me to have lunch. I thank my friends from university, Cristiana Tiago, Joana Guido, Sara Guerreiro, and the other parts of the tri-couple, Inês Bagulho and Sara Costa, for all their support and their help in surviving five years of Biomedical Engineering. Mostly, I'm thankful for all the time we got to spend together, either while studying or partying, for those are the defining moments that should be remembered. I thank my long-time friends, Beatriz Filipe, Catarina Miao, Claudia Florea, Diogo Diogo, Mariana Galiano, Mariana Gomes, Mariana Guttierrez and Tiago Ferreira, for the support and mood-lifting conversations; for always having time to get together after a long week and for all the adventures we lived together the last couple of years. Finally, I thank Pedro Araújo, the other pea in the pod, for the legendary car rides and for his understanding of whatever physics or math course I may have needed to grasp in just 2 days.

On a different note, I thank my parents for the patience and support; for always, and incessantly, trying to push me to go further. Also, I thank you for all the money you have invested in my education, which, as it turns out, has not been invested in vain.

Let it be known that the decision I made, more than a year ago, to develop my thesis on a subject of which I knew so little about was the right one, for I have learned so much more than I foresaw.

"Sometimes you've got to run before you can walk" – Tony Stark

Abstract

Tendons are mechanosensitive tissues that enable skeletal movement by allowing an effective transmission of forces between muscles and bones. Their biomechanical behaviour, particularly their load-bearing capabilities, can be attributed to the anisotropically aligned and hierarchical organization of their extracellular matrix. However, their healing capacity is quite limited, meaning that, in the event of an injury, tendon natural healing will most likely result in a loss of structural and therefore mechanical properties. Thus, the fabrication of scaffolds that synergistically replicate the native tendons structural and mechanical properties and are capable of being remotely actuated to mechanically stimulate cells would be of considerable interest to promote tissue regeneration.

For this purpose, continuous and aligned electrospun nanofibre threads were fabricated and assembled by textile techniques into yarns, 3D hierarchical constructs mimicking the fibrous architecture of native tendons fascicles. These yarns were based on a PCL matrix mechanically reinforced with cellulose nanocrystals (CNCs) decorated with superparamagnetic iron oxide nanoparticles (MNP@CNC). To simultaneously assure these particles chemical and colloidal stability and improve their interfacial compatibility with the polymer matrix, MNP@CNC were coated with thin layers of polydopamine that were further grafted with hydrophobic dodecanethiol (DT-NP). The incorporation of small amounts of DT-NP (0 – 5wt.%) significantly improved the mechanical properties of the nanofibre yarns, simultaneously endowing them with magnetic responsiveness.

Moreover, the biological performance and functionality of the fabricated constructs, namely the capacity to induce tenogenic differentiation, was assessed by culturing human adipose stem cells (hASCs) under the influence or absence of magnetic stimulus. Magneto-mechanical stimulation of cells promoted high expression of tendon-related markers, such as Tenomodulin and Scleraxis, and activation of the YAP/TAZ signalling pathway, that regulates mechanotransduction. Moreover, cells under magneto-mechanical stimulation upregulated genes related with anti-inflammatory cytokines while downregulating pro-inflammatory factors. Overall, the nanofibre yarns were applied to create a magnetically responsive system that, combined with a tendon mimetic architecture, was able to mechanically stimulate cells. As result the proposed system boosted hASCs tenogenic commitment and synergistically had a positive effect on the modulation of their inflammatory response, both of which might play key roles to achieve on tendon regeneration.

Keywords: Tendon, Magnetic nanoparticles, Electrospinning, Hierarchical scaffolds

Resumo

Atualmente, lesões de tendões e doenças relacionadas representam alguns dos problemas músculo-esqueléticos mais frequentes, afetando tanto a população fisicamente activa como indivíduos mais sedentários. Lesões de tendões prejudicam significativamente a qualidade de vida das pessoas afetadas, dado o papel fundamental destes tecidos para o sistema locomotor. A sua capacidade de regeneração é, no entanto, bastante limitada devido à sua natureza hipovascular e hipocelular. Isto significa que, em caso de lesão, o processo natural de cicatrização muito possivelmente resultará numa perda de propriedades estruturais e, consequentemente, mecânicas. Por outro lado, os tratamentos atualmente disponíveis, dos quais a cirurgia é o procedimento mais comum, são pouco eficazes, resultando frequentemente em tecidos pouco funcionais.

Os tendões são tecidos mecanossensíveis essenciais ao funcionamento do sistema locomotor, visto que transmitem forças entre os músculos e o esqueleto, possibilitando o movimento. O seu comportamento biomecânico, particularmente a capacidade de suporte de carga, deve-se à organização hierárquica e anisotrópica da sua matriz extracelular. As células residentes dos tendões (tenócitos) mantêm a homeostase do tecido, remodelando a matriz extracelular em resposta a forças externas, através de um processo denominado mecanotransdução. Os tendões são maioritariamente compostos por Colagénio I (60 - 85 %) agregado em fibrilas alinhadas paralelamente, que por sua vez se agrupam formando fibras. O próprio tendão é composto por estruturas sucessivamente menores encaixadas umas dentro das outras, tal que existem divisões físicas entre aglomerados de fibras de colagénio (fascículos). Estas divisões não só contribuem para as propriedades mecânicas do tendão, como previnem que uma lesão se estenda a todo o tecido. Posto isto, é de extrema importância a produção de *scaffolds* que sinergicamente reproduzam as propriedades estruturais e mecânicas de tendões nativos e sejam capazes de ser atuados de forma remota para estimular mecanicamente as células e subsequentemente promover a regeneração dos tecidos.

Dado que os tendões são tecidos fibrosos, *scaffolds* para regeneração de tendão devem ser igualmente fibrosos e anisotropicamente alinhados. De entre as técnicas de fabrico mais usadas em engenharia de tecidos, *electrospinning* permite obter fibras com diâmetros desde algumas centenas de nanómetros até alguns micrómetros, de modo a que a escala das estruturas do tecido nativo seja replicada. Assim, linhas contínuas formadas por fibras alinhadas (*continuous and aligned fibre threads*,) foram fabricadas por *electrospinning* e posteriormente agregadas em fios (*yarns*). Estes *yarns* são estruturas 3D, organizadas hierarquicamente, que mimetizam a arquitetura dos fascículos em tendões nativos, enquanto os *threads* replicam as respetivas fibras de colagénio. Os *threads* foram produzidos com uma matriz de PCL reforçada por nanocristais de celulose (*cellulose nanocrystals*, CNCs) decorados com nanopartículas superparamagnéticas (MNP) de óxido de ferro. Os CNCs são nanopartículas biocompatíveis e com excelentes propriedades mecânicas que foram obtidas por hidrólise ácida da celulose. Por sua vez, as MNPs possuem uma magnetização elevada na presença de um campo magnético externo, sendo também biocompatíveis. Estas foram adsorvidas aos CNCS através de um método de co-precipitação *in situ*, criando assim um sistema híbrido (MNP@CNC) capaz de reforçar mecanicamente os *yarns* e permtir a sua atuação remota. Para simultaneamente assegurar a estabilidade química e coloidal destas partículas e também melhorar a sua compatibilidade com a matriz polimérica, MNP@CNC foram cobertas com finas camadas de polidopamina, que foram posteriormente modificadas com dodecanetiol (1-DT). A polidopamina é um biopolímero sintético que resulta da auto-oxidação da dopamina, cuja composição química, contendo grupos amina e catecol, permite a formação de camadas com fortes propriedades adesivas em praticamente qualquer superfície. Por sua vez, a longa cadeia alquila do 1-DT confere às partículas um revestimento hidrofóbico, necessário para a incorporação em PCL.

A morfologia dos *threads* aqui produzidos por *electrospinning*, nomeadamente o diâmetro e o alinhamento das fibras, varia consoante a quantidade de nanopartículas incorporadas (0 – 5 wt.%) e a sua velocidade de recolha durante o processo de *spinning*. Verificou-se que existe um aumento do diâmetro tanto das fibras como do próprio *thread* com o aumento de MNP@CNC revestidas (DT-NP). Por outro lado, a velocidade de recolha influencia tanto o diâmetro como o alinhamento das fibras: com o aumento da velocidade há uma diminuição do diâmetro das fibras acompanhado por um aumento do grau de alinhamento das mesmas. Assim, os *threads* produzidos com 0, 2.5 e 5 wt.% DT-NP apresentaram diâmetros mínimos de 44.85 ± 8.26 µm, 65.13 ± 9.99 µm e 62.01 ± 12.27 µm, respetivamente, obtidos com uma velocidade de recolha de 0.73 $cm.s^{-1}$. As fibras correspondentes apresentaram diâmetros de 0.71 ± 0.28 µm, 0.66 ± 0.25 µm e 1.31 ± 0.44 µm, respetivamente. As fibras e fibrilas de colagénio em tendões nativos têm dimensões médias de 1-20 µm e 20-150 nm, respetivamente. Por esta razão, os *threads* produzidos e as correspondentes fibras exibiram dimensões mais próximas às dos fascículos (150-1000 µm) e fibras de colagénio em tendões nativos, do que às das fibras e fibrilas de colagénio, respetivamente. Contudo, a literatura sugere que *scaffolds* produzidos com fibras de dimensões na ordem de alguns micrómetros, não só beneficiam o fenótipo tenogénico como também replicam a topografia de um tendão nativo durante a fase de remodelação do processo regenerativo.

A incorporação de pequenas quantidades (2.5 ou 5 wt.%) de DT-NP nos *yarns* de PCL melhorou significativamente as suas propriedades mecânicas, sendo o aumento proporcional à quantidade de DT-NP incorporadas. O módulo de Young aumentou de 10.88 ± 0.96 para 21.55 ± 4.68 MPa e o limite de resistência à tração (*ultimate tensile strength*) de 2.84 ± 0.48 para 4.22 ± 0.50 MPa em *yarns* com 5 wt.% DT-NP comparativamente a *yarns* não reforçados. Em particular, a incorporação de 5 wt.% DT-NP conferiu aos *yarns* propriedades mecânicas na gama fisiológica dos tecidos nativos (20-1200 MPa e 5-100 MPa para o módulo de Young e limite de resistência à tração, respetivamente). Simultaneamente, a presença de DT-NP possibilitaram a atuação remota dos *yarns*, ao permitirem a sua magnetização em resposta à aplicação de um campo magnético externo. A magnetização foi também proporcional à quantidade de DT-NP incorporadas, sendo, portanto, superior em *yarns* com 5 wt.% DT-NP.

Posteriormente, o desempenho biológico dos *yarns* magnéticos, nomeadamente a capacidade de induzir a diferenciação tenogénica, foi avaliada através da cultura de células estaminais do tecido adiposo humano (*human adipose stem cells*, hASCs) em *yarns* com 5 wt.% DT-NP, sob a influência ou na ausência de um estímulo magnético. Como foi referido, as células adaptam o seu comportamento em resposta a estímulos físicos transmitidos pela matriz extracelular através de mecanotransdução. Neste caso, o campo magnético aplicado atua sobre as nanopartículas magnéticas, o que causa a sua vibração dentro do material e consequentemente induz pequenas deformações nas respetivas fibras. Verificou-se que a topografia dos *yarns*, por si só, induz o alongamento do citoesqueleto bem como o seu alinhamento segundo a direção longitudinal das fibras. No entanto, a estimulação magneto-mecânica induziu um maior grau de alinhamento anisotrópico de células na direção das fibras, relativamente à cultura estática. O alongamento do citoesqueleto é induzido devido à ativação de reguladores de transcrição relacionadas com a mecanotransdução, sendo que a expressão destas proteínas foi significativamente superior em células mecanicamente estimuladas. Deste modo, houve uma transmissão eficaz de estímulos mecânicos que consequentemente promoveu o alongamento de células, que é particularmente importante para o compromisso tenogénico.

A expressão génica das hASCs foi analisada após 11 dias de cultura com o intuito de avaliar o seu compromisso tenogénico, bem como a capacidade de modulação da resposta inflamatória. Dado que um *scaffold* induz inevitavelmente inflamação no local de implantação, é importante que o mesmo promova a remodelação do tecido nativo, sem causar inflamação crónica ou fibrose. Posto isto, verificou-se expressão de marcadores tenogénicos e inibição de marcadores osteogénicos e

condrogénicos. Em particular, hASCs cultivadas sob estimulação magneto-mecânica apresentaram uma maior expressão de marcadores relacionados com o compromisso tenogénico de células estaminais, *TNMD* (Tenomodulina) e *SCX* (Scleraxis). Além disso, houve inibição de citocinas pro-inflamatórias e promoção de citocinas anti-inflamatórias mais acentuadas em hASCs cultivadas sob estímulo mecânico.

Em suma, a incorporação de DT-NP em *scaffolds* cuja estrutura mimetiza a organização da matriz extracelular de tendões, melhorou as suas propriedades mecânicas, colocando-as na gama fisiológica dos tecidos nativos, e conferiu-lhes propriedades superparamagnéticas. A atuação remota dos *scaffolds*, através da aplicação de um campo magnético, provocou a ativação de vias de sinalização relacionadas com a mecanotransdução em células estaminais. Desta forma, confirmou-se uma transmissão eficaz do estímulo mecânico que se traduziu na diferenciação tenogénica de células estaminais e na modulação da resposta inflamatória. Assim, apresenta-se aqui uma estratégia cujas principais características são, de um ponto de vista clínico, vantajosas não só para a recuperação de um tecido totalmente funcional após uma lesão, mas também para a prevenção de fibrose e inflamações crónicas.

Palavras-chave: Tendão, Partículas Magnéticas, Electrospinning, Estrutura hierárquica

Contents

List of Figures

List of Tables

List of Equations

List of Abbreviations

1-DT	Dodecanethiol
2D	2 Dimensional
2D-FFT	2D-Fast Fourier Transform
3D	3 Dimensional
α-MEM	α-Minimal Essential Medium
A	
A/A	Antibiotic-antimycotic Solution
ACAN	Aggrecan
AFM	Atomic Force Microscopy
ANOVA	One-way Analysis of Variance
B	
BMP-12	Bone Morphogenic Protein-12
C	
CANT	Continuous and Aligned Nanofibre Thread
cDNA	Complementary DNA
CHT	Chitosan
CNC	Cellulose Nanocrystals
COL1A1	Type I Collagen
COL3A1	Type III Collagen
COX2	Cyclooxygenase-2
D	
DAPI	4,6-Diamidino-2-phenyindole dilactate
DCN	Decorin
DI	Deionized
DMF	Dimethylformamide
DT-NP	1-DT coated PDA-NP
E	
ECM	Extracellular Matrix
EGF	Epidermal Growth Factor
F	
FBS	Fetal Bovine Serum
FTIR	Fourier Transform Infrared
FWHM	Full Width at Half Maximum
G	
GAPDH	Glyceraldehyde-3-phosphate dehydrogenase
H	
hASCs	Human Adipose Stem Cells
hTDCs	Human Tendon Derived Cells
I	
IL	Interleukin
M	
MCC	Microcrystalline Cellulose
MNP	Magnetic Nanoparticle
MNP@CNC	CNC decorated with MNPs
mRNA	Messenger RNA
Ms	Magnetization of Saturation
MSC	Mesenchymal Stem Cell
MTS	3-(4,5-Dimethylthiazol-2-yl)-5(3-carboxymethonyphenol)-2-(4-sulfophenyl)-2H-tetrazolium
P	
PBS	Phosphate-buffered Saline
PCL	Poly(ε-caprolactone)
PCR	Polymerase-Chain Reaction
PDA	Polydopamine
PDA-NP	Polydopamine coated MNP@CNC
PGA	Poly(glycolic acid)
PDGF	Platelet- Derived Growth Factor
PLA	Poly(lactic acid)
PLLA	Poly(ι-lactic acid)

Q	
qPCR	Quantitative Polymerase-Chain Reaction
R	
RT-PCR	Reverse transcription Polymerase-Chain Reaction
RUNX2	Runt-related Transcription Factor 2
S	
SCX	Scleraxis
SPCL	Starch and PCL
SEM	Scanning Electron Microscopy
STEM	Scanning Transmission Electron Microscopy
T	
TAZ	Transcriptional coactivator with PDZ binding motif
TE	Tissue Engineering
TGA	Thermogravimetric Analysis
THF	Tetrahydrofuran
TNC	Tenascin
TNMD	Tenomodulin
V	
VSM	Vibrating Sample Magnetometer
X	
XRD	X-Ray Diffraction
Y	
YAP	Yes-associated protein

Chapter 1. Introduction

1.1. Incidence of tendon injuries

Currently, tendon injuries and related disorders represent some of the most frequent musculoskeletal problems, significantly impairing the quality of life of those affected. These injuries not only occur among the physically active population, namely due to sport injuries caused by overuse or direct trauma, but also may affect less active or sedentary individuals [1]. In the United States alone, 33 million cases of musculoskeletal problems have been reported annually, in which 50% of these relate to tendon and ligament injuries [2]. Thus, considering the vital role of tendons in the overall functioning of the musculoskeletal system, it is important to ensure the correct regeneration of these tissues. However, tendons have a quite limited healing capacity and current treatments for tendon injuries are inefficient, frequently resulting in low tissue functionality and prolonging of the patients suffering [3].

1.2. Tendon structure and composition

Tendons play a vital role in the overall functioning of the musculoskeletal system, given that they connect muscle to bone allowing an effective transmission of forces that enables skeletal movement [4]. Tendons are dense connective tissues characterized by an abundant extracellular matrix (ECM) that is repaired, remodelled and maintained, by a small resident cell population comprised mostly of tenocytes and a few stem and progenitor cells [5]. The main structural component of the tendon ECM is Type I collagen, representing 60-85 % of its dry weight. These molecules self-aggregate into collagen fibrils (10-500 nm in diameter) to which the tenocytes bind and order into fibres (1-20 µm in diameter) [3,5,6]. Other types of collagen are also present in the ECM in lower quantities. For instance, Type III collagen is involved in tendon repair, while Type V collagen intervenes in Type I collagen self-assembly by stabilizing and ordering its structure. The tendon matrix also accounts for other proteins, such as elastin, which represents 1-2 % of its dry weight and is particularly important for maintaining the matrix structure after mechanical loading, or proteoglycans like decorin or fibromodulin, that play an important role in the collagen fibrils interconnection [3,5].

The tendon ECM has a well-organized hierarchical structure in which the tendon itself is comprised of successively smaller structures encased within each other (Figure 1.1). A tendon unit is comprised of several fascicles encased in a thin sheath of connective tissue, the epitenon. Each fascicle is formed by an ensemble of collagen fibres and is bound by the endotenon. Each fibre is composed of parallel collagen fibrils closely packed together, which in turn result from the aggregation of collagen

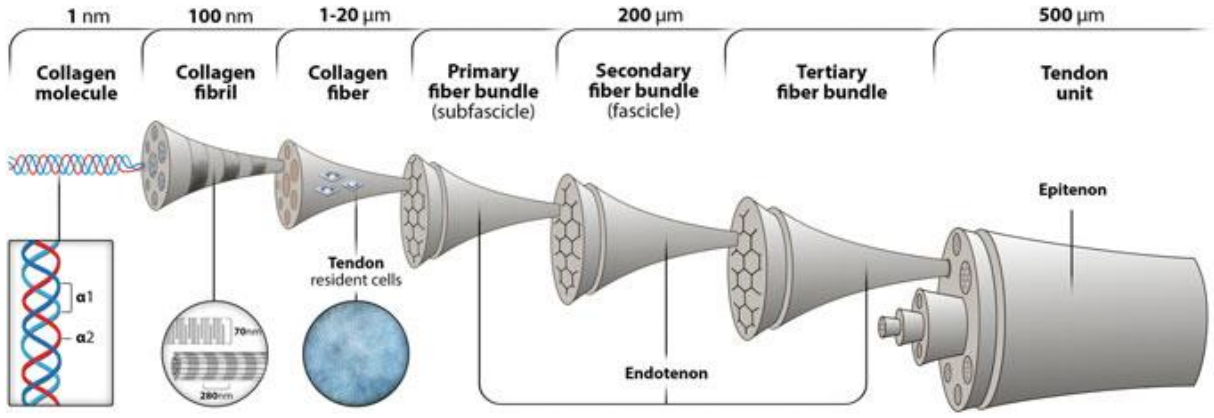

Figure 1.1. Tendon hierarchical structure. A tendon unit is comprised of several fascicles encased in a thin sheath of connective tissue, the epitenon. Each fascicle is an ensemble of collagen fibres bound by the endotenon, which in turn are composed of parallel collagen fibrils closely packed together. Collagen molecules self-aggregate into fibrils, to which the tenocytes bind and organize into fibres. Adapted from ref. [5].

molecules [3,7]. Collagen fibrils present crimps, a characteristic wavy pattern that is ascribed to the bending of the fibrils when they change their plane of running. These crimps stretch when a tensile load is applied to the tendon and revert to their original formation once the load is removed, ultimately contributing to the tendon's flexibility [4,5].

Tendons vary in shape, size and orientation depending on their insertion sites and function of the muscles and bones they are connecting. For instance, extensor muscles like the quadriceps that create powerful forces, have short and wide tendons. On the other hand, muscles like the finger flexors, that are responsible for small and precise movements, have long and thin tendons [6]. Despite these differences in morphology, the internal structure of the tendon, namely its characteristic ECM organization, is common throughout the whole body. In particular, the existence of physically separate divisions of fibres not only prevents that localized damage affects the whole tendon but also provides the tendon with its load-bearing capabilities [5]. Hence, the tendon ECM is directly responsible for the mechanical performance of these tissues regarding their ability to successfully carry out musculoskeletal movement.

1.3. Tendon mechanical behaviour and properties

Tendons are capable of sustaining extremely high tensile forces due to their fibres being aligned longitudinally along the tissues mechanical axis and it is their viscoelastic behaviour that allows these tissues to carry out their mechanical role [4,8]. In this scope, viscoelasticity, referring to the relationship between stress and strain, is a trait of materials in which this relationship is not constant, but instead depends on the period of load or displacement [1]. Namely, when a tensile force is applied, the tendon is stretched and energy is absorbed and stored within the tissue, so when said force is removed, the tissue recovers its original shape and energy is released [1,4]. Regarding these tissues tensile properties, it has been reported that natural tendons have tensile strengths, that is the maximum stress a material can sustain without breaking, and Young's Modulus, which translates the relation between stress and strain, in the range of 5-100 MPa and 20-1200 MPa, respectively [9].

The tendon's stress-strain curve (Figure 1.2) presents three regions: the toe region, the linear region and the yield and failure region. The toe region encompasses the 0-2 % strain of the collagen fibrils and represents the stretching of their crimps, thus presenting a low stiffness. Once every fibril has been flattened, the tendon enters its linear region. At a strain higher than 2 %, the collagen fibril backbone is pulled and the tendons deformation is caused by the collagen molecules sliding between each other. Thus, the deformation is linear and the slope of the curve represents the Young's Modulus of the tendon [1,5,8]. In normal conditions, most tendons function in the physiological range, that is in the toe region and in the beginning of the linear region, given that at strain lower than 4 %, the deformation is reversible and the tendon is able to recover its shape after loading [1]. However, at 4 % strain, individual fibrils start to tear and the tendon enters the yield region. In this region, micro ruptures accumulate, the tendon itself begins to fail and suffers irreversible deformation. Once the strain is higher than 8-10 %, the tendon suffers macroscopic failure [1,8].

1.4. Tendon healing and current treatments

Tendon natural healing can be divided into three overlapping stages: the inflammatory, the reparative and the remodelling phases. First, in the inflammatory phase, the injury site is covered by a blood clot, whose platelets induce the migration of extrinsic inflammatory cells, such as neutrophils and macrophages that phagocyte the necrotic tissue, by releasing of chemoattractants. Later, in the reparative stage, disorganized collagen is laid in large quantities in the injury site, which leads to scar tissue formation. Also, there is intrinsic fibroblastic proliferation and neovascularization along with

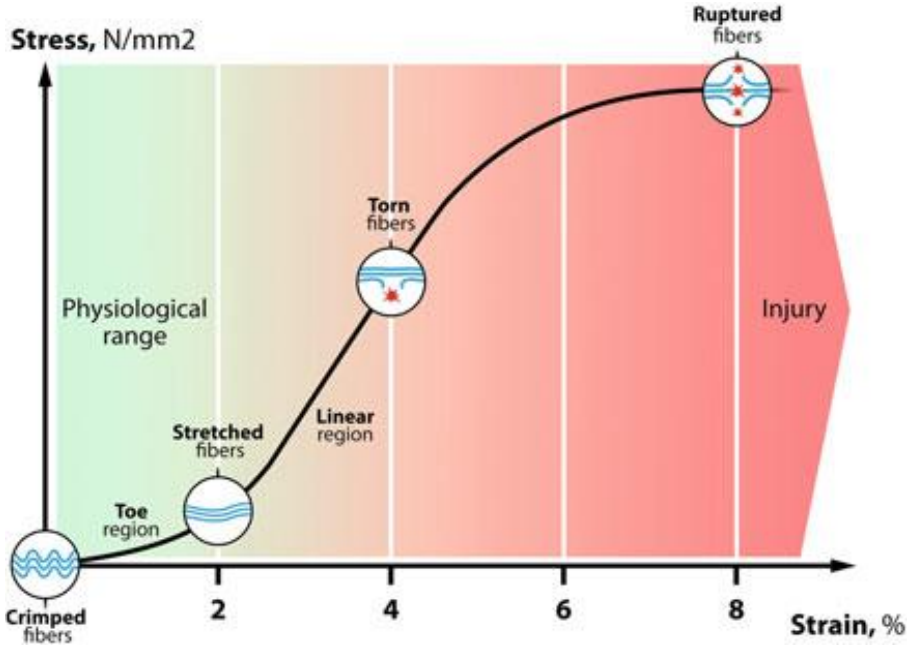

Figure 1.2. Tendon stress-strain curve. This curve presents three regions: the toe region, the linear region and the yield and failure region. The initial toe region (0-2 % strain) represents the stretching of the crimps in the collagen fibrils. The linear region (2-4 % strain) represents the stretching of the fibril backbone and its slope is the tendon's Young's Modulus. In the yield region (strain higher than 4 %) microscopic tears accumulate, eventually leading to a macroscopic rupture and subsequent tendon failure. Adapted from ref. [5].

extrinsic fibroblastic migration into the injury site, which results in the production of large quantities of Type III collagen. Finally, during the remodelling phase, Type III collagen is replaced by Type I collagen and the newly formed fibrous tissue is aligned along the direction of the mechanical loading [1,7,8]. This process is guided by two distinct mechanisms that act simultaneously during these stages: the intrinsic healing, which is mainly governed by the tendon resident cell population; and the extrinsic healing, which encompasses the migration of cells from the surrounding tissues to the injury site and is initiated due to the tendons hypocellular nature and the tenocytes poor reparative capabilities [3,7,10].

Overall, tendon healing can evolve into tendon repair or regeneration. During tendon repair there is inflammatory cell infiltration, fibroplasia, disorderly collagen deposition and although, after this process, the vascular, cellular and collagen content of the remodelled tendon are similar to that of a healthy one, its structural and mechanical properties will be most likely inferior [1,4,11]. Furthermore, this is an extremely long process that can easily take several months or even years for the tissue to fully remodel [7,11]. In contrast, during tendon regeneration there are few inflammatory cells, fibroplasia does not occur and collagen is deposited orderly, so there is no scar tissue formation and the tissues mechanical properties are fully restored [4,5]. Thus, in this scope, the preferred approach following an injury is tissue regeneration rather than tissue repair, so that all the tissue's structural and mechanical properties may be restored.

Nowadays, tendon injuries are treated surgically or by conservative (non-surgical) therapies. Surgical intervention involves the application of implantable devices that are able to cover the defect at the injury site, such as sutures or tissue grafts [10,12]. This type of intervention is followed by a recovery period during which the tendon is immobilized or different types of mechanical loading are applied, aiming at restoring the tendon load-bearing capacity [13]. On the other hand, non-surgical treatment for tendon injuries relies on a combination of different therapies, such as eccentric exercise, extracorporeal shock wave therapy or treatment with low-intensity pulsed ultrasound. Eccentric exercises stimulate tendon remodelling while the latter therapies induce a new trauma to the tendon in order to reinitiate the healing process [14].

Surgery has become the treatment of choice for tendon injuries, given that it has proven to be more successful than conservative therapies. Moreover, a large portion of the patients that resort to conservative therapies need to undergo surgery afterwards due to treatment failure. Regardless, none of the current treatments have been able to fully restore tendon function after injury, in spite of its severity [2,10,11].

1.5. Response to mechanical stimuli

Physiological loads are fundamental for the maintenance of tendon tissue homeostasis by influencing cell behaviour in terms of proliferation, differentiation or even healing mechanisms. In fact, tendon injuries frequently occur as a consequence of inadequate mechanical loading, whether excessive or insufficient, resulting in loss of tissue function [13,15]. In response to external forces, tenocytes remodel the tendon ECM through mechanotransduction, that is, the process by which mechanical stimulus is translated into biochemical signals. Overall, this process depends on interactions between ECM proteins, tenocytes surface receptors and cytoskeleton and several signalling molecules, resulting in the formation and degradation of ECM proteins [16–18]. Also, mechanical loading helps maintain the tenocytes characteristic spindle shape [15]. Thus, mechanical stimulation is an important parameter to consider when aiming at maintaining the tenogenic phenotype and promoting stem cell tenogenic differentiation.

Furthermore, controlled mechanical loading may also be used for clinical purposes to aid the healing process. Although extensive and extended stretching leads to an inflammatory response and promotes osteogenic differentiation of stem cells, the application of forces within the physiologic range can improve the repair process and hence restore most of the normal tissue function [13,15]. The most adequate loading regime should vary with the nature and the site of the injury (Figure 1.3) and should also be combined with any additional therapies that may be applied to correct the tendon defect [13,19]. For instance, complete unloading of an injured tendon leads to a decrease in structural and mechanical properties, while its overloading may reduce its mechanical properties along with its range of motion. On the other hand, passive motion is particularly effective to reduce the formation of adhesions, which hinder the natural gliding of the tendon [19].

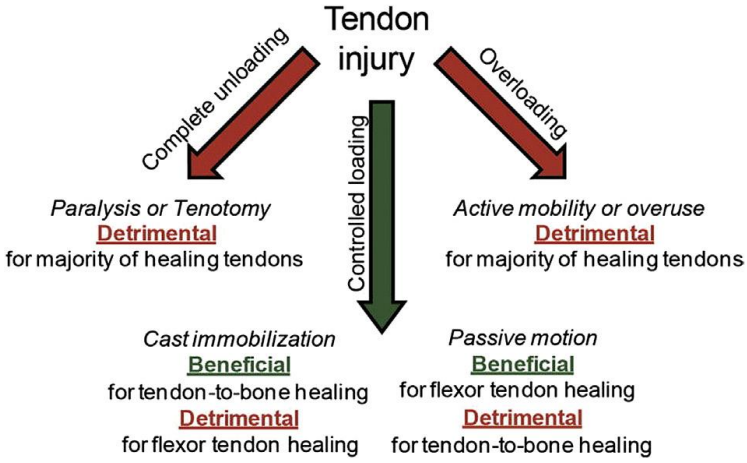

Figure 1.3. Diagram illustrating the effect of different loading regimes in different types of injuries. While complete unloading or overloading impairs the healing process of most injuries, cast immobilization and passive motion are indicated for the treatment of tendon-to-bone interface and flexor tendons, respectively. Adapted from ref. [19].

1.6. Tissue engineering strategies for tendon regeneration

In recent years, several tissue engineering (TE) strategies have been developed in order to promote tendon regeneration, thereby aiming at restoring the tendons normal tissue function in a post injury setting, a requirement that current treatments haven't been able to fulfil. These strategies rely on

a combination of 3D constructs capable of mimicking the key structural aspects of the tissues ECM and of biological agents able to promote a regenerative process, while also supporting cell proliferation.

1.6.1. Cell based approaches

Given the poor regenerative capacity of the tendon resident cell population and these tissues inherent tendency to generate scar tissue and adhesions as a result of an injury, several therapies based on cell harvesting and seeding have been proposed to overcome the limitations of the tendon natural healing process. Moreover, a population of stem and differentiated cells can give rise to a range of bioactive molecules responsible for regulating different physiological processes. For this reason, delivering cells to the injury site could improve the tissues response to the trauma [4,10].

In this scope, the use of the patients own resident tendon cells is an evident option, since an immune response would be avoided. However, the harvesting process is detrimental for the donor tissue, which may lead to tissue morbidity due to its hypocellular nature. On the other hand, cell populations harvested from another donor are prone to induce an immune response, eventually leading to their rejection [11,20]. As an alternative, adult stem cells could be used for this purpose. These cells have the ability to self-renew and are capable of committing and differentiating into different tissue lineages [7]. Also, a population of these cells can be found in almost all tissues of the human body. For instance, adipose tissue is an abundant adult stem cell source, enabling a less invasive harvesting procedure without causing donor tissue morbidity [4,20,21]. Importantly, there is no established method to induce tenogenic differentiation of stem cells, though certain growth factors, such as bone morphogenic protein-12 (BMP-12), epidermal (EGF) and platelet-derived growth factor (PDGF), have promoted the expression of tendon-related markers of stem cells [7,22]. Moreover, it has been suggested that tenogenic differentiation may be enhanced by combining biochemical cues, such as growth factor supplementation, with other biophysical cues, such as surface topography or mechanical stimulus [20,22–24].

Although, stem cells have been extensively investigated for other purposes, the application in tendon TE strategies demands deeper research into the mechanisms underlying tenogenic differentiation. Nonetheless, it is expected that future research may lead to further knowledge on this matter and in particular regarding its role in the regenerative process of tendon tissues.

1.6.2. Scaffold-based approaches

Even though a cell-based approach is an adequate solution for an injured tendon, its individual application may not be sufficient to ensure mechanical properties comparable to that of a native tendon. For this purpose, cell-based approaches can be combined with engineered scaffolds that can provide a suitable environment for cell proliferation while also being able to recapitulate the native tendons mechanical behaviour.

Ideally, scaffolds need to fulfil a few requirements in order to be able to support and guide cell proliferation, eventually originating new and functional tissue. First, and foremost, TE scaffolds must be biocompatible, not to induce an immune response, and biodegradable, degrading at a similar rate as the cells start to produce new ECM. Scaffold architecture is also an important feature to consider: scaffolds should be porous 3D constructs, with a large surface area to allow cell infiltration and nutrient diffusion, and should mimic the overall structure of the tissue ECM. Also, the scaffolds mechanical behaviour should be similar to that of the native tissue, although this requirement depends not only on its architecture but also on the materials with which it is fabricated [12,21,25,26]. In particular, the design of 3D scaffolds for tendon TE applications has been a real challenge given the difficulty in recapitulating the tendons mechanical behaviour, especially at the nanoscale, while ensuring that the remaining requirements are met [27].

Considering the application of an engineered scaffold, the selection of suitable biomaterials is of the utmost importance as it will determine its mechanical properties and degradation time. TE scaffolds can be based on a variety of polymers either of synthetic or natural origin or even on a combination of both. Synthetic polymers are easily processed and modified and can satisfy a multitude of structural features required for the scaffolds specific application, presenting higher mechanical properties than natural polymers. Some of the most common synthetic polymers applied in TE strategies are poly(ε-caprolactone) (PCL), poly(L-lactic acid) (PLLA) and poly(glycolic acid) (PGA) [12,28]. On the other hand, natural polymers, like chitosan or silk, are biocompatible, biodegradable and possess higher cell affinity in comparison with synthetic polymers, since its chemical and biological characteristics are similar to that of the tissues ECM [28,29]. Thus, combining both natural and synthetic polymers leads to the fabrication of a scaffold possessing proper mechanical properties while allowing cell attachment and proliferation [4].

As mentioned in the previous section, tendons are fibrous tissues comprised of a very organized ECM of anisotropically aligned collagen fibres. Thus, scaffolds intended for tendon TE are preferably fibre-based and can be fabricated through several fibre processing techniques, such as melt-spinning, wet-spinning or electrospinning [30]. Fibres fabricated through these techniques can be further assembled into 3D scaffolds that better mimic the tendons ECM structure [12]. Although all these techniques allow the processing of microscaled fibres, through electrospinning one can obtain constructs comprised of fibres scaled from a few hundred nanometres to a few micrometres, therefore allowing the replication of the length scale of the native tendons hierarchical units [30].

1.6.3. Electrospinning

Electrospinning has been among the preferred manufacturing techniques of fibre-based scaffolds for tendon TE applications, given that it allows the production of anisotropically aligned nanofibrous constructions that mimic the highly oriented nanoscale structure of tendon ECM [4]. Overall, electrospinning is a rather simple procedure in which electrostatic forces are used to produce nanofibres with uniform diameters from a polymer solution. A typical setup (Figure 1.4) encompasses four main components: a syringe holding the spinning solution, which is coupled to a syringe pump, a high voltage power supply and a grounded collector. While the syringe pump forces the solution to flow out of the syringe, a high voltage is applied to its needle. A drop will form at the tip of the needle and, when the stresses caused by the electric field overcome the surface tension, the drop is stretched and a jet is formed. Then, while the jet travels in the direction of the grounded collector in an oscillatory movement due to electrostatic repulsion, the solvent evaporates and a nonwoven fibrous mesh is formed in the grounded collector [26,29].

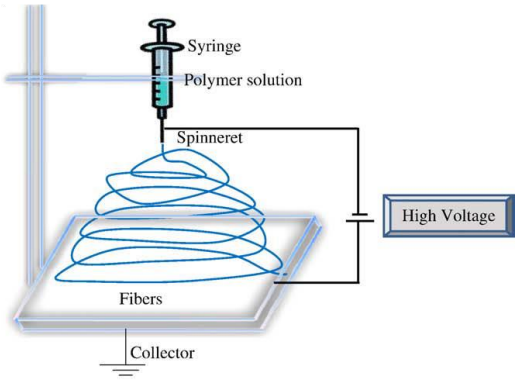

Figure 1.4. Typical setup of an electrospinning procedure. Adapted from ref. [29].

The design of the electrospinning setup significantly impacts the morphology and diameter of electrospun fibres (Figure 1.5), thus several parameters need to be adjusted according to the

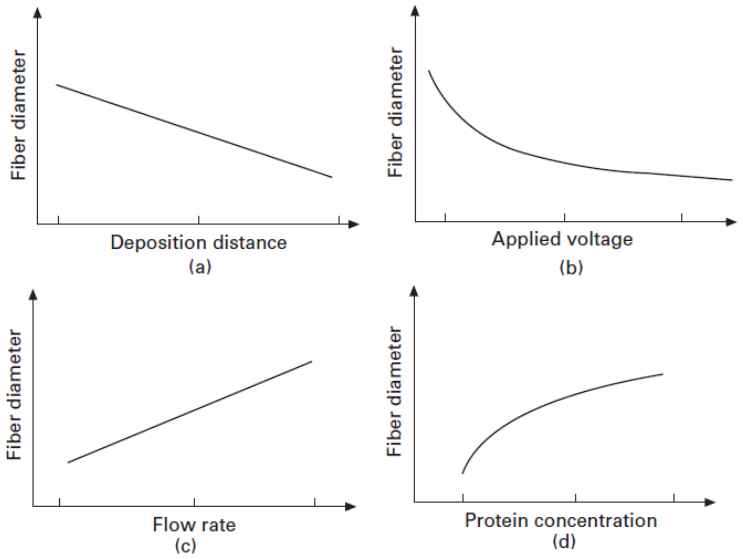

Figure 1.5. Influence of several processing parameters in the diameter of electrospun fibres. Fibre diameter as a function of (a) deposition distance, (b) applied voltage, (c) flow rate and (d) protein or polymer concentration, while keeping the remaining parameters constant. Adapted from ref. [31].

requirements of their intended application. Deposition distance (Figure 1.5a), that is, the distance from the tip of the needle to the grounded collector, is known to influence fibre diameter as its increase leads to further stretching of the spinning jet, thereby causing a decrease in the fibre diameter. Also, there is a required minimum distance to allow the solvent to evaporate before the fibres are deposited in the collector [29]. The voltage applied to the polymer solution (Figure 1.5b) is an essential requirement of this procedure, since there is a threshold below which jet formation does not occur [31]. However, once the applied voltage threshold is reached and the solution is jetted in the direction of the collector, an increase in the applied voltage frequently leads to greater stretching and subsequent decrease of the fibre diameter, although there is a higher probability of causing bead formation [29]. On the other hand, a higher flow rate (Figure 1.5c), that is the speed at which the solution is jetted out of the syringe, tends to lead to thicker fibres. Furthermore, a lower flow rate is usually indicated to allow the fibres enough time to dry, thereby preventing the formation of beads [29]. Finally, protein or polymer concentration (Figure 1.5d) has to be carefully adjusted since it influences the viscosity of the solution. At lower concentration, beads are formed instead of fibres and at higher concentration continuous formation of fibres is interrupted due to the difficulty in maintaining the flow rate at the tip of the needle. Nonetheless, higher polymer concentration causes an increase in the fibre diameter [29,31].

Another important feature to consider during the electrospinning process is the type of the collector that is used, since it determines the alignment of the electrospun fibres. In a typical electrospinning setup (Figure 1.4), the grounded collector is a flat surface which leads to the formation of randomly aligned fibre meshes [29]. However, the ECM from the majority of native tissues has an anisotropic organization that is essential for its overall functioning [26]. Therefore, numerous strategies were developed to allow the fabrication of electrospun scaffolds with different types of alignment. Among these, the use of high speed rotating collectors, such as rotating disks, to force an aligned deposition of nanofibres has been the preferred approach to produce anisotropically aligned nanofibrous scaffolds intended to tendon TE [4,26].

1.6.4. 2D vs 3D Scaffolds

In the scope of tendon TE, anisotropically aligned nanofibrous scaffolds showed to be able to provide the necessary topographical cues to guide the adhesion and proliferation of tenocytes, thereby proving its ability to maintain the tendon phenotype [32]. In Figure 1.6, human tenocytes seeded onto

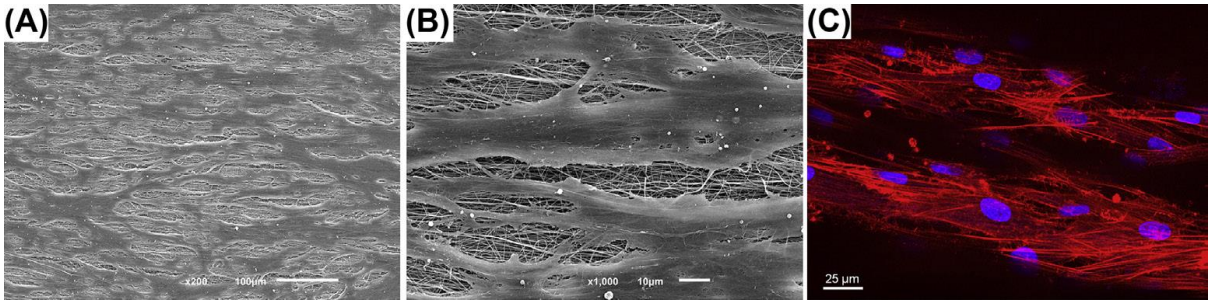

Figure 1.6. Scanning electron microscope images (SEM) of hTDCs cultured on anisotropically aligned electrospun PCL/CHT scaffolds for 10 days. Magnification (A) X200 and (B) X1000. (C) Confocal microscopy images of hTDCs on aligned electrospun PCL/CHT scaffolds (actin filaments stained in red and nuclei in blue). Adapted from ref. [30].

anisotropically aligned electrospun scaffolds, fabricated from a polymer blend of PCL and chitosan (CHT), clearly show a preferential direction of alignment. Also, these aligned nanofibre mats were able to induce the differentiation of human tendon stem/progenitor cells by promoting an increase in the expression of tendon-specific genes, in regard to random nanofibrous scaffolds. [4,30].

Although these constructs are able to fulfil the biological requirements for tendon TE, their mechanical properties can only ensure the load-bearing capabilities of tendons during the regenerative process to some extent [33]. Indeed, scaffolds intended for tendon TE applications should be mechanically similar to the native tissue, thus minimizing stress-shielding effects, which can cause disorganized tissue growth, and providing a temporary replacement for immediate function that is unlikely to rupture after repair and that enables tissue regeneration at the same time. However, the mechanical properties of electrospun scaffolds are generally much inferior to that of native tendons (1-25 MPa in ultimate tensile strength and 1-350 MPa in Young's modulus) [4]. Therefore, it is necessary to improve the mechanical properties of electrospun nanofibrous scaffolds, without impairing their biological performance, thereby maximizing their application for tendon TE.

In order to improve the electrospun scaffolds mechanical performance, reinforcement nanofillers, such as cellulose nanocrystals (CNCs) may be incorporated into the fibres . These are biocompatible rod-shaped nanoparticles with exceptional mechanical properties (7.5-7.7 in ultimate tensile strength and 110-220 GPa in axial elastic modulus) and low cytotoxicity, which allows them to be used as load-bearing components for tendon directed scaffolds [34].

For this purpose, CNCs were incorporated in electrospun nanofibrous scaffolds, both randomly and anisotropically aligned, based on a polymer blend of PCL and chitosan (PCL/CHT) and intended for tendon TE applications (Figure 1.7) [33]. The incorporation of small CNC contents up to 3 wt.% (weight percentage) proved to have a significant reinforcement effect on the nanofibrous scaffolds by increasing their mechanical properties to the range of native tendons. In particular, when 3 wt.% CNC content was added to the polymer blend (PCL/CHT/CNC3), the aligned nanofibrous scaffolds suffered a substantial increase in their ultimate tensile strength (Figure 1.7B), from 21.4 ± 2.2 MPa to 39.3 ± 1.9 MPa, and Young's modulus (Figure 1.7C), from 230.0 ± 2.2 MPa to 540.5 ± 83.7 MPa, which represents an improvement of 132% and 83%, respectively. Moreover, the enhancement of the mechanical performance of the scaffolds was achieved without compromising their biological performance, since the aligned nanofibrous scaffolds reinforced with CNCs were able to promote cell alignment, along the axis of orientation of the fibres, and induce an elongated cell morphology, unlike the random nanofibrous scaffolds (Figure 1.7D, E and F). The stress-strain profiles of the aligned nanofibrous scaffolds (Figure 1.7A), though showing a significant improvement for the PCL/CHT/CNC3 in comparison with the PCL/CHT, lack the characteristic toe region of native tendon mechanical behaviour, which is attributed to the uncramping of the collagen fibres (see Tendon mechanical behaviour section). This region appears at low strains and represents a shock-absorbing feature of

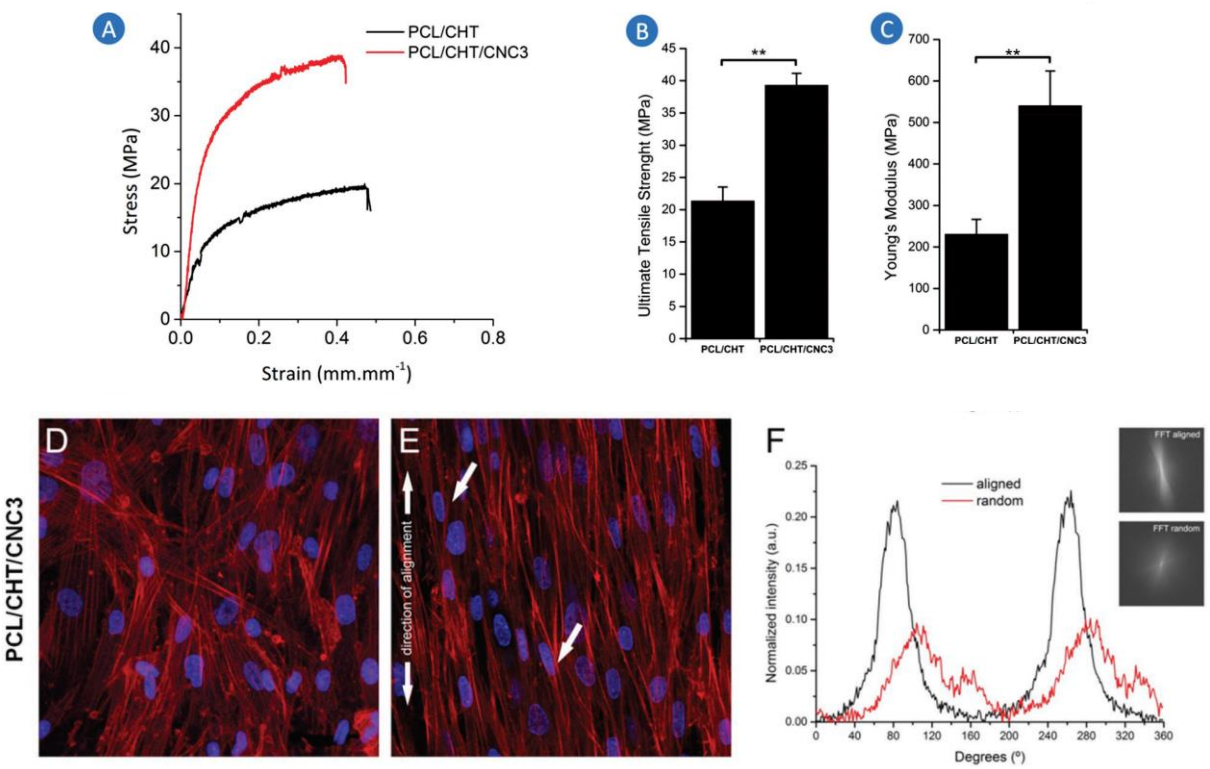

Figure 1.7. Mechanical assessment of anisotropically aligned nanofibrous scaffolds of PCL/CHT and PCL/CHT/CNC3 and biological performance of aligned PCL/CHT/CNC3 scaffolds against its random counterpart. (A) Stress-strain profiles; (B) Ultimate tensile strength. (C) Young's modulus. Confocal microscopy images of the hTDCs seeded on randomly oriented PCL/CHT/CNC3 scaffolds (D) and on anisotropically aligned ones, after 10d of culture (blue: nuclei; red: actin filaments). (F) 2D FFT frequency plots and normalized radial intensity plotted against the angle of rotation for hTDCs cultured on aligned nanofibres of PCL/CHT/CNC3. Adapted from ref. [33].

tendons to prevent tissue damage. Nonetheless, these results substantiate the use of CNCs as reinforcement nanofillers for electrospun nanofibrous scaffolds intended for tendon TE [33].

Despite these reinforced aligned nanofibrous scaffolds possessing adequate mechanical properties and biological performance for tendon TE, they lacked the ability to replicate the native tendon tri-phasic biomechanical behaviour and the length scale of their hierarchical units. Furthermore, these scaffolds are usually fabricated as 2D membranes, limiting their dimensions and making them difficult to handle for practical TE approaches. As such, a new electrospinning system has been developed to fabricate scaffolds that may overcome these limitations.

Thus, continuous and aligned nanofibre threads (CANT) were fabricated from a PCL/CHT/CNC blend (with 3wt% CNC content) and were then assembled into 3D hierarchical scaffolds, through different textile techniques (Figure 1.8) [35]. CANT are intended to mimic the basic unit of a native tendon, that is, the collagen fibres, while the higher hierarchical constructs mimic different length scale structures from the native tendons ECM. These constructs address several requirements of a tendon directed scaffold, namely regarding its structural, mechanical and biological properties, by presenting an anisotropic hierarchical structure and a nonlinear biomechanical behaviour. Moreover, the newly devised system for the production of CANT provides the necessary conditions to ensure a scalable production of 3D scaffolds while allowing the adaptation of their dimensions to fit the demands of the target tissue.

Three textile techniques with different levels of complexity were used to assemble CANTs. First, by twisting 6, 9 or 12 CANT together, nanofibre yarns were obtained in order to replicate the architecture of the native tendons fibre bundles (Figure 1.8A i), ii), and iii)). Mechanical assessment of these yarns showed that an increase in the number of CANT has no significant effect on its Young's modulus and ultimate tensile strength, as opposed to their tensile load (maximum load sustained before

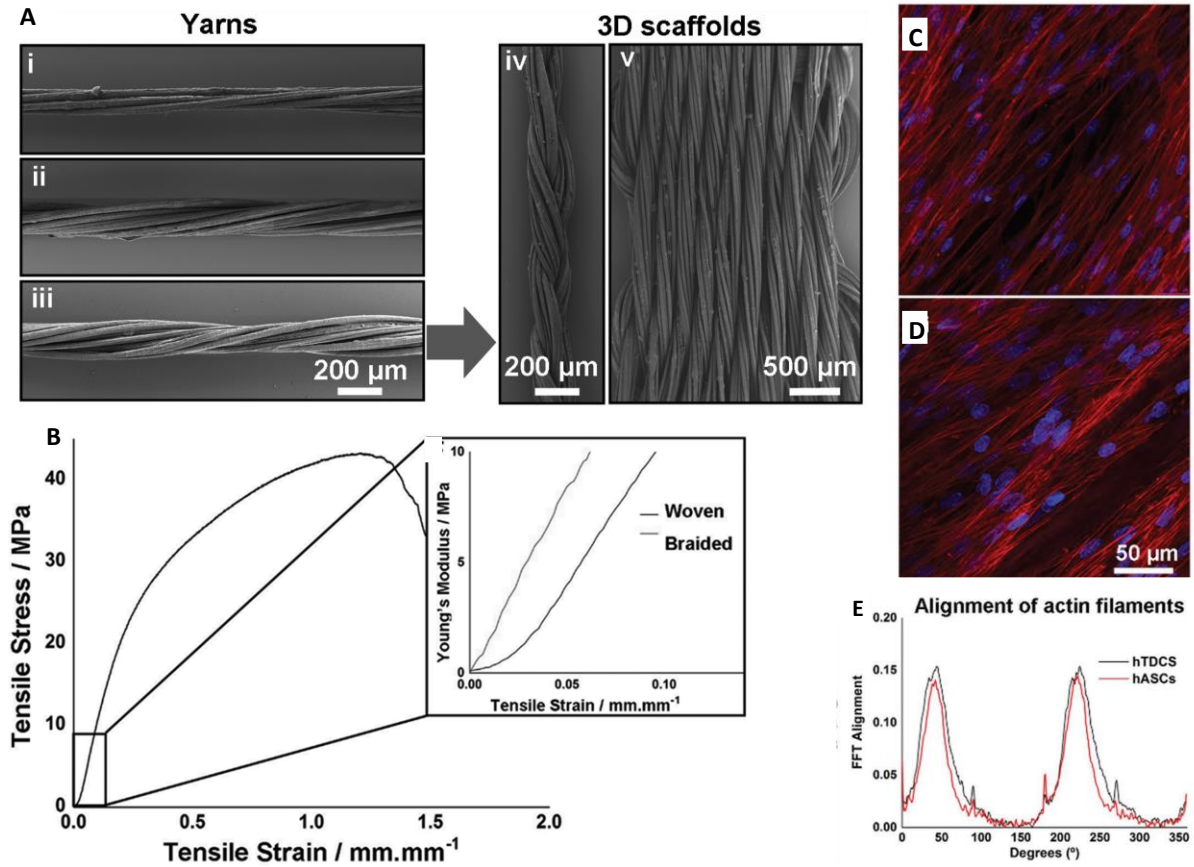

Figure 1.8. Characterization of CANT, Yarns and 3D scaffolds. (A) SEM images of Yarns comprised of i) 6, ii) 9 or iii) 12 CANT, and of iv) braided and v) woven 3D scaffolds. (B) Tensile-strain curve of the woven scaffolds and close up comparing the toe region from woven scaffolds and braided scaffolds. High magnification confocal images of (C) hTDCs and (D) hASCs cultured onto woven scaffolds, at day 7 (nuclei is stained in blue and the cytoskeleton in red). (E) 2D-FFT frequency plots of actin filaments alignment in hTDCs and hASCs cultured onto woven scaffolds for 21 days. Adapted from ref. [35].

breaking) and toughness (ability of a material to deform plastically without breaking), which were considerably enhanced. Thus, 3D scaffolds, mimicking the native tendon unit architecture, were fabricated through braiding and weaving of yarns comprised of 12 CANT (Figure 1.8A iv) and v)). Although braided scaffolds presented higher ultimate tensile strength and Young's modulus in comparison to the woven scaffolds, the latter had a significantly higher toughness and tensile load. Moreover, the woven scaffolds were able to mimic the stress-strain profile of a native tendon, unlike the braided scaffolds, which lacked the characteristic toe region at low strains (Figure 1.8B). Given the superior mechanical performance of woven over braided scaffolds, their biological performance was assessed in terms of tendon-phenotype maintenance and induction of stem cell tenogenic differentiation, by seeding hTDCs (human Tendon Derived Cells) and hASCs (human Adipose Stem Cells), respectively. Indeed, the topography of the woven scaffolds induced an elongated morphology and alignment of the seeded cells, for both cell types (Figure 1.8C and D), after 7 days of culture. The 2D-FFT plots in Figure 1.8E show two distinct peaks at 90° and 180°, which translates the high alignment of cells after 21days, for both cell types. These plots further confirm the effect of these scaffolds topography in the maintenance of the tendon phenotype and induction of tenogenic differentiation of stem cells. Thus, the results herein support the need for target tissue mimicry when developing a scaffold for tendon TE applications [35].

1.6.5. Mechanical stimulation and magnetic actuation

As mentioned before, tendons are mechanosensitive load-bearing tissues and, as such, without appropriate mechanical stimulus, collagen alignment and organization are affected during new tissue formation, thereby impairing its load-bearing capabilities [27]. Moreover, mechanical stimulation has been linked to enhanced cell proliferation and alignment, as well as tenogenic differentiation and ECM synthesis [36–39].

Nowadays, bioreactors are the preferred approach to mechanically stimulate cells seeded onto scaffolds, therefore guiding tissue remodelling and ultimately enhancing the performance of said scaffold [27,38]. A bioreactor system (Figure 1.9) is comprised of a motion component, which grips on both ends of a scaffold and applies physical stimulus; a culture chamber, in which the seeded scaffold is incubated under controlled conditions and continuously perfused with growth media; and a control component that allows the regulation of the parameters for mechanical stimulation and the conditions of incubation [37,40]. In short, this equipment applies cyclic tensile strains to a construct by gripping on its ends, while providing a dynamic environment with the suitable conditions to sustain a cell culture.

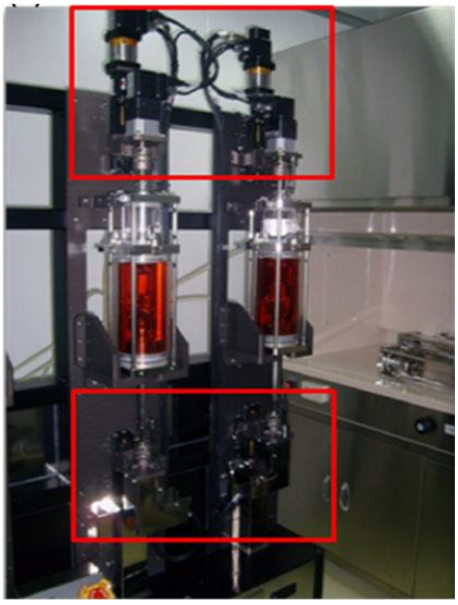

Figure 1.9. Example of a mechanical bioreactor. The motion component is highlighted by the red rectangles. The red tubes are the incubation chambers. Adapted from ref. [40].

Indeed, bioreactors have proven to be an important tool to enhance the performance of TE constructs through mechanical stimulation. These systems have not only been able to induce new tissue formation with the characteristic structural organization of native tendon ECM, but also enhance the mechanical properties of loaded tendon TE constructs [21,36,37]. However, this approach may only be applied for *in vitro* studies, due to the need to physically hold onto the ends of the scaffolds to provide the mechanical stimulus [38]. Nonetheless, tendon TE directed scaffolds may be mechanically stimulated *in vitro* before their implantation *in vivo*, which enhances their maturation, ECM fibre alignment and overall mechanical properties [21,40].

The perspective of manufacturing a scaffold capable of replicating the native tendons structural and mechanical properties, while also being able to be remotely actuated to mechanically stimulate cells, thus promoting tissue regeneration, would be of considerable interest. The remote actuation of scaffolds would allow mechanical stimulation of cells without needing to restrict the scaffold when applying external loads. Furthermore, bioreactors would no longer be necessary for this purpose and scaffolds possessing this feature would enable mechanical stimulation *in vivo*, in a post implantation setting.

In this scope, magnetic nanoparticles (MNPs) could be combined with the scaffolds biomaterials, thereby creating a mechanically responsive system capable of being magnetically actuated to stimulate cells (Figure 1.10). As previously mentioned, cells adjust their behaviour in response to external mechanical stimuli through mechanotransduction [17]. In this sense, physical cues, such as substrate deformation or ECM stiffness, are recognized by cells due to the direct contact between their F-actin cytoskeleton and the ECM, provided by focal adhesions. As such, cells compensate extracellular forces by reorganizing their cytoskeleton, thereby causing tension within the cell. Besides the direct impact on cell geometry, cytoskeletal tension also activates signalling pathways that regulate proliferation and differentiation of stem cells [16,17,41]. Thus, the local substrate deformations caused by the magnetic actuation of MNPs [42], should activate mechanotransduction mechanisms that ultimately drive cellular responses towards the desired behaviour [43,44].

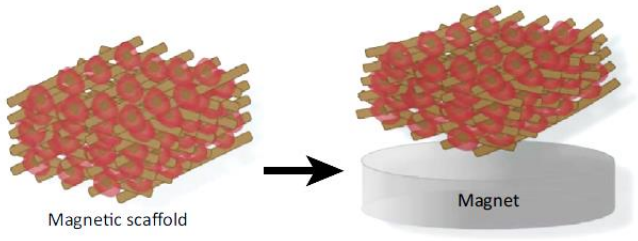

Figure 1.10. Magnetically actuated scaffold. In the presence of a magnet, the magnetic field induces structural deformation of the scaffold, and consequently of the seeded cells as well. Adapted from ref. [43].

Although the development of magnetic responsive scaffolds for tendon TE is relatively new, this approach has been successfully applied to bone TE strategies. For instance, Singh *et al.*, 2014 [45] reported on the osteogenic potential of electrospun nanofibre mats produced from a blend of PCL and iron oxide MNPs exhibiting ferromagnetic behaviour. Results indicate that the incorporation of MNPs enhanced Mesenchymal Stem Cells (MSCs) adhesion and spreading and promoted their osteogenic differentiation *in vitro*. When implanted *in vivo* in rat models for 4 weeks, the scaffolds elicited minimal inflammatory reactions, promoted neovascularization and cell migration through the scaffolds and presented a degradation rate comparable to that of the native tissue. Additionally, magnetic responsive scaffolds were rolled in a cylindrical form and applied to rat segmental defects: these scaffolds promoted neobone formation after 8 weeks and exhibited a higher degradation rate than bare PCL scaffolds. Meng *et al.*, 2013 [46] assessed the *in vivo* osteogenic potential of superparamagnetic nanocomposite electrospun scaffolds of a blend of PLA (poly lactide acid), iron oxide MNPs and hydroxyapatite nanoparticles (nHA). For this purpose, the scaffolds were implanted in rabbit model defects and an external static magnetic field was applied for 110 days. Results indicate that magnetic actuation of these scaffolds induced earlier and faster bone formation, in comparison to scaffolds implanted in the absence of magnetic field. Also, the degradation rate of the scaffolds was enhanced under magnetic actuation, suggesting higher activation of recruited macrophages. Finally, Hao *et al.*, 2017 [47] reported on the use of the aforementioned superparamagnetic nanocomposite electrospun scaffolds to modulate the function of macrophages related to bone regeneration. Firstly, macrophages were cultured on magnetic responsive scaffolds under a static magnetic field alternatively applied in intervals of 12h. Results indicate that macrophages under magnetic stimulation expressed higher levels of a key marker for the pro-resolving phenotype, than those in static culture, while suppressing a key marker for the pro-inflammatory phenotype. Analogously, macrophages under magnetic stimulation increased the production of anti-inflammatory and wound-healing associated cytokines while supressing the secretion of pro-inflammatory cytokines, in comparison to those in static culture. Moreover, pre-osteoblasts were seeded onto the magnetic scaffolds and cultured on the macrophage-conditioned medium, under magnetic stimulation, to assess the osteogenic potential of macrophages. After 24h there was a higher migration rate, as well as, higher intensity of mineralization, characteristic of the later phases of

osteoblast maturation, in pre-osteoblasts cultured under magnetic stimulation than in those in static culture. Analogously, when seeded pre-osteoblasts were cultured in a combination of macrophage-conditioned medium and osteogenic induction medium, there was higher intensity of mineralization among pre-osteoblasts under magnetic stimulation than those in static culture. Therefore, magnetic stimulation has a significant impact on the recruitment of pre-osteoblasts and on the induction of osteogenesis mediated by macrophages. Overall, these studies highlight the efficacy of the proposed strategy on the promotion of osteogenesis, both *in vitro* and *in vivo* [45,46], and on the modulation of the inflammatory response by regulating the polarization of macrophages phenotype [47]. Moreover, due to the versatility of the electrospinning technique, magnetic responsive scaffolds with different architectures can be designed for TE strategies directed at other tissues, thereby eliciting equivalent responses regarding stem cell differentiation, new tissue formation and modulation of the inflammatory response.

Regardless, magnetically actuated scaffolds, intended for tendon TE, were fabricated through rapid prototyping technology, by incorporating iron oxide nanoparticles into aligned arrangements of fibres based on a polymer blend of starch and PCL (SPCL) (Figure 1.11A) [48]. Besides exhibiting a superparamagnetic behaviour, these materials containing iron oxide MNPs had no effect on the viability of seeded cells, thereby proving the MNPs biocompatibility. Magnetic stimulation of the scaffolds had a positive impact on the viability and proliferation of hASCs: the application of an oscillating magnetic field resulted in a significant increase in cellular metabolic activity in both magnetic and non-magnetic constructs, although metabolic activity was higher in magnetic scaffolds under static and dynamic conditions. Thus, cells respond to magnetic stimulus both in the presence and in the absence of MNPs, meaning cellular behaviour can be influenced by indirect magnetic forces. Also, the combination of magnetic stimulation and MNPs seems to have a synergistic effect on cellular mechanisms by benefiting the proliferation of cells [48].

The effect of combining structural cues and magnetic stimuli on guiding hASCs towards a tenogenic lineage was assessed by culturing cells onto SPCL and magnetic SPCL scaffolds under magnetic stimulation. The results showed that hASCs undergo tenogenic commitment, developing a type I collagen matrix, that appears to be more abundant in scaffolds cultured under magnetic stimulation, and especially in magnetic SPCL scaffolds (Figure 1.11B). Also, under magnetic stimulation was observed a more aligned arrangement of collagen fibres that better replicated the ECM structure of native tendons. Furthermore, higher production of Tenascin C, a tendon marker whose expression is upregulated as a result of mechanical loading, was observed in both types of scaffolds

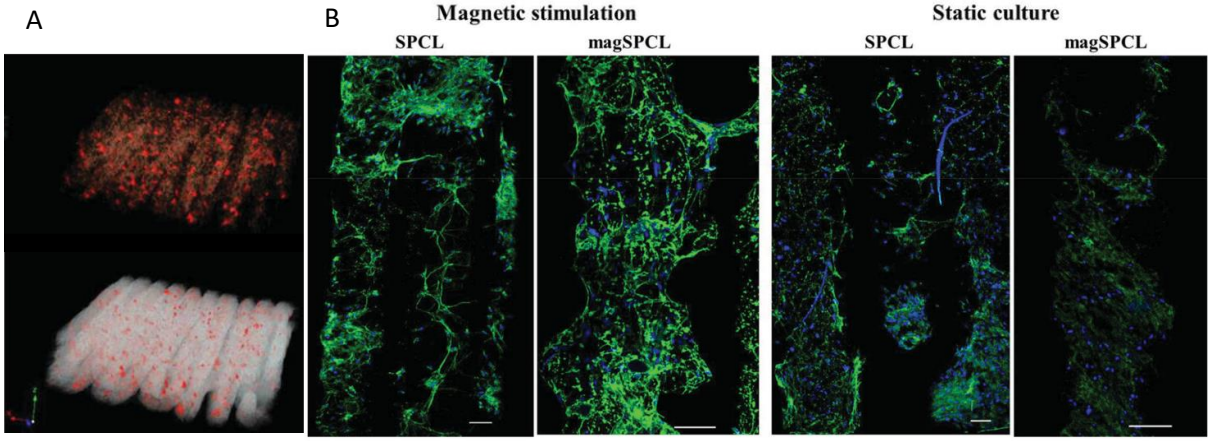

Figure 1.11. Magnetically actuated scaffolds for tendon TE applications fabricated from a blend SPCL and iron oxide nanoparticles. (A) 3D reconstructed model by micro-CT analysis showing the aligned architecture of these scaffolds (the polymeric matrix is presented in grey and the MNPs in red). (B) Type-I collagen immunolocation in hASCs seeded onto bare and magnetic SPCL (magSPCL) scaffolds, cultured for 7 d under magnetic stimulation or static culture. These images represent 1 or 2 fibres from the aligned scaffolds (blue stains the nuclei while green indicates type-I collagen). Scale bar represents 100 µm. Adapted from ref. [48].

cultured under magnetic stimulation, although showing a tendency to increase in magnetic scaffolds, in comparison with those in static culture. Overall, the results herein indicate that the combination of magnetic stimulation with the aligned structure of the scaffolds was determinant in promoting the tenogenic commitment of hASCs [48].

Furthermore, it has also been shown that magnetic fields may be used to remotely guide tissue regeneration, by acting as a mechanical stimulatory cue, and modulate the inflammatory response of these tissues [49]. When studying the effects of low-frequency magnetic fields on the behaviour of tendon-derived cells, it was observed that short and prolonged exposures to this stimulus altered the production of tendon ECM proteins [49]. Namely, a regime of 8h of exposure to magnetic stimulus every 24h showed a positive effect on the preservation of tenogenesis, while exposing hTDCs to magnetic stimulation every 48h resulted in an increase of the type I collagen/type III collagen ratio, thereby promoting collagen deposition. Also, continuous exposure of cultured hTDCs to magnetic stimulation promoted an increase in the secretion of IL-10, an anti-inflammatory cytokine, while inhibiting the secretion of pro-inflammatory IL-1β [49].

Tendon injuries currently represent some of the most common musculoskeletal problems, significantly impairing the quality of life of those affected. Given the importance of tendons to the overall functioning of the musculoskeletal system, ensuring it is correct healing in a post-injury setting is of the utmost importance. Although, current conventional treatments are the preferred approach to these injuries, they frequently result in low tissue functionality. Thus, tissue engineering may give rise to new strategies that may overcome the limitations of conventional treatments, thereby resulting in the full regeneration of injured tissues and most importantly of its natural biomechanical behaviour.

Herein were discussed several tendon tissue engineering approaches addressing different issues in the regeneration of an injured tissue, such as mimicry of the native tendons ECM architecture, replication of its original biomechanical behaviour and external mechanical stimulation of the regenerative process. The following work will thus combine the advantages each approach offers in order to create a broader solution.

Chapter 2. Materials and Methods

The main goal of this project is the fabrication of multifunctional woven electrospun nanocomposite scaffolds capable of mimicking tendon tissue architecture, composition and mechanical properties, while also being able to be magnetically actuated to guide cellular responses. The project herein is divided into three main tasks (Figure 2.1): (1) Production and characterization of magnetic nanoparticles, (2) Fabrication of 3D textile electrospun scaffolds and (3) Assessment of the biological performance of electrospun scaffolds. In the first task, magnetic nanoparticles were produced and incorporated in the scaffolds biomaterials, thereby allowing their magnetic actuation. During the second task, electrospun fibre threads were produced and assembled into higher hierarchical constructs to mimic different length scale structures from the native tendons ECM. Finally, the biological performance and the functionality of the fabricated scaffolds, namely the capacity to induce and boost tenogenic differentiation, were assessed by culturing human adipose stem cells under the influence or absence of magnetic stimuli.

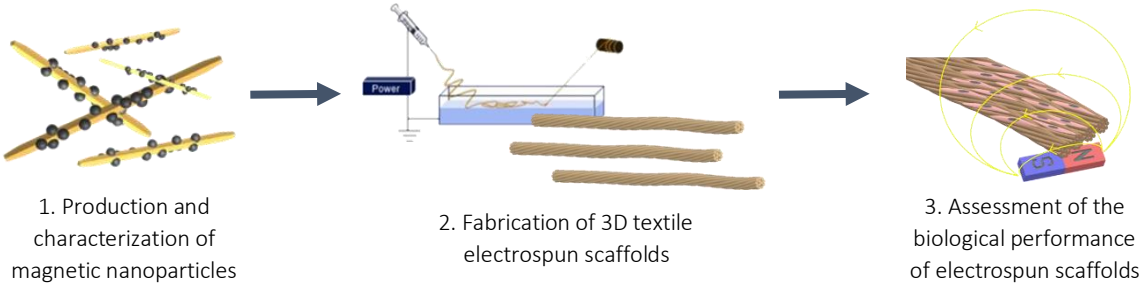

Figure 2.1. Schematic illustrating the tasks involved in the project. First, magnetic nanoparticles were produced and incorporated with the scaffolds biomaterials (1). Then, 3D nanofibrous scaffolds were produced through electrospinning and further assembled into hierarchical constructs through a textile technique (2). Finally, the biological performance of the scaffolds was assessed under magnetic stimulation conditions (3).

The core materials used to produce the magnetic nanoparticles and their main characteristics, as well as the processes through which these were synthesized and characterized are detailed in the following sections.

2.1. Production and characterization of magnetic nanoparticles

Herein, Cellulose Nanocrystals (CNCs) were used as reinforcement nanofillers for the electrospun nanofibre threads, as well as nucleating sites and reducing agents for the incorporation of superparamagnetic iron oxide nanoparticles (Figure 2.2). Then, the produced nanoparticles surface was modified to assure their chemical and colloidal stability while improving their compatibility with the polymeric matrix.

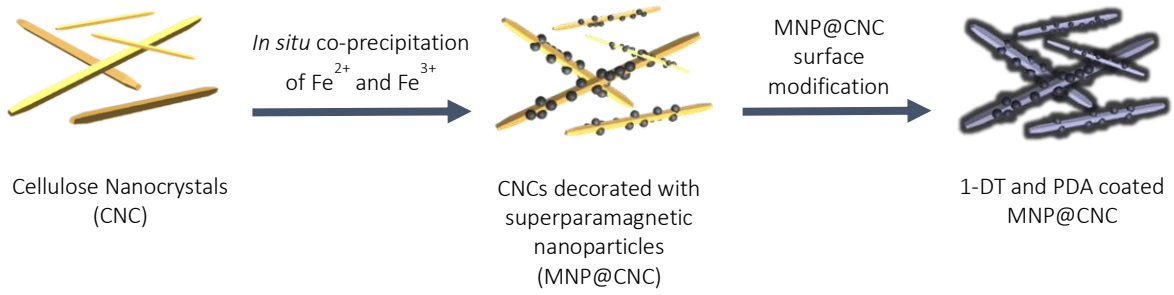

Figure 2.2. Schematic illustrating the different steps involved in the production of the magnetic nanoparticle hybrid system. Cellulose Nanocrystals (CNCs) were produced through sulphuric acid hydrolysis and then decorated with superparamagnetic iron oxide nanoparticles (MNP@CNC) through *in situ* co-precipitation of Fe^{2+} and Fe^{3+} in the presence of CNCs. MNP@CNC surface was coated with thin layers of Polydopamine (PDA) and further grafted with hydrophobic Dodecanethiol (1-DT).

2.1.1. Cellulose Nanocrystals (CNCs)

Cellulose is a polysaccharide consisting of a long-chain of repeating units of a glucose dimer, cellobiose, and is one of the most abundant and available biopolymers on earth, given that it can be extracted from a multitude of sources, such as wood, cotton and certain bacteria. Analogous to tendon tissues, cellulose presents a hierarchical structure in which cellulose chains aggregate into elementary fibrils through hydrogen bonds and van der Waals forces, which subsequently are assembled into microfibrils (5-50 nm diameter) and then into fibres. Moreover, the cellulose microfibrils structure exhibits crystalline regions of highly ordered cellulose chains separated by amorphous regions of disordered cellulose (Figure 2.3). When extracted from the microfibrils, these crystalline regions in the CNCs [34,50].

CNCs are usually obtained through strong acid hydrolysis, particularly sulphuric acid hydrolysis (Figure 2.3). During this process, the amorphous regions of the cellulose microfibrils are degraded and the resulting CNCs present a rod-like shape (Figure 2.2) and a negatively charged surface with numerous hydroxyl and sulphate ester groups that can be exploited for covalent surface modifications. Furthermore, the negatively charged surface improves the colloidal stability of these nanoparticles in aqueous suspensions [34,51].

CNCs present high aspect ratio, with dimensions of 2-50 nm in width and 100-2000 nm in length, depending on both the cellulose source and the conditions of the hydrolysis process [34,52]. Also, CNCs have exceptional mechanical properties with Young's modulus and tensile strengths ranging between 110-220 GPa and 7.5-7.7 GPa, respectively [34]. Nonetheless, it is due to their biocompatibility and low cytotoxicity [34,51] that CNCs are particularly attractive for applications in TE strategies. In particular, CNCs may be used as reinforcement nanofillers for the electrospun scaffolds herein proposed, providing these with the characteristic load bearing capabilities of native tendons [33,35].

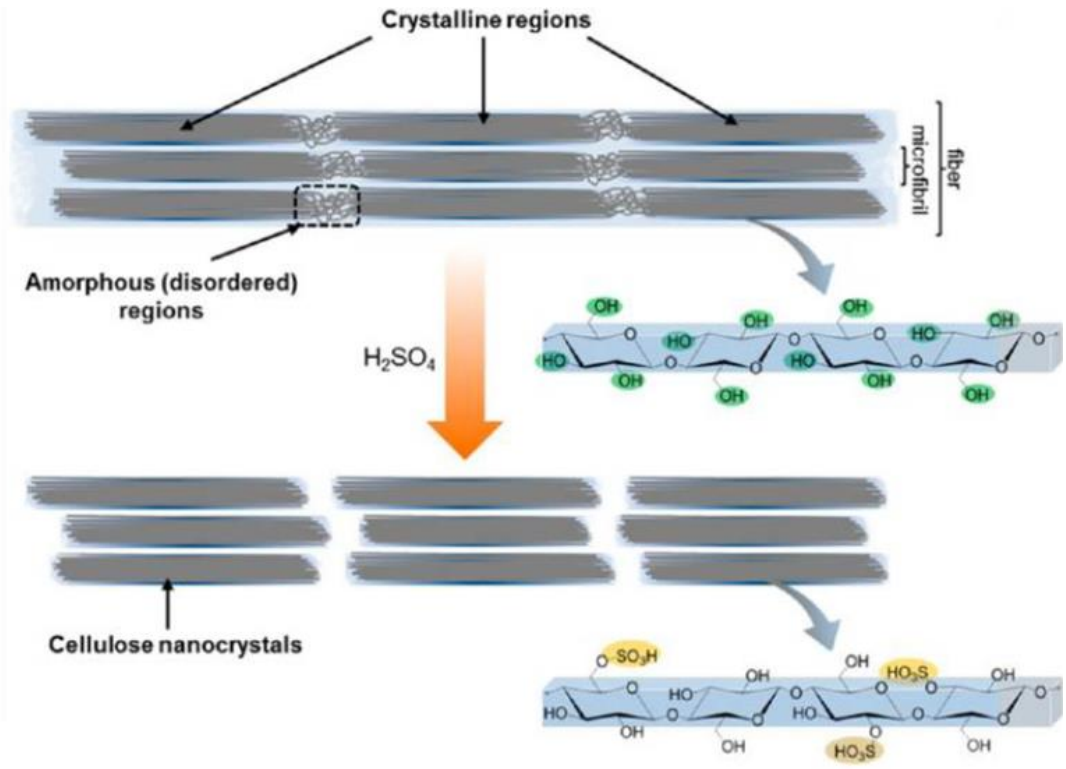

Figure 2.3. Production of cellulose nanocrystals through sulphuric acid hydrolysis. The cellulose nanocrystals result from the hydrolysis of the cellulose microfibrils amorphous regions and present a negatively charged surface of numerous hydroxyl and sulfate ester groups. Adapted from ref [34].

2.1.1.1. Synthesis of CNCs

CNCs were prepared through sulphuric acid hydrolysis of microcrystalline cellulose powder (MCC), following the procedure described on Bondeson *et al.*, 2006 [53] and on Domingues *et al.*, 2016 [33] and adapted according to the reports from Chen *et al.*, 2015 [52]. Hydrolysis was performed with 62 wt.% sulphuric acid at 60 °C for 40 minutes under mechanical stirring.

First, 42g of MCC (Sigma-Aldrich, USA) were suspended in 217 mL of deionized (DI) water under mechanical stirring (500 rpm), followed by the slow addition of 203 mL of sulphuric acid 95-97 % (Honeywell Fluka, Germany) under ice cooling to prevent overheating, taking no longer than 10 minutes to accomplish this step. Then, the suspension was heated to 60 °C and left to react for 30 minutes, under continuous mechanical stirring. Hydrolysis was quenched by adding an excess of cold DI water (5 times the initial volume), previously cooled for 2 hours at 4 °C, and the resulting suspension was left to decant at 4 °C.

Then, the supernatant was discarded and the remaining suspension was centrifuged (Sigma 2-16K, Sigma-Aldrich, USA) at 9000 rpm and 5 °C in 10 minute cycles, until the supernatant became turbid. Between centrifugation cycles, the supernatant was replaced by ultrapure water. The resulting suspension was collected and dialyzed for 7 days, using cellulose dialysis tubing membranes (MWCO: 12-14 kDa, 0-76 mm width, Sigma-Aldrich, USA). Prior to use, dialysis membranes were prepared by washing with hot water for 3 hours. Dialysis was performed against DI water and in the last day against ultrapure water until neutral pH.

After dialysis, the membranes content was subjected to 5 sonication cycles (VCX-130PB-220, Sonics, USA) of 5 minutes each, using an ultrasound probe (Horn ½" SOLID vc 70/13c 3 – 0561) at 60 % of amplitude output, under ice cooling to prevent overheating. The cloudy suspension was then centrifuged for 10 minutes at 9000 rpm and 5 °C to remove big particles. The resulting supernatant containing CNCs was collected and degassed with a vacuum pump. Finally, the CNC suspension was stored at 4 °C until further use.

2.1.2. Magnetic nanoparticle hybrid system

To endow the proposed scaffolds with magnetic properties, CNCs were decorated with iron oxide magnetic nanoparticles (MNPs). Among the different forms of iron oxides, magnetite (Fe_3O_4) and maghemite (γ-Fe_2O_3) are the most commonly used for biomedical applications, due to their low toxicity and biocompatibility as well as their excellent magnetic properties. Magnetite is a black ferromagnetic material containing both Fe^{2+} and Fe^{3+} and presenting the strongest magnetic behaviour among iron oxide forms. On the other hand, maghemite results from the oxidation of magnetite and consequently exhibits weaker magnetic properties, in comparison with magnetite [25,54].

MNPs are commonly produced through co-precipitation methods, in which homogeneous and highly pure, spherical particles can be obtained in aqueous solutions, under relatively low temperatures. This method also allows control over the size of the particles, by varying the pH, temperature and stirring rate of the process, which is of extreme importance since MNPs dimensions directly impacts their magnetic properties. In particular, the MNPs magnetization value increases with their size [55].

For biomedical applications, such as targeted tissue repair, MNPs with high magnetization values and a superparamagnetic behaviour are of particular interest [54,55]. Superparamagnetism refers to materials exhibiting zero magnetic moment in normal conditions, that magnetize upon application of an external magnetic field, with its individual magnetic moments aligning along the magnetic field. Interestingly, MNPs smaller than 20 nm exhibit enhanced superparamagnetic behaviour [25,54].

As mentioned before, MNPs may be anchored to the surface of CNCs (Figure 2.2), thereby creating a hybrid nanocomposite system (MNP@CNC) that simultaneously reinforces the mechanical

properties and provides magnetically responsiveness to the proposed scaffolds. The numerous hydroxyl groups on the CNCs surface (Figure 2.3) function as nucleating sites and reducing agents for the formation of MNPs. Moreover, anchoring MNPs to CNCs improves the dispersion and chemical stability of MNPs [56].

2.1.2.1. Synthesis of magnetic nanoparticle hybrid system

The CNCs decorated with MNPs (MNP@CNC) were produced by co-precipitation of Fe^{2+} and Fe^{3+} with ammonium hydroxide in the presence of CNCs and under N_2 environment. First, 40 mL of 0.3 % CNC aqueous suspension were placed in a triple bottleneck flask at 70 ºC and under continuous N_2 purging. It is important that the whole reaction occurs in anaerobic conditions to prevent magnetite (Fe_3O_4) oxidation[55]. MNP salt precursors, 0.1 g of $FeCl_3 \cdot 6H_2O$ (Sigma Aldrich, USA) and 0.04 g of $FeCl_2 \cdot 4H_2O$ (Sigma Aldrich, USA) (2/1 molar ratio of Fe^{3+}/Fe^{2+}), were dissolved in 10 mL of ultrapure water and added to the CNC suspension, which was left under vigorous stirring for 2 hours. Co-precipitation of Fe^{2+} and Fe^{3+} was induced by adding 100 mL of 3 % (v/v) ammonium hydroxide solution (Sigma Aldrich, USA) and the resulting suspension turned black immediately upon MNP formation. After 1 hour under vigorous stirring, MNP@CNC were magnetically separated using a permanent neodymium magnet (DX=X=_N52, K&J Magnetics, USA) and subjected to several washing and centrifugation cycles (10 min, 5 °C, 9000 rpm) against DI water until neutral pH was achieved. Finally, MNP@CNC were dispersed in ultrapure water and stored at 4 ºC until further use.

2.1.3. MNP@CNC Surface modification

Iron oxide MNPs produced through co-precipitation methods exhibit high surface energy, due to their high surface area to volume ratio, which subsequently leads to MNP aggregation in order to minimize these energies. Furthermore, iron oxide MNPs are easily oxidised which leads to a decrease in the magnetization and dispersion of the particles [54,55]. Thus, to simultaneously assure MNP@CNC chemical and colloidal stability and improve their compatibility with the polymer matrix, MNP@CNC were coated with thin layers of polydopamine (PDA) that were further grafted with hydrophobic dodecanethiol (1-DT) (Figure 2.4).

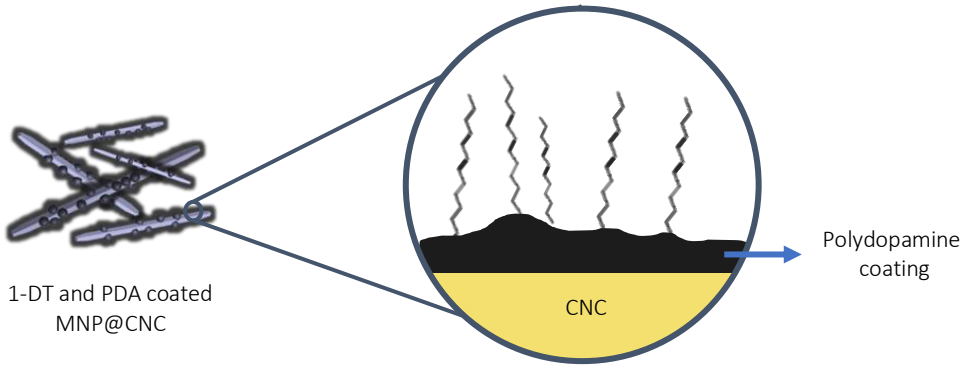

Figure 2.4. Schematic illustrating the magnetic nanoparticles surface modification. MNP@CNC were first coated with thin layers of polydopamine (PDA) and further grafted with hydrophobic dodecanethiol (1-DT).

PDA (Figure 2.5) is a synthetic biopolymer that results from the autoxidation of dopamine and is analogous to the naturally occurring melanin, thus exhibiting high biocompatibility [57]. Dopamine is a biomolecule containing both catechol and amine functional groups (Figure 2.5) , whose co-occurrence is believed to be essential for the formation of strong adhesive films onto virtually any material surface [58]. This monomer polymerization occurs spontaneously under alkaline and aerobic conditions through oxidation of its catechol group to quinone, which reacts with other catechol and amine groups

establishing different covalent and noncovalent bonds, consequently leading to the formation of a polymeric film [57,59]. Thin PDA layers can be obtained through a simple dip-coating procedure, in which the substrate is immersed in an alkaline dopamine hydrochloride solution during 12-18 h. The thickness of the coating increases with immersion time, stabilizing at around 50 nm after 24 h [58].

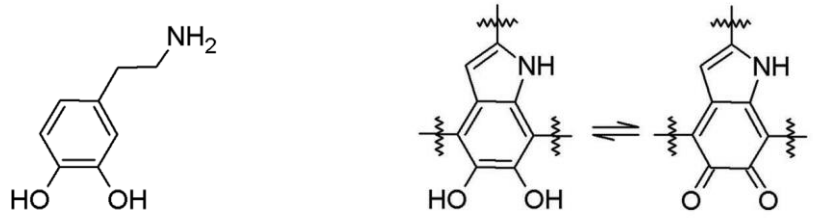

Dopamine Polydopamine (PDA)

Figure 2.5. Chemical structure of dopamine and polydopamine (PDA). Dopamine is a biomolecule containing both catechol and amine functional groups. Polydopamine is a synthetic biopolymer, analogous to the naturally occurring melanin, that results from the autoxidation of dopamine, under alkaline and aerobic conditions. Adapted from Ref [57].

Moreover, PDA films can be further easily functionalized, thereby acting as advantageous mediators for the conjugation of other material or biomolecule to any surface. Catechol and quinone functional groups are able to react with nucleophilic groups, such as amines and thiols, through Michael addition (Figure 2.6) or with amines through Schiff base reactions, subsequently forming covalent bonds with these moieties [57,58,60].

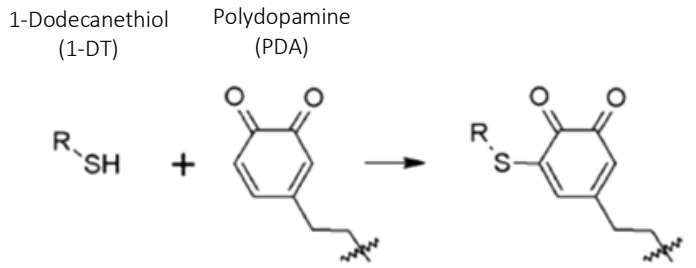

Figure 2.6. Modification of polydopamine (PDA) with a thiol through Michael addition reaction. Through Michael addition, the nucleophile (thiol) donates an electron pair to a carbonyl compound (PDA) resulting in the formation of a covalent bond between the two species [124]. Adapted from ref. [57].

Due to the hydrophilic nature of PDA and its excellent chelation properties towards metallic ions, this strategy results in a robust coating that ensures the steric stabilization of MNP@CNC, thereby preventing particle aggregation in aqueous suspensions [57,61,62]. On the other hand, functionalization of the PDA coating with 1-DT increases the hydrophobicity of MNP@CNC [63–65], improving their dispersion in organic solvents, such as those commonly used for electrospinning purposes [66], as well as their compatibility with the hydrophobic scaffolds' polymer matrix, PCL.

From here on, for the sake of clarity and simplicity, PDA coated MNP@CNC and 1-DT and PDA coated MNP@CNC will be referred to as PDA-NP and DT-NP, respectively

2.1.3.1. Polydopamine Coating

MNP@CNC were coated with PDA following the procedure described on Shi *et al.*, 2015[61]. Previously prepared MNP@CNC were dispersed in tris buffer solution, so that the concentration of MNP@CNC in suspension was 0.2 %. Tris buffer solution (10 mM, pH 8.5) was prepared by dissolving tris((hydroxyethyl)aminomethane) (Sigma Aldrich, USA) in ultrapure water and adjusting the pH with an HCl solution. The resulting suspension was subjected to a 1 minute sonication cycle using an Ultrasonic Processor (VCX-130PB-220, Sonics, USA) at 40 % amplitude output. 2 mg/mL of dopamine

hydrochloride (Sigma Aldrich, USA) were added to the suspension, which was then placed in an ultrasonic bath for 5 minutes to promote the homogenous dispersion of dopamine hydrochloride. The MNP@CNC/dopamine hydrochloride suspension was left stirring overnight, in an opened container and at room temperature. Polydopamine coated MNP@CNC (PDA-NP) were collected through magnetic separation using a permanent neodymium magnet (DX=X=_N52, K&J Magnetics, USA) and subjected to several washing and centrifugation cycles (20 minutes, 5 °C, 9000 rpm) against DI water until neutral pH was achieved. Finally, PDA-NP were dispersed in ultrapure water and stored at 4 ºC until further use.

2.1.3.2. 1-DT Grafting

PDA-NP surface was further modified with hydrophobic Dodecanethiol (1-DT) adapting the procedure described by Lee *et al.*, 2007[58]. Previously prepared PDA-NP were dispersed in absolute ethanol solution, so that the concentration of PDA-NP in suspension was 0.2 %. The resulting suspension was subjected to a 2 minutes sonication cycle using an Ultrasonic Processor (VCX-130PB-220, Sonics, USA) at 40 % amplitude output. After bubbling with N_2, 20 mM of 1-DT (Sigma Aldrich, USA) and then 10 mM triethylamine (Sigma Aldrich, USA), final concentration, were added to the PDA-NP suspension, which was left stirring overnight, in a closed container and at room temperature. 1-DT coated PDA-NP (DT-NP) were subjected to several washing and centrifugation cycles (20 minutes, 5 °C, 9000 rpm) against ethanol and finally dispersed in DMF solution (Thermo Fisher Scientific, USA) and stored at 4 ºC until further use.

2.1.4. Characterization of the produced nanoparticles

In this section, the methods through which the produced nanoparticles were characterized in terms of morphological and chemical properties, as well as the preparation of the respective samples, are presented.

2.1.4.1. Atomic Force Microscopy (AFM)

Atomic Force Microscopy (AFM) is a type of scanning microscopy that obtains high-resolution images at the atomic scale, by measuring the force created by the proximity of a probe to the surface of a sample, without damaging the sample [67].

AFM was used to study the morphology and dimensions of the produced nanoparticles, namely CNCs, MNP@CNC, PDA-NP, DT-NP. For this purpose, a 0.015 % (w/v) solution of each sample was prepared in ultrapure water. A drop of each solution was placed on a freshly cleaved mica disk (9.9 mm diam. 0.27 mm thick), so that the solution covers the entire surface of the latter. After 15 min excess solution was removed and the mica disks were left drying overnight in an exicator, at room temperature. Images were obtained in tapping mode with a Dimension Icon equipment from Bruker with a range of xy – 1 nm to 90 μm. These were later treated and analyzed using Gwyddion software (version 2.49), namely, to obtain CNCs length and height.

2.1.4.2. Scanning Transmission Electron Microscopy (STEM)

Scanning Transmission Electron Microscopy (STEM) is an imaging technique that relies on a focused electron beam to scan a sample in a raster pattern. The acquired image is reconstructed from the transmission signal detected by the equipment [68].

STEM (Auriga Compact, Zeiss, Germany) images were obtained to further assess the morphology of the produced nanoparticles, namely MNP@CNC, PDA-NP, DT-NP. For this purpose,

a 0.015 % (w/v) solution of each sample was prepared in ultrapure water. 7 μL of each solution were dropped in TEM grids (Carbon Type B, 400M Cu, Monocomp) and left to dry for 15 minutes, after which excess solution was removed. STEM images were obtained with magnifications of 30-100 kx and with acceleration voltage of 25-30 kV.

2.1.4.3. Fourier Transform Infrared (FTIR)Spectroscopy

Fourier Transform Infrared (FTIR) Spectroscopy is a chemical characterization technique, in which a sample is exposed to IR radiation, absorbing it at specific frequencies that are characteristic of their chemical composition. The obtained IR spectrum translates the excitation of the molecules vibrational modes, thus allowing the identification of functional groups and chemical bonds in the chemical structure of the sample [69].

FTIR spectra were obtained to assess the chemical composition of MNP@CNC, by comparison with the MNPs and CNCs spectra, as well as to confirm the success of the coating strategies of PDA-NP and DT-NP, by comparison with the MNP@CNC spectrum. For this purpose, 150 μL of 0.5 % (w/v) nanoparticle aqueous suspension were dropped on 120 mg of KBr (221864, Sigma Aldrich) placed on a petri dish, which was then left to dry at 70 ˚C for 2 hours. Then, using a manual press (hand press, Pike technologies, Madison, WI), pellets were made from the dried KBr/nanoparticle samples. The Spectra were obtained using an IRPrestige 21 FTIR spectrophotometer (Shimadzu, Japan), within the wavelength range of 400-4000 cm^{-1}, with 32 scans per sample and resolution of 4 cm^{-1}.

2.1.4.4. X-Ray Diffraction (XRD)

X-Ray Diffraction (XRD) is a technique used to determine the crystalline structure of a material. For this purpose, a sample is subjected to an X-ray beam causing its diffraction into specific diffraction angles. By scanning the sample in a range of 2θ angles and assessing the direction of the diffracted beams relatively to the incident X-ray beam, the crystalline structure of the analyzed sample can be deduced [70].

The crystallinity of the produced nanoparticles, namely CNCs, MNP@CNC, PDA-NP and DT-NP, was evaluated by acquiring x-ray diffractometry profiles of 20 mg freeze-dried nanoparticle pellets, over the 2θ range of 10-90° (0.05° scanning step, 2 seconds per step), on a Bruker D8 Advance diffractometer (Bruker, Germany) operating at 40 kV and 40 mA with a Cu Kα X-ray source.

The average crystallite size was calculated according to the Scherrer equation[71] (Equation 2.1),

$$D_{hkl} = \frac{K}{\beta \cos \theta} \qquad \textbf{Equation 2.1}$$

in which, where D_{hkl} is the crystallite size, according to the reflection planes (hkl), K represents the shape factor, here assumed as 0.9, ʎ is the X-Rays wavelength (1.541Å for Cu Kα radiation), Θ is the Bragg's diffraction angle, and β is the full width at half maximum (FWHM) peak intensity.

2.1.4.5. Thermogravimetric Analysis (TGA)

Thermogravimetric Analysis (TGA) is used to characterize a system, such as a compound or a mixture, in terms of variations of physico-chemical properties occurring at high temperatures. In particular, sample weight variations can be measured as a function of temperature, as the latter increases over time. Thus, TGA can be used to quantify the content of different compounds within a sample [72].

TGA was performed using a Simultaneous Thermal Analyzer (Hitachi, Japan), in which freeze dried samples of CNCs and MNP@CNCs were subjected to temperatures within a range of 40-600 °C,

at a heating rate of 10 °C/min, using crucibles of platinum as a support, under 1:7 oxygen/nitrogen atmosphere with a flow rate of 200 mL.min^{-1}. Sample weight at 105 °C (after residual moisture evaporation) was taken as reference for residual mass calculation after thermal degradation.

2.1.4.6. Vibrating Sample Magnetometer (VSM) Studies

Vibrating Sample Magnetometer (VSM) is an instrument used to quantify the magnetic properties of materials, in which a sample is magnetized under a uniform magnetic field and then vibrated perpendicularly to that same field. Consequently, an oscillating magnetic field is created by the vibrating sample, which induces a voltage in stationary detection coils that is proportional to the magnetic moment of the sample [73].

The magnetic properties of the produced magnetic nanoparticles, that is, of MNPs, MNP@CNCs and coated MNP@CNCs, were evaluated using a superconducting quantum interference device (SQUID-VSM) magnetometer (Quantum Design, USA). Thus, 10 mg of each sample were freeze-dried and analysed under a magnetic field up to 20 kOe, at room temperature.

2.2. Fabrication of 3D textile electrospun scaffolds

The scaffolds herein proposed were fabricated using a system (Figure 2.7) developed by Laranjeira *et al.*, 2017 [35]. As stated in the previous chapter, this system allows the production of CANTs, constructs designed to replicate the structural organization of collagen fibres, while also ensuring their scalable and tuneable production, specifically regarding their dimensions. Moreover, the fibre threads were also assembled into yarns (Figure 2.7) to study the influence of magnetic stimulation of the material at a higher length scale of the tendon-like hierarchical structure.

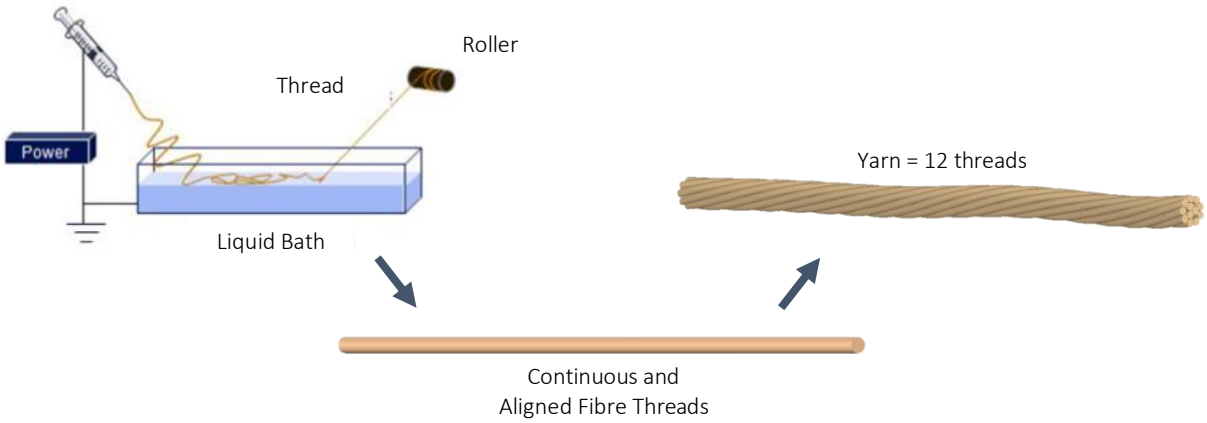

Figure 2.7. Schematic illustrating the steps involved in the fabrication of 3D textile electrospun scaffolds. On the left is illustrated the electrospinning setup (adapted from ref [35]) used to produce continuous and aligned fibre threads of PCL and in which the produced nanoparticles were incorporated. Twelve threads were then twisted into a yarn to replicate the hierarchical structure of the tendon ECM.

For tendon TE applications, previously developed electrospun constructs were based on a synthetic/natural polymer blend of PCL and chitosan, reinforced with CNCs, due to their mechanical performance being comparable to that of native tendons [33,35]. The incorporation of chitosan is beneficial for cell attachment and proliferation, however its processing for electrospinning purposes is more complicated than that of PCL and other synthetic polymers and the particular system developed in the previous study does not allow to incorporate the magnetic particles here developed. As chitosan needs to be dissolved in acid solutions [74], in the scope of this project that is far from ideal since acid solvents

would also dissolve any iron oxide nanoparticle adsorbed in the CNCs surface. Thus, continuous fibre threads were based solely on PCL and reinforced with DT-NP.

2.2.1. Poly(ε-caprolactone) (PCL)

Poly(ε-caprolactone) (PCL) is one of the most commonly used synthetic polymers for biomedical applications and, in particular, for electrospinning purposes. PCL is a linear aliphatic polyester (Figure 2.8) with a semicrystalline structure, composed of repeating units of hexanoate [75]. This polymer is hydrophobic and therefore soluble in a multitude of different organic solvents, such as chloroform, dichloromethane and dimethylformamide [66,75,76].

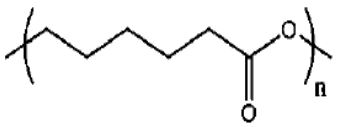

Figure 2.8. Chemical structure of Poly(ε-caprolactone) (PCL). Adapted from ref [66].

The current interest behind the extensive application of PCL within the biomedical field is due to its biocompatibility, low melting point, superior viscoelastic properties, excellent blend-compatibility, high processing versatility and relative low-cost in comparison with other synthetic polymers [66,76,77]. Moreover, PCL exhibits a slow *in vivo* degradation rate, spanning from several months to several years, depending on its molecular weight, degree of crystallinity and degradation environment [75–77]. PCL degradation occurs as a two-step process: first, water diffusion causes degradation of the amorphous regions due to ester bond cleavage, thus resulting in a decrease of the molecular weight and an increase of the crystallinity; then, the crystalline domains suffer hydrolytic degradation until the molecular weight is decreased enough to allow intracellular degradation [75–77]. Many TE applications demand scaffolds possessing higher degradation rates, however for tendon TE strategies the low degradation rate of PCL may be beneficial given the slow healing process of these tissues [1,11].

As mentioned previously, the grafting of hydrophobic 1-DT onto the magnetic nanoparticles surface aims at improving their compatibility with the scaffolds PCL hydrophobic matrix, as well as their dispersion in the organic solvents that are generally used to dissolve PCL for electrospinning procedures.

2.2.1.1. Preparation of electrospinning solutions

The PCL/DT-NP solutions for electrospinning were prepared with 17% (w/v) PCL and 2.5, 5 or 7.5 wt.% DT-NP (PCL/DT-NP2.5, PCL/DT-NP5 and PCL/DT-NP7.5, respectively). Depending on the necessary volume for electrospinning purposes, the intended amount of DT-NP was dispersed in DMF (Thermo Fisher Scientific, USA) and THF (AppliChem, Germany) solution (1:1 (v/v) ratio DMF/THF) and subjected to 3 sonication cycles of 1 min each using an Ultrasonic Processor (VCX-130PB-220, Sonics, USA) at 40% amplitude output. PCL was added to the MNP@CNC suspension, which was then left stirring at room temperature for 3-4h, until PCL was completely dissolved. Prior to use, the solution was again subjected to 3 sonication cycles of 1 min each, under ice bath to prevent overheating, to ensure the proper dispersion of all components.

PCL solutions without nanoparticle addition were prepared following similar procedures to ensure that all samples are subjected to the same treatments, prior to electrospinning.

2.2.2. Production of PCL/DT-NP constructs

2.2.2.1. Fabrication of PCL/DT-NP continuous fibre threads

As mentioned previously, continuous fibre threads were produced using a customized electrospinning system (Figure 2.7) developed by Laranjeira *et al.,* 2017 [35]. The electrospinning solution was loaded into a syringe with a 21G needle and connected with a syringe pump to control the solution flow rate during the spinning process. A high voltage power supply was used to create an electric field between the needle (positive electrode) and a grounded water/ethanol liquid bath (8:2 (v/v)). This bath was placed directly below the spinning needle, at 14 cm from the surface of the liquid bath. A roller was used to pull the produced threads (Figure 2.7) from the liquid bath and was placed 20 cm away from the needle. Additionally, threads with randomly oriented fibres were fabricated, as a negative control for the fibre alignment, by placing the roller 16 cm away from the spinning needle.

The electrospinning solution was jetted at constant flow rate (0.4 mL/h) towards the liquid bath and under a voltage of 9 kV. The produced fibre threads were pulled by the roller at constant speed and collected at room temperature (24 ± 2ºC) and at 45-50 % humidity.

2.2.2.2. Assembly into yarns and scaffolds

The produced fibre threads were then assembled into yarns (Figure 2.7), as described by Laranjeira *et al.,* 2017 [35], in which the mechanical and biological performance of the proposed strategy was assessed. Each yarn is formed by 12 threads twisted together at 4 turns/cm. Additionally, the produced yarns were woven into scaffolds as previously described [35], thereby creating higher 3D hierarchical constructs in which the potential to induce tenogenic differentiation and matrix production was assessed.

2.2.3. Characterization of the produced nanofibre threads

In this section, the methods through which the produced nanofibre threads were characterized in terms of morphological and physical properties, as well as the preparation of the respective samples, are presented.

2.2.3.1. High-Resolution Field Scanning Electron Microscopy (SEM)

High-Resolution Field Scanning Electron Microscopy (SEM) is an imaging technique in which the surface of a sample is scanned by an electron beam, that is accelerated by a high electrical potential in a high vacuum environment. SEM images result from the electron signal detected at each pixel, that is generated by the sample in response to the electron beam scanning [78].

SEM (JSM-6010LV, JEOL, Japan) was used to assess the morphology, alignment and dimensions of the electrospun CANT. For this purpose, the fibre threads were mounted on SEM stubs (TAAB, UK) using coverslips (13 mm, Sarstedt, Germany) to prevent collapsing of the fibres resultant of taping the threads to the stubs. The specimens were previously coated with approximately 2 nm of platinum (Cressington, UK) and images were collected with different magnification (500-5000 x) and acceleration voltage at 10 kV.

2.2.3.2. Directionality Analysis

Fibre alignment in the produced threads was assessed through the directionality plugin (https://imagej.net/Directionality) from ImageJ (version: 1.51f, NIH, USA). For this purpose, SEM

images of CANT were converted to 8-bit grayscale, then cropped to 450 by 450 pixels and their contrast enhanced to 0.5 % pixel saturation. Directionality histograms were generated to translate the amount of structures in the image along an angle of orientation (-90 – 90º). Histograms of each condition (n=3) were fitted with a Gaussian function using Origin Lab software (version: 9.0.0, OriginLab Corporation, USA). To assess nanofibre alignment, the height and full width at half maximum (FWHM) of the peaks from each condition was evaluated. The quality of the fitting was evaluated according to the value of Adjusted R^2, which ranges from 0, indicating a poor fit, to 1, indicating a good fit. For an average R^2 lower than 0.75, the FWHM of the peak was considered 180º, meaning the lack of any preferential domains of alignment.

2.2.3.3. Assessment of the Mechanical Properties of Yarns

Mechanical properties of yarns fabricated with and without DT-NP were assessed using a universal mechanical testing machine (5543, Instron, UK) equipped with a 1kN load cell. 3 cm long specimens of each yarn were cut and two of these were fixed in square paper frames with a 1x1 cm window, making sure the yarns are straightened and not touching each other. These were then mounted onto the tester grips at a gauge length of 1 cm. Before testing, the paper frames were cut laterally, and the test was performed at a crosshead speed of 10 $mm.min^{-1}$. Prior to testing, images from each specimen were acquired with an optical microscope (Stemi 2000-C, Zeiss, Germany) for cross-sectional area calculations. Cross-sectional area was estimated from yarn diameter measurements at three different locations along the length of the specimen, which were obtained using ImageJ software. Moreover, the frames were placed in vacuum overnight to remove any residual solvent and to assure uniform testing conditions.

From the data acquired during the tensile tests, several parameters were calculated using MATLAB software (R2015b, MathWorks, USA). For this purpose, the stress-strain curve of each specimen was drawn until its breakpoint. Young's modulus was determined by linear regression of the linear region of the stress-strain curves. Yield Stress and Strain were estimated by tracing a line parallel to the linear region, with a 0.5 % strain offset. The coordinates of the intersection of this line with the stress-strain curve correspond to the yield strain and yield stress of the specimen, respectively. Ultimate tensile strength was determined by calculating the maximum of the stress-strain curve, while the Strain at Break was determined by identifying the strain value corresponding to the breakpoint. The respective MATLAB script can be found in the Appendix section (FigureA.1).

2.2.3.4. Vibrating Sample Magnetometer (VSM)

Similarly to the method used for the magnetic nanoparticles (section 2.1.4.6), the magnetic properties of the PCL/DT-NP2.5 and PCL/DT-NP5 yarns were evaluated under a magnetic field up to 20 kOe, at room temperature.

2.3. Assessment of the biological performance of electrospun scaffolds

Considering the mechanical and magnetic properties of the different formulations, PCL/DT-NP5 yarns were selected as representative building blocks of 3D scaffolds to assess the biological performance of magnetically actuated constructs. hASCs were seeded onto individual yarns and cultured under magnetic stimulated conditions for up to 21 days, to assess their potential to induce and boost tenogenic differentiation (Figure 2.9). Cells seeded on yarns were also cultured in static nonstimulating conditions as an experimental control. Cultured constructs were investigated over time for cell metabolic activity, for activation of mechanotransduction pathways and for tenogenic

differentiation by immunocytochemistry. Moreover, real time RT-PCR analysis of tendon and nontendon specific markers and of inflammatory cytokines was performed.

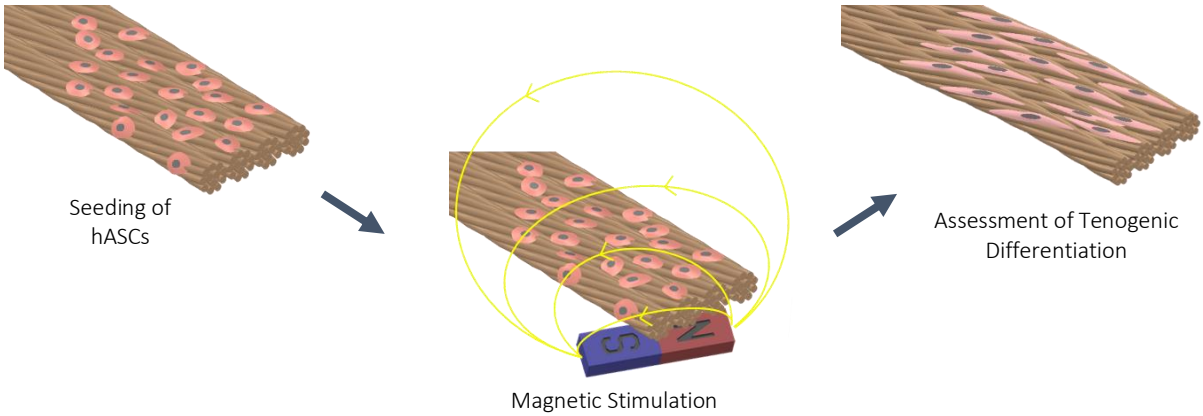

Figure 2.9. Schematic illustrating the steps involved in the assessment of the biological performance of electrospun scaffolds. Human Adipose Stem Cells (hASCs) were seeded onto the electrospun nanofibre yarns under magnetic stimulation conditions to assess the scaffolds ability to induce tenogenic differentiation of stem cells.

Additionally, hASCs were seeded onto woven scaffolds of PCL/DT-NP5 and cultured under magnetic stimulated conditions for 21 days. Cultured scaffolds were investigated for tenogenic differentiation and tendon-like ECM deposition by immunocytochemistry.

2.3.1. Cell Sources

All biological studies were performed using cells isolated from human adipose tissue sources, obtained under previously established protocols with Hospital da Prelada (Porto) and with informed consent of the patients. The content of the written informed consent and related procedures were reviewed and approved by the Hospital Ethics Committee.

2.3.2. Isolation of hASCs

HASCs were isolated from tissue samples and cultured as previously described [79,80], and have been previously characterized by RT-PCR for CD44, STRO-1, CD105 and CD90 markers [79]. First, the tissue was rinsed in phosphate-buffered saline (PBS, Life Technologies, USA) containing 10 % (v/v) of an antibiotic-antimycotic solution (A/A) (Thermo Fisher Scientific, USA). Then, the fat solution was immersed in a 0.05 % collagenase type II (C6885, Sigma-Aldrich, USA) solution for 45 min at 37º C under mild agitation. The digested tissue was centrifuged at 800 G for 10 min at 4 º C, after which the supernatant was discarded. Finally, cells were expanded in basic culture medium composed of α-minimal essential medium (α-MEM; Life Technologies, USA) supplemented with 10% Fetal Bovine Serum (FBS, Life Technologies, USA) and 1 % A/A solution (Life Technologies, USA).

2.3.3. Cell Seeding onto electrospun yarns and scaffolds

Prior to cell seeding, the yarns were mounted onto CellCrown inserts (Sigma-Aldrich, USA) and sterilized by immersion in 70 % ethanol for 1 h. The woven scaffolds were sterilized in the same way by immersion in 70 % ethanol for 1 h. Then, samples were washed 4 times with PBS (Life Technologies, USA), to remove the remaining ethanol and immersed in basal culture medium composed of α-MEM (Thermo Fisher Scientific, USA) supplemented with 10 % FBS (Thermo Fisher Scientific, USA) and 1 % A/A solution (Thermo Fisher Scientific, USA) for 1h to improve cell attachment. hASCs were seeded at a density of $5x10^4$ cells onto each yarn and of $15x10^4$ cells onto each scaffold and

incubated overnight to allow cell adhesion. Samples were then transferred to a new plate and fresh culture medium was added to each well. Experiments were conducted under static (control group) and magnetic stimulating conditions (oscillation frequency of 2 Hz and 0.2 mm of displacement) in a magnefect nano device (nanoTherics Ltd, UK) composed by an oscillating magnet array system (0.35 T per magnet per sample) for 21 days, as described by Gonçalves *et al.*, 2016 [48].

2.3.4. Biological Characterization of cell constructs

2.3.4.1. Cell Viability by MTS Assay

The MTS assay (3-(4,5-Dimethylthiazol-2-yl)-5(3-carboxymethonyphenol)-2-(4-sulfophenyl)-2H-tetrazolium, inner salt) is a colorimetric method to determine the amount of viable cells. MTS is reduced to a water-soluble brown coloured formazan product by the mitochondria of viable cells. By measuring the absorbency at 490 nm, the number of viable cells can be estimated [81].

Cell metabolic activity of hASCs was evaluated by MTS assay (CellTiter 96® AQueous One Solution Cell Proliferation Assay, Promega, USA) after 11 and 21 days of culture. Constructs were rinsed in PBS and then incubated in a mixture of FBS-free culture medium without phenol red and MTS solution (5:1 ratio) for 3 h, at 37 °C and 5% CO_2 atmosphere. Then, 100 µL of each sample was transferred to a new 96-well plate and the absorbance read at 490 nm (Synergy HT, Bio-TeK Instruments, USA). The absorbance of each sample was measured in triplicates and blank readings were performed for correction purposes.

2.3.4.2. mRNA extraction and real-time RT-PCR

Polymerase-Chain Reaction (PCR) is an *in vitro* method commonly used to evaluate gene expression in tissues by detecting and quantifying a specific DNA or RNA segment [82]. For this purpose, messenger RNA (mRNA), which is transcribed from DNA to code specific proteins, is extracted from the cells and complementary DNA (cDNA) is synthetized according to the former with reverse transcriptase [83]. Specific primers and a fluorescent dye are combined with cDNA and as it is being amplified , the fluorescence is evaluated for relative quantification of specific genetic markers [82]. The level of fluorescence is proportional to the expression of genes.

Total RNA was extracted from the constructs using TRI reagent (VWR, USA) according to the manufacturer's instructions. RNA quantity and purity were determined with a NanoDrop ND-1000 spectrophotometer (NanoDrop, ThermoScientific, USA). The cDNA synthesis was performed with the qScript cDNA Synthesis kit (Quanta Biosciences, USA) and using the Mastercycler Realplex (Eppendorf, Germany) with a total RNA of 1 µg in a volume of 20 µL. The quantification of the transcripts was carried out by quantitative polymerase chain reaction (qPCR) using the PerfeCTA SYBR Green FastMix kit (Quanta Biosciences, USA) following the manufacturer's protocol, in a Real-Time Mastercycler Realplex thermocycler (Eppendorf, Germany). The primers were pre-designed with PerlPrimer v1.1.21 software (Table 2.1) and synthesized by MWG Biotech. GAPDH (glyceraldehyde-3-phosphate dehydrogenase) was used as the housekeeping gene. The $2^{-\Delta\Delta Ct}$ method was selected to evaluate the relative expression level for each target gene [84]. All values were first normalized against GAPDH values, and then to hASCs cells collected at day 0.

2.3.4.3. Immunofluorescence

Immunofluorescence is a biological assay in which antibodies and fluorescent molecules are used to detect biomolecules, such as proteins, in cells and tissues. First, a primary antibody is used to

Table 2.1. Primers used for real-time RT-PCR.

Target	NCBI reference	Sequence 5' - 3'
ACTB	AK223055	F: CTGGAACGGTGAAGGTGACA R: AAGGGACTTCCTGTAACAA
COL1A1	NM_000088.3	GCCAAGACGAAGACATCCCA GGCAGTTCTTGGTCTCGTCA
COL3A1	NM_000090.3	CCTGAAGCTGATGGGGTCAA CAGTGTGTTTCGTGCAACCAT
DCN	NM_001920.4	CACAAGTTTCCTGGGCTGGA AGATGGCATTGACAGCGGAA
SCX	NM_001080514.2	CAGACGGACGTACAGACAGG CAGCGCAGAAAGTTCCAGTG
TNC	NM_002160.3	ACTGCCAAGTTCACAACAGACC CCCACAATGACTTCCTTGACTG
TNMD	NM_022144.2	CCGCGTCTGTGAACCTTTAC CACCCACCAGTTACAAGGCA
IL4	NM_000589.3	GCACCGAGTTGACCGTAACA AGGAATTCAAGCCCGCCAG
IL6	NM_000600.4	AGGAGACTTGCCTGGTGAAA GCATTTGTGGTTGGGTCAG
IL10	NM_000572.2	AAGACCCAGACATCAAGGCG AATCGATGACAGCGCCGTAG
COX2	NM_000963.3	ATGGGGTGATGAGCAGTTGT GAAAGGTGTCAGGCAGAAGG
ACAN	NM_013227.3	TAGAGTCCTCAAGCCTCCTGT TGGTCTGCAGCAGTTGATTC
RUNX2	NM_001024630	TTCCAGACCAGCAGCACTC CAGCGTCAACACCATCATTC

bind to a specific antigen of interest. Then, a fluorescent-labelled secondary antibody, from the same species used to produce the primary antibody, binds to the primary antibody enabling the detection of that biomolecule under fluorescence microscopy [85].

For this purpose, at 11 and 21 days, hASCs constructs were rinsed with PBS and fixed with 10% neutral buffered formalin (Thermo Fisher Scientific, USA) prior to the detection of YAP/TAZ (SC-101199, SantaCruz Biotechnology, USA), Scleraxis (SCX, ab58655, Abcam, UK) and Tenomodulin (TNMD, SC-49324, Santa Cruz Biotechnology, USA) in yarns and TNMD and Type I Collagen (COL1A1, ab90395 Abcam, UK) in scaffolds. After cells permeabilization with 0.1 % Triton X-100/PBS (Thermo Fisher Scientific, USA) solution, for 20 min at room temperature, and washing with PBS, samples were blocked with RTU Normal Horse Serum (RTU Vectastain Kit, PK-7200, Vector, USA) for 40 min. Then, cells were incubated overnight with primary antibodies against YAP/TAZ, Tenomodulin, Scleraxis and Type I Collagen, diluted in antibody diluent with background reducing components from Dako (Dako, USA) at 4 °C. Samples were then rinsed in 0.1 % Triton X100/PBS (Thermo Fisher Scientific, USA) solution followed by incubation for 1 h at room

temperature with the respective Alexa fluor 488 (Invitrogen, USA) considering the host species of the primary antibodies. Samples were stained with DAPI (4,6-Diamidino-2-phenyindole, dilactate, 5 μg/μL, 40009, VWR, USA) for 10 min and with Phalloidin (Phalloidin-Tetramethylrhodamine B isothiocyanate, 424203, BioLegend, USA) for 20 min for cell nuclei and cytoskeleton labelling, respectively. Immunolabeled samples were analysed by confocal laser scanning microscopy (Leica TCS SP8, Microsystems, Wetzlar, Germany).

2.3.4.4. Cytoskeleton Organization

Cell alignment was assessed according to a similar method as the one previously described for analysing PCL nanofibre alignment (Section 2.1.1.1.). Thus, using the directionality plugin from ImageJ, confocal microscopy images were converted to 8-bit greyscale and their contrast was enhanced to 0.1 % pixel saturation. Directionality histograms were generated to translate the amount of structures in the image along an angle of orientation (-90 – 90º). Histograms of each condition (n=5) were fitted with a Gaussian function using Origin Lab software. To assess actin filament organization, the height and FWHM of the peaks from each condition was evaluated.

2.3.4.5. YAP/TAZ Quantification

The ratio of nuclear/cytoplasmatic YAP/TAZ in cells cultured for 11 days was assessed by calculating the intensity of the nuclei and of the respective cytoplasm in confocal microscopy images ($n > 6$). For this purpose, ImageJ was used to adjust image brightness and contrast and remove the resulting outliers, followed by image segmentation using MATLAB software. Finally, the nuclear/cytoplasmatic YAP/TAZ ratio was obtained by dividing the intensity of the segmented nuclei by the intensity of the segmented cytoplasm. The respective MATLAB script can be found in the Appendix section (FigureA.2).

2.4. Statistical Analysis

Statistical analysis of data was performed using GraphPad PRISM version 6.01. One-way analysis of variance (ANOVA) was performed in normal distributed populations and the Kruskal-Wallis non-parametric test was performed otherwise, both followed by Tukey post hoc test for multiple comparisons, unless specified otherwise. Analogously, unpaired t test was performed to compare two normal distributed populations. The statistical significance was set to $p<0.05$ and results are presented as mean ± standard deviation.

Chapter 3. Results and Discussion

Tendons are load-bearing mechanosensitive tissues and, as such, scaffolds envisioned to aid in their regeneration should not only mimic the native ECM architecture, but also ensure the biomechanical performance of these tissues in a post-injury setting, while providing mechanical stimulation of cells to guide tissue remodelling. The strategy herein proposed combines CNCs and iron oxide MNPs with a biomimetic scaffold, thereby simultaneously reinforcing its mechanical properties and endowing it with magnetic responsiveness to be able to be remotely actuated to mechanically stimulate cells.

3.1. Characterization of magnetic nanoparticles

The morphology and dimensions of the produced nanoparticles was assessed through AFM and STEM (Figure 3.1). CNCs produced through sulfuric acid hydrolysis (Figure 3.1A) presented the characteristic rod-shape[34,53] with 216.5 ± 71.4 nm length and 4.3 ± 1.7 nm height. MN@CNC (Figure 3.1B) obtained through co-precipitation of Fe^{2+} and Fe^{3+} in the presence of CNCs show spherical MNPs attached to the CNCs, indicating successful adsorption of the iron oxide nanoparticles. As previously mentioned, MNP@CNC were coated with thin layers of PDA and further grafted with 1-DT to simultaneously improve their chemical and colloidal stability as well as their interface compatibility with the scaffold polymer matrix. Figure 3.1C shows that the nanoparticles morphology is maintained after the coating and that, although a few particle aggregates can be noticed, DT-NP are well dispersed and individualized. Moreover, STEM analysis (Figure 3.1D) indicates that the coating involves both CNCs and MNPS as the images show the coating in grey surrounding both the CNCs and the anchored MNPs here displayed in black.

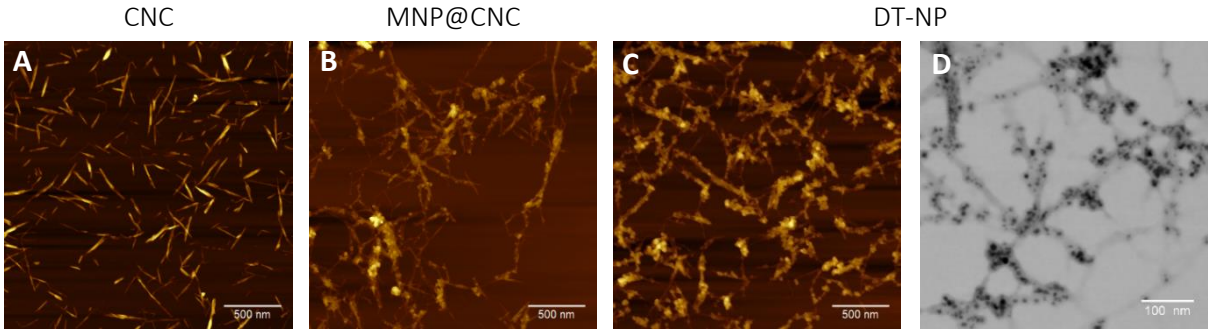

Figure 3.1. Morphology of the produced nanoparticles. AFM images of CNCs (A), MNP@CNCs (B) and of DT-NP (C) (scale bar 500nm); STEM image of DT-NP (D) (scale bar 100nm).

FTIR Spectroscopy (Figure 3.2A and B) was performed to study the chemical composition of the nanoparticles as well as to confirm the successful building of the coating layers. CNCs spectrum displays characteristic peaks of cellulose at 3347 and 2900 cm^{-1} (–OH and –CH stretching, respectively) (Figure 3.2A.i), 1163 cm^{-1} (C-O-C stretching), 1113, 1059 and 1034 cm^{-1} (C-OH stretching) (Figure 3.2Aii) [56]. MNP spectrum exhibits the characteristic iron oxide absorption peak at 583 cm^{-1} (Figure 3.2Aiii) corresponding to the Fe-O vibrational frequencies [55]. Consequently, MNP@CNC spectrum shows characteristic peaks of both cellulose and iron oxide confirming the formation of iron oxide nanoparticles on the CNCs surface. Regarding Figure 3.2B, the success of the PDA coating in PDA-NP was translate in the appearance of the polydopamine characteristic bands appearing at 1612, 1501 and at 1280 cm^{-1} (Figure 3.2Bv), due to N-H bending in the primary amine, C=C phenylic stretching and stretching of the phenolic OH (C-O), respectively [62,86]. Finally, the functionalization of PDA-NP with dodecanethiol was confirmed by two well defined peaks at 2920 and 2848 cm^{-1} (Figure 3.2Biv), due to CH_2 stretching from the long alkyl chain of Dodecanethiol [65,86] appearing only in the DT-NP spectrum.

The identity of the nanoparticles crystalline phase was assessed through XRD (Figure 3.2C). The CNCs diffractogram shows characteristic peaks at 2θ = 15.4°, 15.9°, 22.7° corresponding to the 1-10, 110 and 200 crystalline reflection planes, respectively [56]. The MNP@CNC diffractograms are dominated by the characteristic peaks of magnetite (Fe_3O_4) nanoparticles at 2θ = 30.2°, 35.7°, 43.3°, 53.7°, 57.3°, 62.8°, corresponding to the (220), (311), (400), (422), (511) and (440) reflection planes respectively [56], along with the highest intensity peak of CNC at 22.7°, confirming the presence of iron oxide MNPS on the CNCs surface. On the other hand, the diffractogram of coated MNP@CNC exhibit a similar pattern to that of bare MNP@CNC which indicates that the coating strategies did not impact the nanoparticles crystallinity. Additionally, the crystallite size of the anchored MNPs was calculated through Scherrer's equation[71] using the magnetite peaks corresponding to the (311) and (400) reflection planes (Table 3.1), from which the estimated MNPs size was 7.41 ± 0.45 nm of diameter.

TGA was performed to evaluate the amount of MNPs adsorbed onto the CNCs (Figure 3.2B). The CNC degradation profile exhibits two distinct phases: the first, in the range of 100–300 °C, is attributed to residual moisture and scission of sulphate groups from the CNCs surface; from around 300 °C on, there is degradation of cellulose [56]. Given the organic nature of CNCs, the sample was fully degraded, with 0.36 % of the initial mass remaining after analysis. Analogously, the MNP@CNC degradation profile also presents two steps, as well as superior thermal stability in comparison with the CNCs due to the incorporation of iron oxide nanoparticles, which are thermodynamically stable at temperatures superior to 570 °C [55,56]. From the thermographs in Figure 3.2B, the content of magnetic material in MNP@CNC was estimated to be 32.38 wt.%, considering the remaining weight of the sample consists only in inorganic material.

Finally, the magnetic properties of the nanoparticles were assessed through VSM studies (Figure 3.2C). Bare iron oxide MNPs present high magnetization of saturation (Ms), usually higher than 40 emu/g depending on particle size [55,87,88]. After anchoring on CNCs, there is a decrease in the particles Ms due to the lower magnetic content of the particles [89]. Results indicated that the produced MNP@CNC have a Ms of 18.2 emu/g. Although lower than expected, previously developed MNP@CNC have shown higher Ms values due to a higher magnetic content (~50 wt.%) and larger adsorbed MNPs (18–30 nm) [56]. The magnetization of saturation of MNP@CNC decreased to 11.1 emu/g after polydopamine coating [90] and then to 8.4 emu/g after grafting with 1-DT, given the decrease in the magnetic material content in the nanoparticles. The low coercivity (intensity of the magnetic field required to reduce the magnetization of the material to zero after saturation), the absence of distinct hysteresis loops and of remanence (magnetization remaining in the absence of a magnetic field, after the application of a magnetic field capable of inducing saturation) confirm the superparamagnetic behaviour of these nanoparticles.

3.2. Characterization of electrospun fibre constructs

To fabricate electrospun constructs displaying magnetic responsiveness, DT-NP were added to a 17 % PCL solution. For this purpose, different nanofiller contents (0 – 7.5 wt.% DT-NP) were tested in order to simultaneously maximize the mechanical and magnetic properties of the electrospun threads and SEM was used to assess its influence on the threads morphology (Figure 3.3). There is an overall and significant increase in both thread and fibre diameters with the increase in nanofiller content (Figure 3.3A and C). Higher nanofiller contents lead to increasingly viscous solutions, in which nanoparticles may not disperse homogeneously, thereby generating larger nanofibres. However, the addition of DT-NP to PCL threads only has a more significant impact on these constructs dimensions for concentrations above 2.5 wt%, given the similar dimensions of the PCL and PCL/DT-NP2.5 threads and fibres (Figure 3.3C). Although the quality of nanoparticles dispersion could not be evaluated at high nanofiller concentrations due to their fibre thickness, at 2.5 wt% it shows homogeneous dispersion within the core of the electrospun fibres without apparent aggregates (Figure 3.3B). Moreover, the increase in nanofiller content doesn't impair the spinning of these constructs, as well as its nanofibres alignment, until 7.5

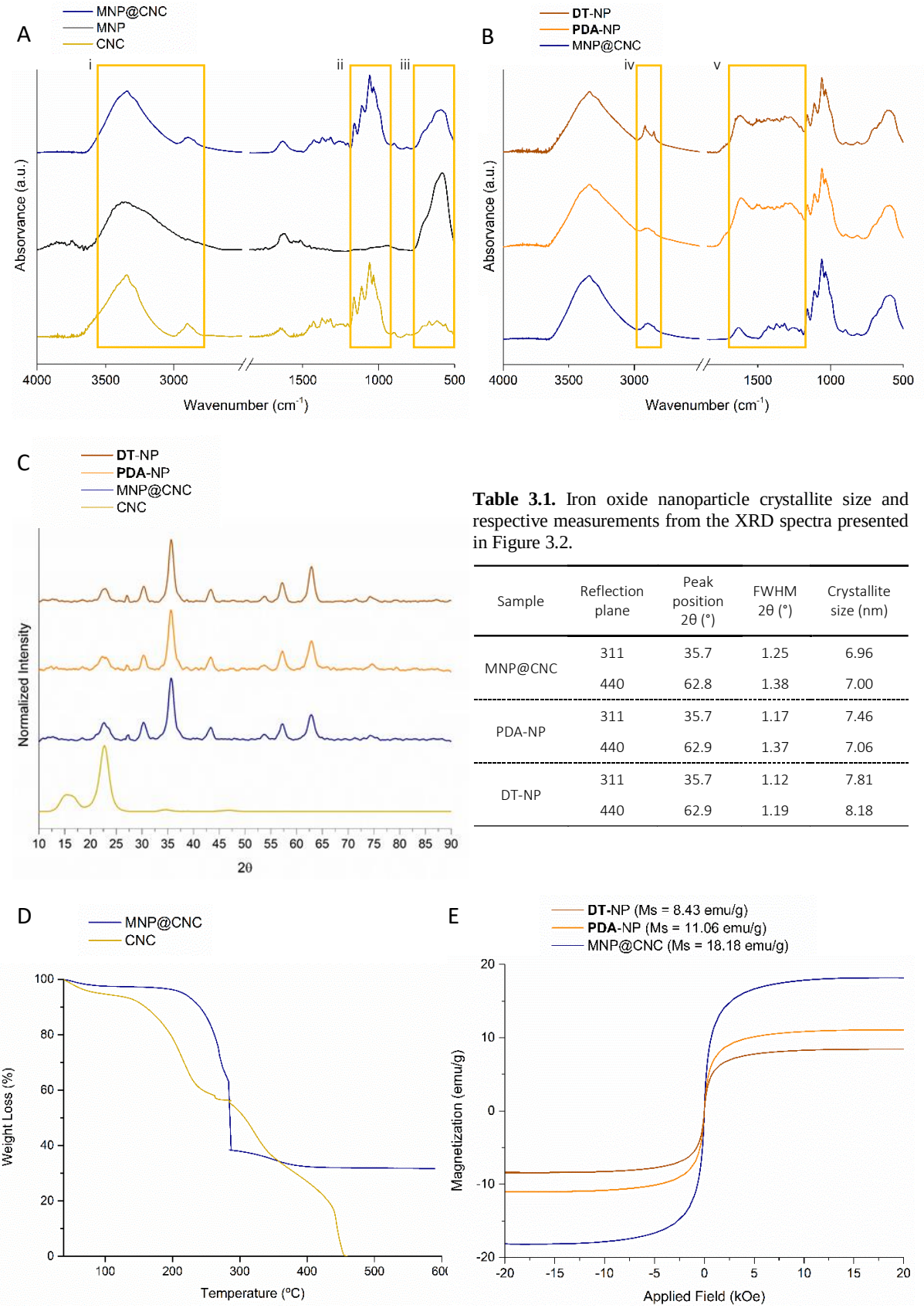

Table 3.1. Iron oxide nanoparticle crystallite size and respective measurements from the XRD spectra presented in Figure 3.2.

Sample	Reflection plane	Peak position 2θ (°)	FWHM 2θ (°)	Crystallite size (nm)
MNP@CNC	311	35.7	1.25	6.96
	440	62.8	1.38	7.00
PDA-NP	311	35.7	1.17	7.46
	440	62.9	1.37	7.06
DT-NP	311	35.7	1.12	7.81
	440	62.9	1.19	8.18

Figure 3.2. Characterization of magnetic nanoparticles. (A) Comparison between the FTIR spectra of neat CNCs and iron oxide MNPs with the MNP@CNC hybrid system spectrum and (B) comparison between the FTIR spectrum of neat MNP@CNC with those of PDA-NP and DT-NP. Yellow squares represent regions of the spectra in which characteristic peaks of the different species can be identified. (C) XRD spectra of CNC, MNP@CNC, PDA-NP and DT-NP. (D) TGA thermograph of CNCs and MNP@CNC. (E) Magnetic hysteresis curves of MNP@CNC, PDA-NP and DT-NP. Magnetization of saturation (Ms) of each sample is shown next to the respective label.

wt% is reached (Figure 3.3A). Electrospinning solutions of 17 % PCL and 7.5 wt.% DT-NP (PCL/DT-NP7.5) were very viscous, which hindered the jetting of the solution during the spinning process [29]. Thus, the high concentration of nanofiller might prevent its homogeneous dispersion in the polymeric solution, resulting in particle aggregation. Both these factors lead to brittle fibre threads with visually variable diameters along their length (Figure 3.3C). As shown in Figure 3.3A, PCL/DT-NP7.5 fibres have low anisotropic alignment and tended to curl within the threads. On the other hand, all the other formulations generated threads of consistent diameters and with smooth, bead-free nanofibres presenting high anisotropic alignment (Figure 3.3A).

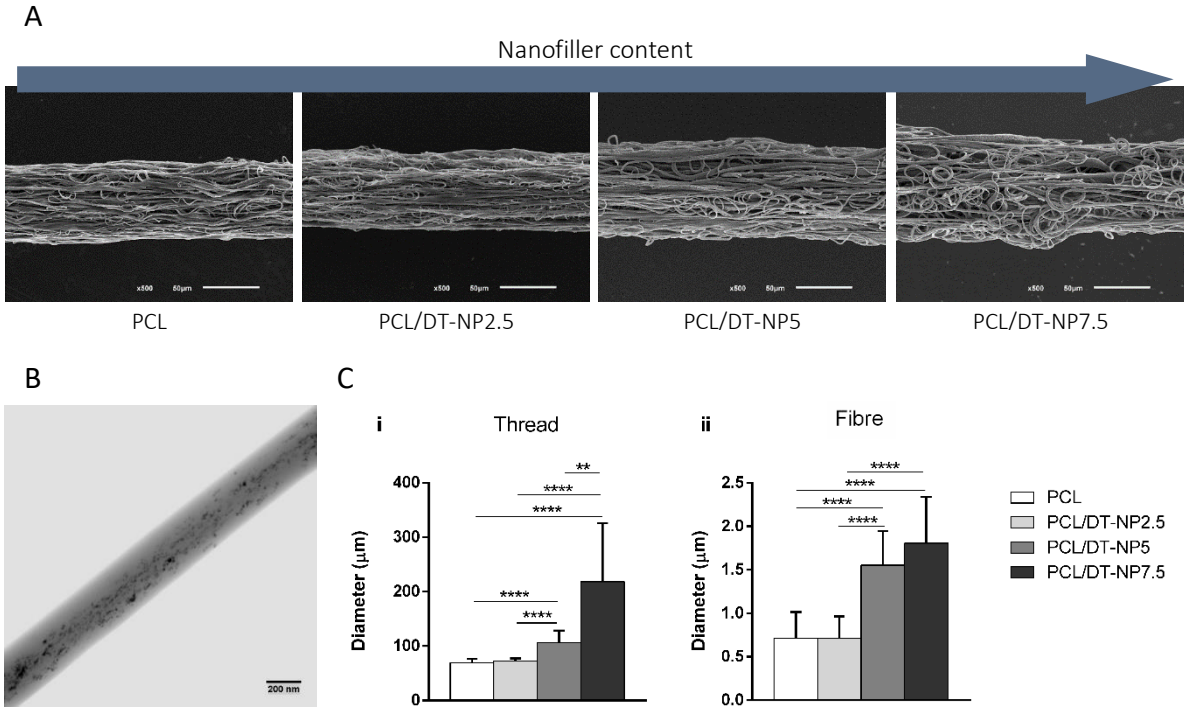

Figure 3.3. Influence of the nanofiller content on the thread and nanofibre diameters of PCL threads. (A) SEM characterization images of PCL threads fabricated with different nanofiller content (0 - 7.5%) under the same spinning conditions (scale bar 50 µm). (B) STEM image of PCL/DT-NP2.5 fibre showing the dispersion of magnetic nanoparticles within the constructs nanofibres (scale bar 200nm). (C)Variation of the diameter of PCL threads (i) and respective fibres (ii) with the increase in nanofiller content (**$p \leq 0.01$****$p \leq 0.0001$).

Thread morphology can be modulated by varying the take-up speed, meaning, the rotation speed of the roller, during the spinning process. An increase in the take-up speed of these constructs leads not only to a higher anisotropic alignment of fibres but also to thinner threads (Figure 3.4A). Threads fabricated through the proposed method presented diameters between 89.22 ± 24.46 and 44.85 ± 8.26 µm for bare PCL, between 127.24 ± 27.10 and 65.13 ± 9.99 µm for PCL/DT-NP 2.5 and between 184.88 ± 39.12 and 62.01 ± 12.27 µm for PCL/DT-NP5. Regarding their fibres, diameters between 1.07 ± 0.28 and 0.71 ± 0.28 µm, 1.15 ± 0.26 and 0.66 ± 0.25 µm and between 1.93 ± 0.39 µm and 1.31 ± 0.44 µm were obtained for threads reinforced with 0, 2.5 and 5 wt% of DT-NP, respectively (Figure 3.4B).

The dimensions obtained for constructs produced with any of the proposed formulations are superior to those of native tendons. Collagen fibrils usually present diameters in the range of 20-150 nm [5,6], and the closest of any of the produced synthetic equivalents was attributed to PCL/DT-NP2.5 nanofibres in threads taken-up at 0.73 cms^{-1}, which presented 600 nm of average diameter. Analogously, collagen fibres usually exhibit diameters in the range of 1-20 µm [5,6], which could not be matched by any of the fabricated constructs, and the smallest threads of each of the formulations were 2-3 times thicker. In this sense, the obtained threads and the corresponding fibres exhibited dimensions closer to

those of native tendon fascicles (150-1000 µm [5,6]) and collagen fibres, rather than those of collagen fibres and fibrils, respectively. The threads with the smallest dimensions, for any of the tested formulations, were fabricated using 0.73 cm.s^{-1} (v5) take-up speed. Interestingly, increasing the speed to 0.86 cm.s^{-1} (v6) lead to an increase in the constructs dimensions. Moreover, at this take-up speed, the threads were more prone to breaking, due to the increase in the speed at which they were being pulled from the support bath.

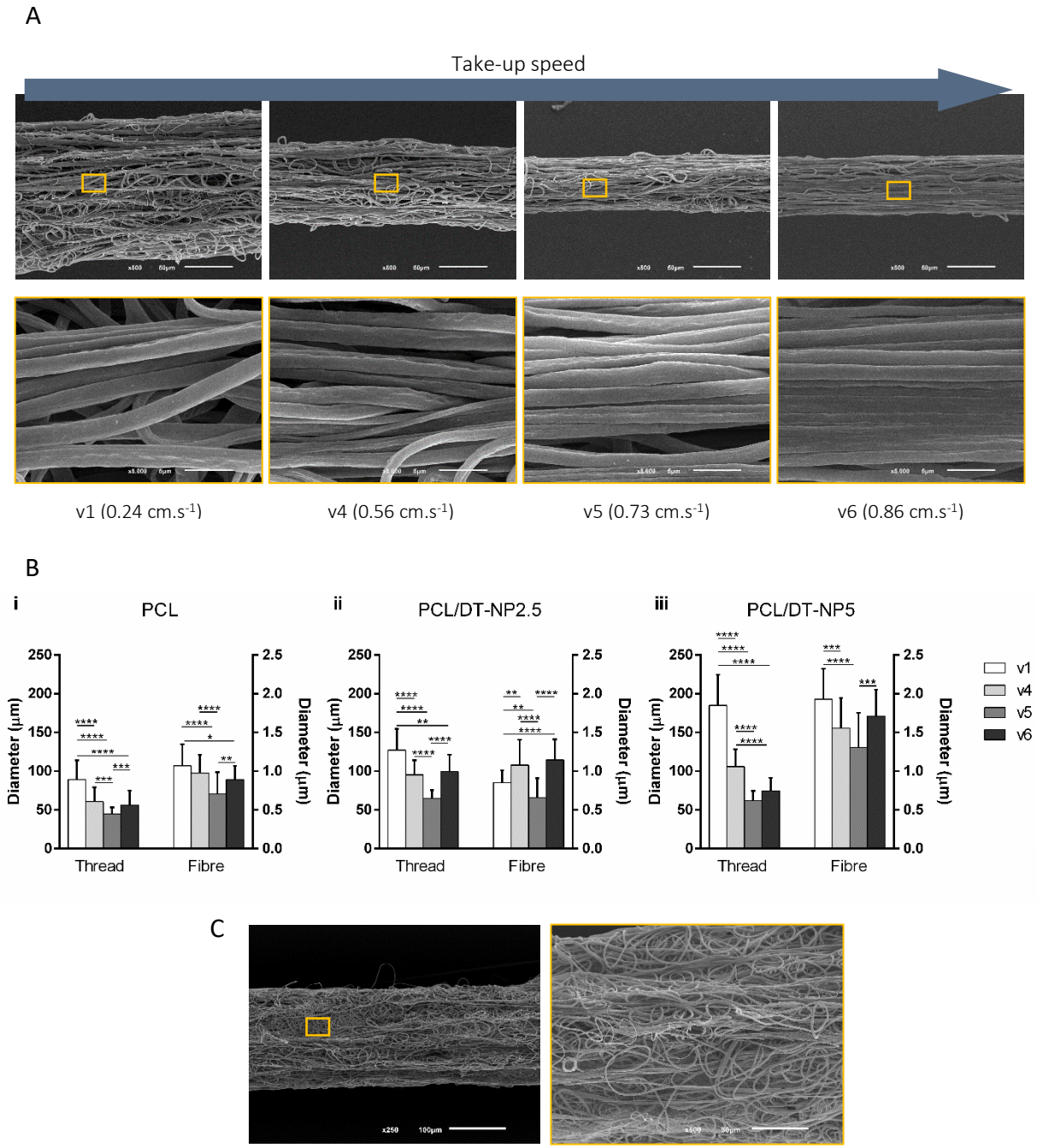

Figure 3.4. Influence of the take-up speed on the thread and nanofibre diameters of PCL threads. (A) SEM characterization images of PCL/DT-NP5 threads fabricated with increasing take-up speed (0.24–0.86 cm.s^{-1}) and respective magnifications. Top row (scale bar 50 µm) demonstrates the effect of take-up speed on the thread diameter, while the bottom row (scale bar 5 µm) highlights the influence on fibre alignment. (B) Variation of the diameter of PCL threads with 0 % (i), 2.5 % (ii) and 5 % (iii) DT-NP and of the respective fibres with the increase in the constructs take-up speed (*p≤ 0.05 **p ≤ 0.01***p≤ 0.001 ****p ≤ 0.0001). Tested speeds were 0.24 cm.s^{-1} (v1), 0.56 cm.s^{-1} (v4), 0.73 cm.s^{-1} (v5) and 0.86 cm.s^{-1} (v6). (C) SEM characterization images of PCL/DT-NP5 thread taken up at 0.24 cm.s^{-1} (v1) and at 16 cm from the spinning needle (scale bar 100 µm). Right image highlights the nanotopography of the threads (scale bar 50 µm).

Nevertheless, the fibres of the produced constructs are within the range of those in previously developed aligned nanofibrous electrospun scaffolds, based of PCL for tendon TE (~ 400 nm to over 1 µm in diameter) [91–95]. Also, the produced threads were generally thinner than previously reported scaffolds with an equivalent structure (~150 µm to ~200 µm) [93,95,96]. Additionally, it has been shown that fabricating electrospun scaffolds comprised of microfibres (~1.40 µm to ~1.80 µm), such as those obtained here from PCL/DT-NP5, rather than nanofibres (~300 nm to ~650 nm) is beneficial to maintain tenogenic phenotype [97,98]. Such behaviour is justified based on the fact that nano sized fibres recapitulate the early stages of tissue repair, in which there is disorganized collagen fibre deposition and scar tissue formation [98], while micron sized fibres resemble the remodelling phase, a later stage of the repair process in which the fibres display a closer diameter and organization to those of healthy tendons [97]. For this reason, microfibrous scaffolds would not only promote higher cell alignment and elongation [97,98], but would also reduce scar-like collagen matrix deposition [97,98], in comparison with nanofibrous scaffolds. Moreover, cells seeded onto microfibres have shown an upregulation of tenogenic markers, such as type I collagen and tenomodulin [97].

Threads comprised of randomly oriented fibres were also fabricated (Figure 3.4C), both as a negative control for fibre alignment and as proof of concept of the development of threads with different degrees of fibre alignment that might be used to develop scaffolds with topographical gradients from random to aligned. Although that not complete within the scope of this study, such concept could be advantageously explored to engineer the tendon-to-bone interface, a complex tissue that has a random to aligned ECM organization [99]. These random threads were obtained by taking up the electrospun fibres at 0.24 $cm.s^{-1}$ (v1) and at 16 cm away from the spinning needle. Reducing the distance between the needle and the roller reduces the distance through which the fibres are pulled and stretched, thereby leading to thicker fibres with low anisotropic alignment. Random PCL/DT-NP5 threads exhibited 213.37± 22.35 µm and 1.83± 0.37 µm for thread and fibre diameter, respectively.

Fibre alignment was evaluated on SEM images of PCL/DT-NP5 (Figure 3.5). For this purpose, directionality histograms of fibres of each condition were calculated and one of each is presented in Figure 3.5A for comparison. Moreover, to quantify the differences between spectra of different conditions, the respective peaks were fitted with a Gaussian function and the average FWHM and height are compared in Figure 3.5B. As shown, there is an increase in the peak height and a subsequent decrease in the FWHM as the take-up is increased, indicating an increase in the anisotropic alignment of fibres, specifically around 0°. As expected, threads taken-up at 0.73 $cm.s^{-1}$ (v5) and 0.86 $cm.s^{-1}$ (v6) exhibited a similar degree of fibre alignment, with those taken-up at 0.73 $cm.s^{-1}$ being slightly more aligned.

For the reasons stated above, threads with aligned topography were, from here on, fabricated using 0.73 cms^{-1} take-up speed (v5) as it leads to the formation of thinner fibres, and therefore thinner threads, with higher degrees of anisotropic alignment. These threads were then assembled into yarns, whose mechanical properties were evaluated in terms of nanofiller content (Figure 3.6Ai-iii). Additionally, random PCL/DT-NP5 threads were produced to assess the influence of fibre alignment on the mechanical properties of these constructs (Figure 3.6Aiv). For this purpose, 12 threads of each condition were twisted together at 4 turns/cm and tensile strain tests were performed in 3 cm long specimens at crosshead speed of 10 $mm.min^{-1}$. Yarns comprised of anisotropically aligned threads displayed 346.93 ± 31.08 µm, 313.08 ± 33.48 µm and 326.45 ± 33.09 µm diameter for 0, 2.5 and 5 wt% DT-NP, respectively, while yarns comprised of randomly oriented fibre threads exhibited 601 ± 37.24 µm diameter. These yarns are intended to mimic the native tendons fascicles that usually exhibit diameters within the range of 150-1000 µm [5,6].

Tensile strain tests revealed that the addition of DT-NP to the constructs had a significant and positive impact on their mechanical properties (Figure 3.6Bi-iii), thereby confirming the reinforcement effect of the CNCs. The Young's modulus increased 98 % (from 10.88 ± 0.96 to 21.55 ± 4.68 MPa, Figure 3.6Bi), the yield strength increased 68 % (from 1.32 ± 0.10 to 2.22 ± 0.29 MPa, Figure 3.6Bii) and the ultimate tensile strength increased 49 % (from 2.84 ± 0.48 to 4.22 ± 0.50 MPa, Figure 3.6Biii)

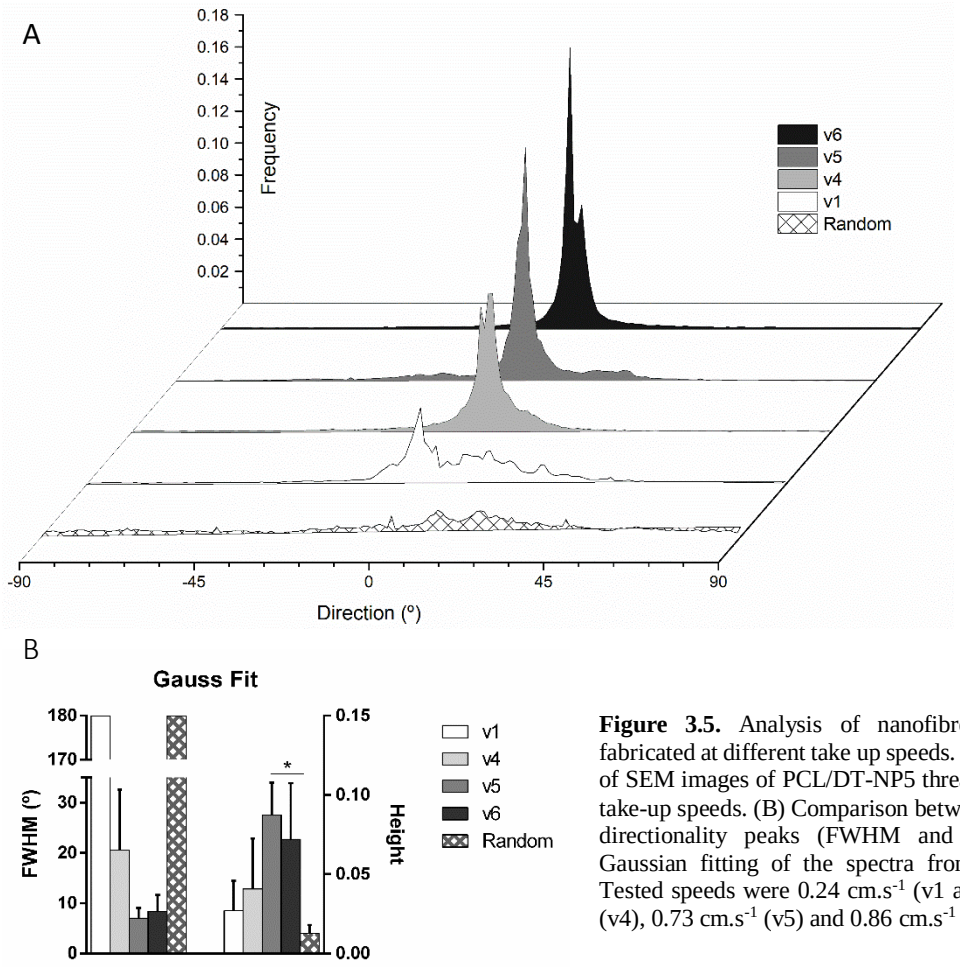

Figure 3.5. Analysis of nanofibre alignment in threads fabricated at different take up speeds. (A) Directionality spectra of SEM images of PCL/DT-NP5 threads fabricated at different take-up speeds. (B) Comparison between the dimensions of the directionality peaks (FWHM and Height) obtained after Gaussian fitting of the spectra from each condition (n=3). Tested speeds were 0.24 $cm.s^{-1}$ (v1 and Random), 0.56 $cm.s^{-1}$ (v4), 0.73 $cm.s^{-1}$ (v5) and 0.86 $cm.s^{-1}$ (v6).

in PCL/DT-NP5 threads in comparison to bare ones. Analogously, yield strain and strain at break increased 7 % (from 0.14 ± 0.01 to 0.15 ± 0.01 mm/mm) and 68 % (from 2.79 ± 0.42 to 4.70 ± 0.51 mm/mm) respectively, in threads of PCL/DT-NP5 in comparison to bare ones (Figure 3.6Bii-iii).

Aligned PCL/DT-NP5 yarns displayed Young's modulus and ultimate tensile strength within the lower range of native tendons tensile properties (20-1200 MPa and 5-100 MPa, respectively [9]). Their yield strain, although just 0.15 ± 0.01 mm/mm (Figure 3.6Bii), that is 15 % strain, is adequate for tendon TE applications given that native tissues physiological range is 4 % strain [8]. On the other hand, randomly oriented threads of the same material exhibited Young's modulus (7.56 ± 0.48 MPa, Figure 3.6Biv) and ultimate tensile strength (1.07 ± 0.12 MPa, Figure 3.6Bvi) 3-4 times inferior to those of their aligned counterpart, thereby emphasizing the importance of fibre alignment to the mechanical properties of the constructs. Interestingly, the yield strain of the random threads (0.24 ± 0.01 mm/mm Figure 3.6Bv) was significantly superior to that of aligned threads. Unlike anisotropically aligned fibres, that are generally stretched, randomly oriented fibres tend to curl within the threads and, as such, their higher yield strain over aligned threads may be attributed to the uncoiling of the fibres rather than to their actual stretching.

The characteristic stress-strain curves of PCL constructs with different nanofiller contents are shown in Figure 3.6C. All the tested formulations were able to mimic the non-linear biomechanical behaviour of native tendons [8], namely its linear and yield regions. The toe region, however, characteristic of native tendons and comprising the behaviour at low strains [8], could not be mimicked by these constructs. Nonetheless, it was shown before that aligned electrospun yarns could not mimic the behaviour ascribed to the uncrimping of collagen fibrils and that only scaffolds of higher hierarchical organization, comprised of woven yarns, were able to do so, thereby replicating the triphasic behaviour of native tendons [35]. Also, PCL/DT-NP5 threads would most likely be implanted into injured tendons

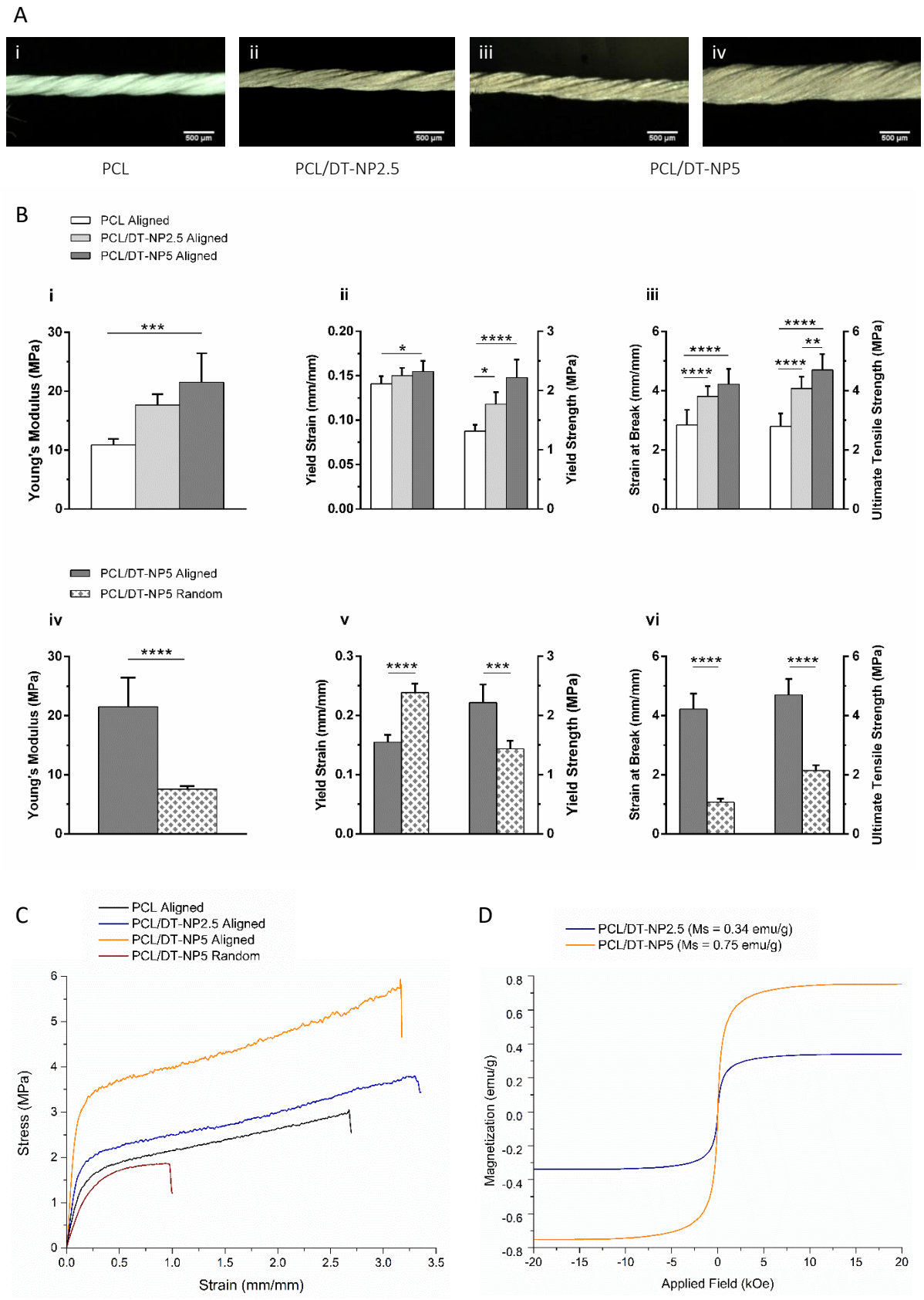

Figure 3.6. Mechanical and magnetic properties of PCL yarns with different nanofiller contents and nanofibre orientation. (A) Optical microscopy images of yarns with 0 (i), 2.5 (ii) or 5% (iii, iv) DT-NP, with aligned (i - iii) or randomly oriented nanofibres (iv), that were taken up at 0.73cm.s^{-1} and 0.24 cm.s^{-1}, respectively (scale bar 500 µm). (B) Mechanical properties of electrospun yarns with different nanofiller contents and nanofibre orientation (*p≤ 0.05 **p ≤ 0.01***p≤ 0.001 ****p ≤ 0.0001). (C) Representative tress-strain curves of the fabricated yarns. (D) Hysteresis curves of PCL/DT-NP2.5 and PCL/DT-NP5 yarns. Magnetization of saturation (Ms) of each sample is shown next to the respective label.

in the form of woven scaffolds [35], thereby improving the constructs overall mechanical properties which are essential to provide sufficient biomechanical support in a post-injury setting.

The magnetic properties of reinforced yarns were evaluated through VSM studies (Figure 3.6D), similarly to the produced nanoparticles. As expected, increasing the content of magnetic nanoparticles in the constructs leads to an increase in their Ms, from 0.34 to 0.75 emu/g. These Ms values, namely the one for PCL/DT-NP5 yarns are similar to previously developed electrospun scaffolds comprising similar amounts of iron oxide magnetic nanoparticles [45,47]. Importantly, scaffolds with Ms of similar magnitude as that of PCL/DT-NP5, showed to be able to influence cellular responses [45,47,48,100]. Moreover, as concluded for the magnetic nanoparticles, the low coercivity, the absence of remanence magnetization and of distinct hysteresis loops confirm the superparamagnetic behaviour of the material.

Overall, the aligned PCL/DT-NP5 constructs not only displayed the best mechanical properties, similar to those of previously reported electrospun constructs with an equivalent structure [93,96,101,102], but were also closer to the physiological range of native tendons. Additionally, the PCL/DT-NP5 constructs showed the highest magnetization, making them the best candidates to evaluate the influence of magneto-mechanical stimulation in synergy with tendon biomimetic scaffolds on boosting the commitment of stem cells toward the tenogenic lineage.

3.3. Assessment of the biological performance of electrospun scaffolds

hASCs were seeded onto PCL/DT-NP5 yarns for up to 21 days to evaluate whether the tendon mimetic morphology of the constructs combined with magneto-mechanical stimulation synergistically contribute to promote the tenogenic commitment of stem cells. Cell morphology and organization, as well as expression of tendon-related markers were assessed by immunocytochemistry after 11 and 21 days of culture against the results from the experimental control, cultured under static conditions. Additionally, RT-PCR was performed after 11 days of culture.

Metabolic activity of seeded hASCs was assessed through MTS assay (Figure 3.7D). Cells remained viable over time showing a significant increase in cell density between day 11 and day 21 for both culture conditions. No significant differences were observed between the metabolic activity of cells cultured under magnetic stimulation and those in static culture, suggesting that the mechanical loading via magnetic actuation does not affect cell viability. Cell morphology and organization were evaluated over time by quantifying the development of uniaxial alignment of the actin filaments (Figure 3.7A-C). As expected, cells cultured under both conditions, static and magnetic stimulated, exhibit high anisotropic alignment along the direction of the polymer fibres induced by the known contact guidance mechanisms [32,103] (Figure 3.7A). Irrespective of the stimulation regime to which the cells were subjected, the aligned topography set by the constructs fibres induced a tenocyte-like morphology [32,35,48], which is mainly characterized by an elongated cell shape [6,15]. After 21 days of culture, a thick, well-aligned layer of cells can be observed on the yarns surface indicating that cell organization is maintained during proliferation [35]. Furthermore, the degree of alignment of the cytoskeleton was quantified by calculating the directionality histograms of F-actin staining images acquired for each condition (Figure 3.7B). Similarly to the analysis performed to assess fibre alignment within electrospun threads, the resultant histograms were fitted to a Gaussian function and their FWHM and height were calculated (Figure 3.7C). Higher FWHM, and subsequent lower height, indicate that the actin filaments orientation are scattered across a wider range of directions domains. Overall, although there is a preferential direction of alignment, specifically around 45°, for all the tested conditions, histograms of cells cultured under magnetic stimulation for 21 days show monomodal directionality peaks with significantly lower FWHM accompanied by a higher peak height trend. These results suggest that, compared with the static culture conditions, the mechanical loading of cells, herein

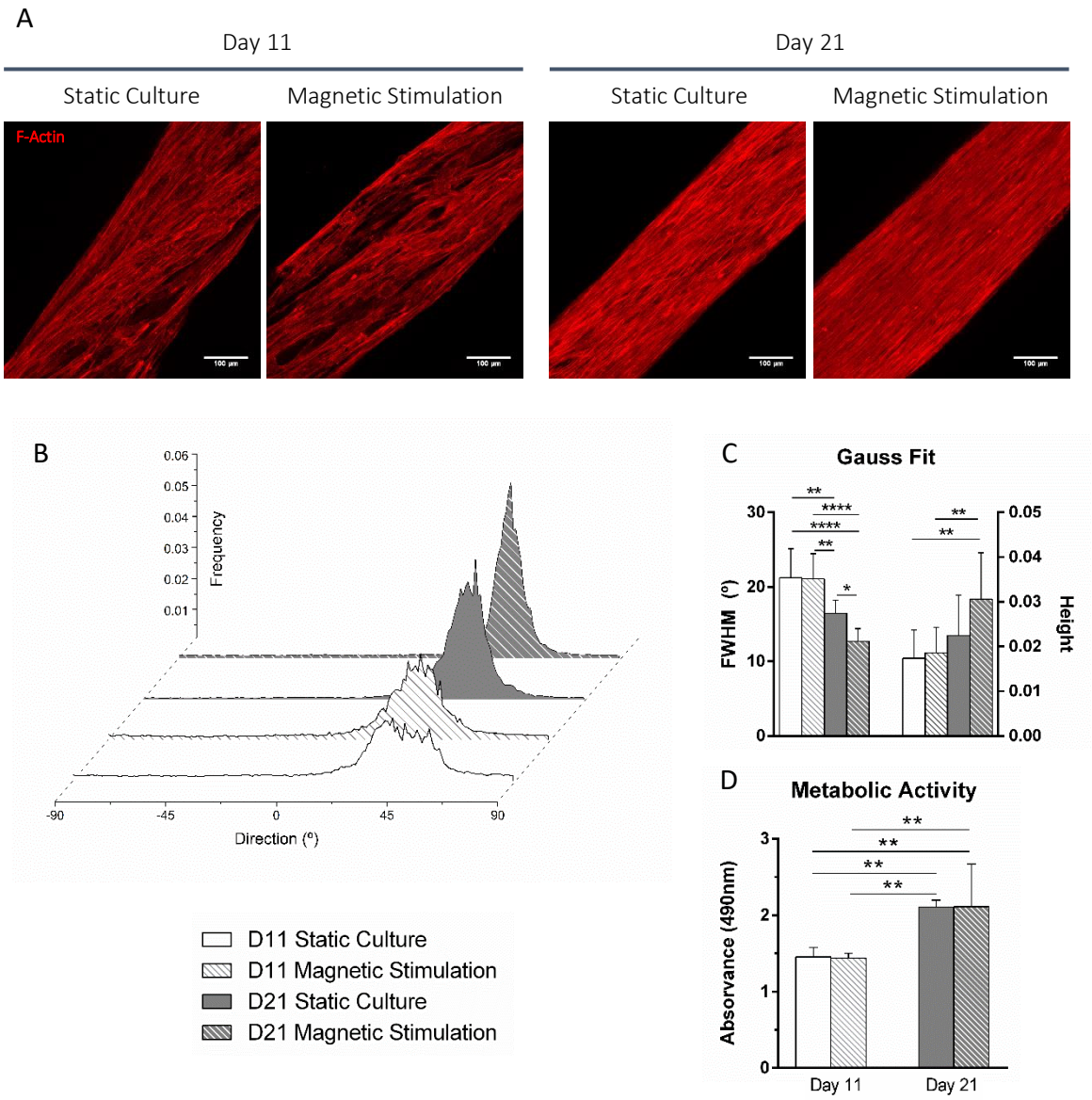

Figure 3.7. Morphometric analysis and metabolic activity of hASCs seeded onto PCL/DT-NP5 yarns. (A) Confocal microscopy images of the cytoskeleton of hASCs (red: phalloidin) seeded PCL/DT-NP5, after 11 and 21 days of culture, under static and magnetic stimulation conditions (scale bar 100 µm) and (B) the respective directionality spectra. (C) Comparison between the dimensions of the directionality peaks (FWHM and Height) obtained after Gaussian fitting of the spectra from each condition (n=5) (**p ≤ 0.01 ****p ≤ 0.0001). (D) Metabolic activity of hASCs assessed by MTS assay (**p ≤ 0.01).

performed through remote magnetic actuation of the constructs, enhances cell uniaxial alignment and elongation along the longitudinal direction of the fibres.

Related with cytoskeleton organization is the ability of cells to perceive external mechanical cues, which, as mentioned previously, is extremely important for regulation of tendon tissue homeostasis [49,104] and directing its regeneration [8,13]. Cells can adapt their behaviour, in terms of proliferation, differentiation or tissue phenotype maintenance, in response to mechanical input transmitted by their extracellular environment, following a process called mechanotransduction [17]. Mechanotransduction relies on the physical connection between cells and the ECM, in which focal adhesions provide a direct contact between ECM and the F-actin cytoskeleton of cells [16]. Thus, external physical signals such as ECM stiffness, the area available for cells to spread or even the degree of deformation of the substratum, herein induced by the magneto-mechanical actuation of the magnetic nanoparticles within the material, directly influence key cell functions [41]. One of the suggested mediators between the mechanical stimulus perceived by the cytoskeleton and the correspondent cell

response are two transcriptional activators, YAP (Yes-associated protein) and TAZ (transcriptional coactivator with PDZ binding motif) [105]. Although, YAP/TAZ are major components of the Hippo signalling pathway, which regulates tissue and organ growth [16,17], recent studies have shown that these proteins respond to mechanical signals independently from the Hippo pathway [106–108]. YAP/TAZ are predominantly cytoplasmatic, though upon activation, they shuttle from the cytoplasm to the nucleus where they promote specific gene expression [106–108] (Figure 3.8B). Importantly, an increase in nuclear YAP/TAZ is indicative of tension of the cytoskeleton which is likely caused by its adjustment to the external physical stimulus [41,109]. This phenomenon is common in cell spreading and proliferation [108] and stem cell differentiation towards the osteogenic lineage [110], for instance.

Thus, the expression of YAP/TAZ was investigated in hASCs cultured for both 11 and 21 days (Figure 3.8) to assess the ability of PCL/DT-NP5 yarns to induce mechanotransduction as a promoter

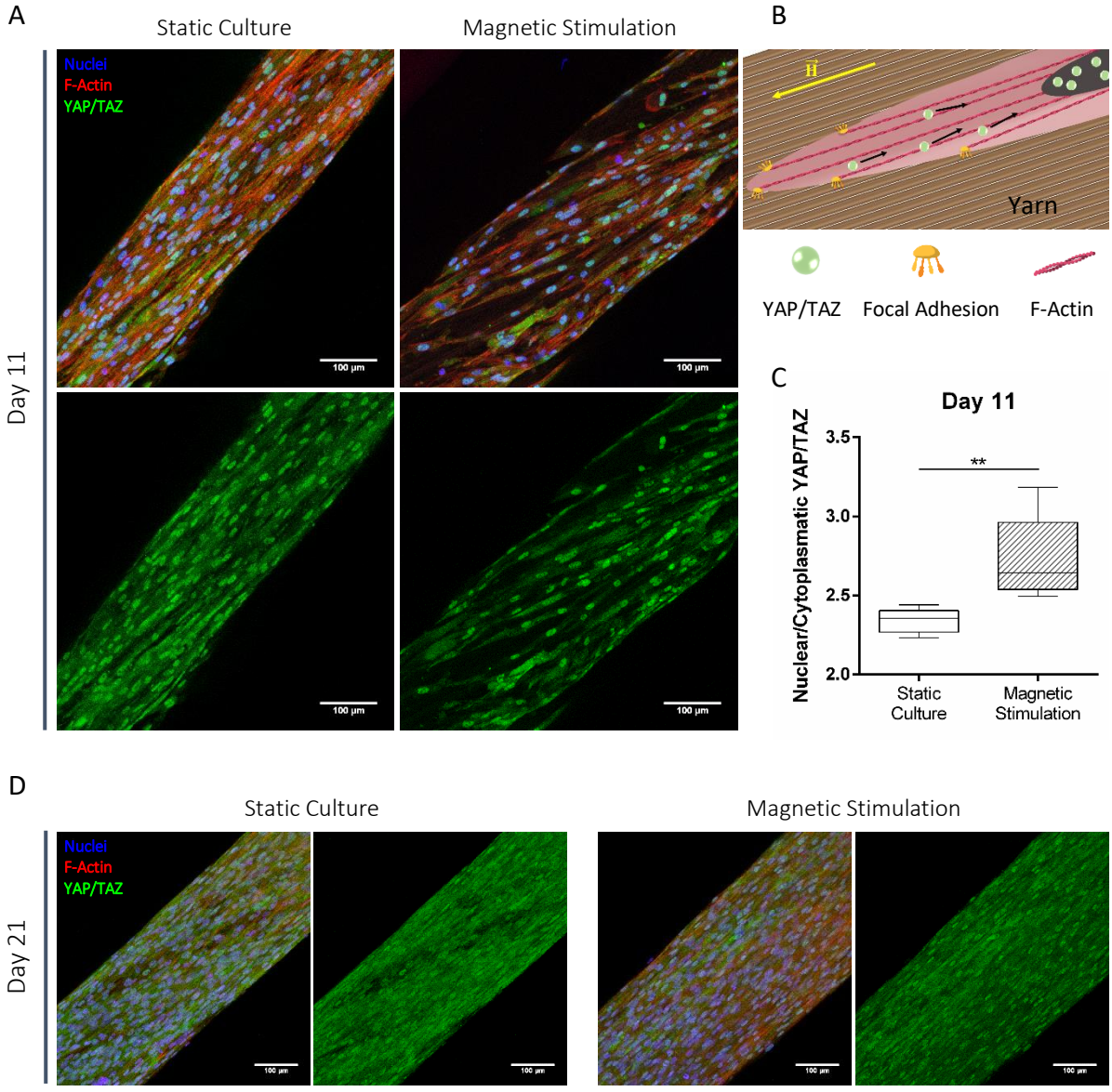

Figure 3.8. Analysis of the mechanotransduction mechanism resultant of the mechanomagnetic stimulation of hASCs. (A) Confocal microscopy images of hASCs seeded onto PCL/DT-NP5 yarns and cultured for 11 days under static and magnetic stimulated conditions (scale bar 100 µm). (B) Schematic illustrating the shuttling of nuclear/cytoplasmatic YAP/TAZ in response to substrate deformations caused by the applied magnetic field ($\vec{H}$). (C) Ratio of nuclear/cytoplasmatic YAP/TAZ in hASCs cultured for 11 days (** $p \leq 0.01$). (D) Confocal microscopy images of hASCs seeded onto PCL/DT-NP5 yarns and cultured for 21 days under static and magnetic stimulated conditions (scale bar 100 µm). Nuclei are stained in blue (DAPI), actin filaments in red (phalloidin) and YAP/TAZ in green.

for tenogenic commitment, particularly upon magneto-mechanical actuation. In this sense, the applied magnetic field acts on the magnetic nanoparticles that can be seen as remote actuators, to induce small deformations on the respective nanocomposite fibres. As a result, the cells cytoskeleton is subjected to increasing tension, thus transmitting more strain to the nucleus while activating YAP/TAZ shuttling [106] (Figure 3.8B). Immunofluorescence images of hASCs cultured under both stimulation conditions for 11 days (Figure 3.8A) clearly display expression of nuclear YAP/TAZ. The fact that the constructs were able to induce YAP/TAZ activation under both non-stimulating and stimulation conditions indicates that their aligned topography is sufficient to induce cell spreading and stretching, as previously shown [35,106]. Additionally, the nuclear to cytoplasmatic YAP/TAZ ratio was calculated in cells cultured for 11 days under static and magnetic stimulation (Figure 3.8C), by segmenting the nuclei in the YAP/TAZ stained images according to the respective DAPI staining (nuclei) and calculating the overall intensity of each of the resulting images. The results show that the nuclear to cytoplasmatic YAP/TAZ in magnetically stimulated cells is significantly superior to that of cells in static culture, which not only suggests a more effective transmission of mechanical signals but also a higher proliferation rate [109]. In contrast, immunofluorescence images of hASCs cultured for 21 days (Figure 3.8) showed predominantly cytoplasmatic YAP/TAZ, most likely due to cell crowding, which has been shown to be a sign of a decrease in proliferation [108]. Overall, magneto-mechanical stimulation of cells was capable of activating YAP/TAZ, suggesting an effective transmission of mechanical stimulus. This mechanical stimulus consequently enhances cell cytoskeleton elongation, which is in agreement with the results of cytoskeleton organization (Figure 3.7) and is particularly important for tenogenic commitment, as it might boost these cell fate pathways, vital when envisioning the applicability of these constructs for post-injury and post-implantation settings.

To have a first assessment on the impact of magneto-mechanical stimulation on cell commitment towards the tenogenic lineage, gene expression was assessed by real time RT-PCR. It should be noted that there are no specific markers for tenocytes and tendon progenitors, as the main genes that regulate tenogenesis have yet to been identified. Moreover, most of the markers expressed by cells committed to the tenogenic lineage, such as tenomodulin (*TNMD*) or type I collagen (*COL1A1*) which is the main component of tendons, are expressed by other cell types as well [111]. Nevertheless, *TNMD*, *COL1A1*, decorin (*DCN*), tenascin-C (*TNC*), type III collagen (*COL3A1*) and the transcription factor scleraxis (*SCX*) are collectively abundant in tendons [18,23]. RT-PCR results (Figure 3.9) suggest that cells cultured on PCL/DT-NP5 under both static and magnetic conditions present a tenogenic-like

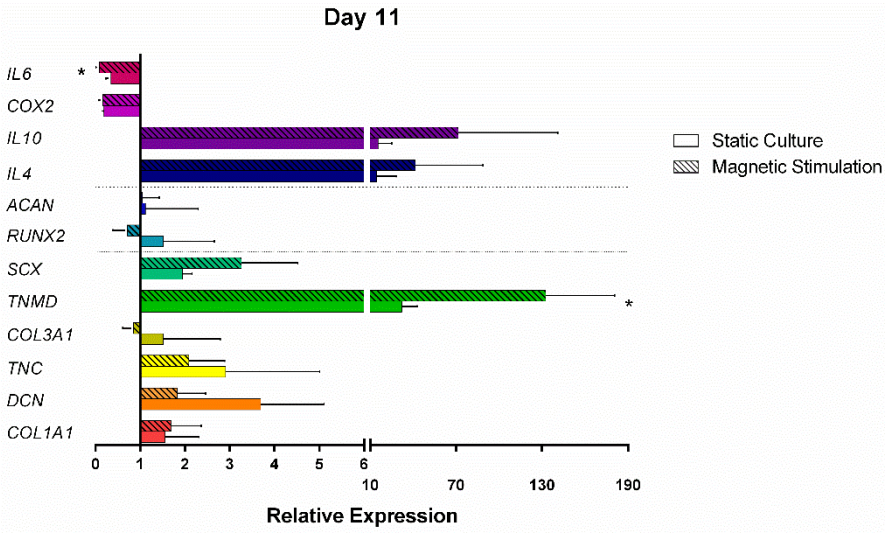

Figure 3.9. Real time RT-PCR analysis of tenogenic (*COL1A1*, Type I Collagen; *DCN*, Decorin; *TNC*, Tenascin; *COL3A1*, Type III Collagen; *TNMD*, tenomodulin; *SCX*, scleraxis), chondrogenic (*ACAN*, Aggrecan) and osteogenic (*RUNX2*) gene expression, as well as anti-inflammatory (*IL-4* and *IL-10*) and pro-inflammatory (*IL-6* and *COX2*) cytokines of hASCs cultured on PCL/DT-NP5 yarns for 11 days under static and magnetic stimulated conditions (*$p \leq 0.05$).

behaviour: in general, the aforementioned tendon-related markers were upregulated after 11 days of culture, with the exception of *COL3A1* which was downregulated in cells cultured under magnetic stimulation, suggesting that the yarns topographical cues are themselves strong inducers of hASCs tenogenic commitment [32,35]. In contrast, magneto-mechanical stimulation of hASCs leads to higher expression of *SCX* and *TNMD*. Scleraxis is responsible for the promotion and consequent regulation of the expression of *TNMD* in mature tenocytes [112], as well as for directing mesenchymal stem cell differentiation towards the tenogenic lineage in response to mechanical stimulus, while suppressing commitment towards other lineages [113]. In turn, tenomodulin is a transmembrane glycoprotein expressed mainly in tenocytes, that regulates their proliferation and is involved in the calibration of collagen fibrils [114]. Moreover, although, Type III collagen is essential for the regulation of type I collagen assembly [115], it is associated with the early stages of tendon repair in which the first laid down matrix is significantly weaker and more disorganized than the healthy tissue [3,7]. Therefore, the trend for lower expression level of this collagen type promoted by magneto-mechanical stimuli might indeed be a desirable effect for tendon regeneration. Additionally, the gene expression of non-tendon-related markers, namely *RUNX2* and *ACAN*, which are related with the osteogenic and chondrogenic lineages, respectively [116], was investigated against the aforementioned tendon-related markers. Cells under magneto-mechanical stimulation presented a lower expression of these markers, with downregulation of *RUNX2*, in comparison to those cultured under static conditions. Overall, these results indicate that magneto-mechanical stimulation of hASCs cultured on PCL/DT-NP5 yarns tends to increase the gene expression of markers that are crucial in inducing the tenogenic commitment of hASCs and regulating tenocyte proliferation, while decreasing expression of genes specific of the osteogenic and chondrogenic lineages.

Although biomimetic scaffolds are an effective strategy to promote tissue regeneration in defects of considerable size, their implantation will most likely lead to inflammation at the injury site, thus compromising the healing process [47]. Macrophages are essential regulators of tissue homeostasis as well as tissue healing, by eliciting the inflammatory response in a post-injury setting [117]. These cells can be activated into two distinct subpopulations in response to different inflammatory cues: M1 macrophages are induced in the presence of pro-inflammatory cytokines and are predominantly present during the first stage of tendon healing (inflammatory), while M2 macrophages are activated in the presence of anti-inflammatory cytokines and are characteristic of the later stages of healing (reparative and remodelling) [117,118]. As such, induction of the M2 phenotype would be preferential when implanting scaffolds in a tissue with such particularly complicated healing process. For this reason, the modulation of the inflammatory secretome of stem cells cultured on PCL/DT-NP5 yarns under static and magnetic conditions, namely the expression of both pro (*COX2* and *IL6* [119]) and anti-inflammatory markers (*IL4* [120] and *IL10* [121]), was assessed after 11 days. RT-PCR (Figure 3.9) revealed that there is an upregulation of anti-inflammatory markers and a downregulation of pro-inflammatory markers in cells cultured under both conditions. These results suggest that the yarns aligned topography should induce a positive immunomodulatory behaviour of hASCs, with the subsequent potential impact on the induction of polarization of macrophages towards the M2 phenotype inducing a pro-healing inflammatory response [107]. Moreover, according to previous reports, the yarns topography may have a direct effect on the polarization of macrophages. By promoting the elongation of the macrophages, which is characteristic of the M2 phenotype, aligned nano- and micro-patterned surfaces were able to modulate their polarization towards the pro-resolving phenotype without cytokine induction [122,123]. Thus, the aligned nanofibrous structure of PCL/DT-NP5 yarns might potentially have a similar effect. Furthermore, RT-PCR also revealed that magneto-mechanical stimulation of hASCs leads to a higher expression of anti-inflammatory markers and a significantly lower expression of *IL-6*. Interestingly, it has been recently demonstrated that magneto-mechanical stimulation of macrophages through magnetic responsive materials also has a positive effect on their polarization towards an M2-like phenotype [47]. Altogether,

these results suggest that magnetic actuation of implanted PCL/DT-NP5 constructs should not only promote tenogenic commitment of stem cells but also modulate the inflammatory response of the native tissue, thus preventing chronic inflammation and scar tissue formation. Therefore, although not investigated in detail under the scope of this study, the immunomodulatory potential of the proposed scaffolds should be the focus of future studies.

Immunocytochemistry analysis was performed to further assess the presence of tenogenic-related markers, such as TNMD and SCX, at 11 and 21 days of culture (Figure 3.10). hASCs cultured under static and magnetic stimulating conditions express SCX at day 11 but not at day 21, implying that there is a substantial decrease in the activation of this transcription factor between the two timepoints. In contrast, the deposition of TNMD protein suffers an evident increase from day 11 to day 21 in cells cultured under both conditions. At day 11, TNMD deposition is visibly superior in constructs under magneto-mechanical stimulation than those in static culture, further confirming the results of RT-PCR analysis. This tendency is maintained on day 21 with higher expression of TNMD by cells magneto-

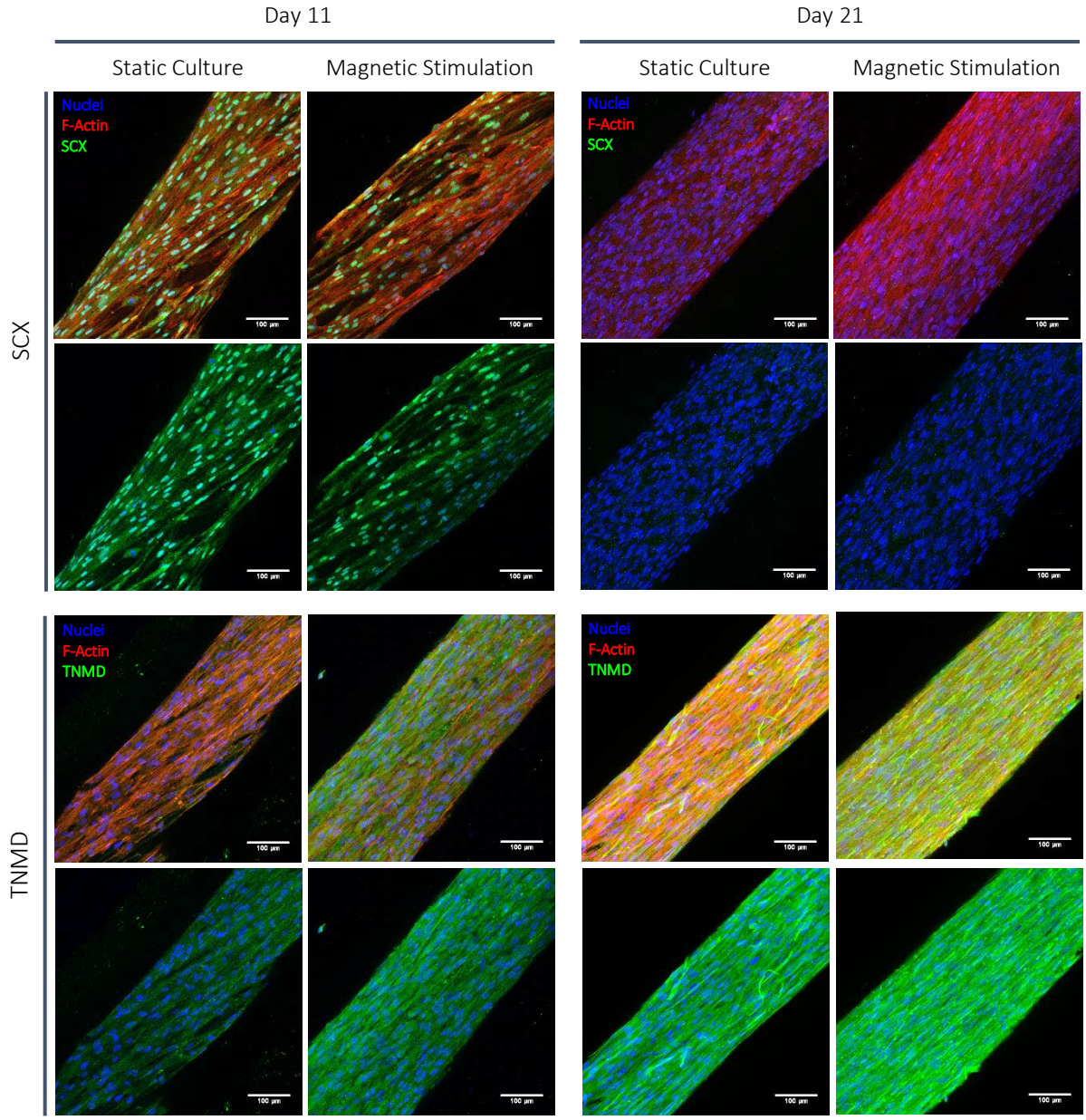

Figure 3.10. Expression of tendon-related markers. Confocal microscopy images of hASCs cultured on PCL/DT-NP5 yarns for 11 and 21 days of culture under static and magnetic stimulated conditions (scale bar 100 µm). Nuclei are stained in blue (DAPI), actin filaments in red (phalloidin) and SCX/TNMD in green.

mechanically stimulated. These results suggest that there is a peak of SCX expression, that may occur before day 11, appearing long before the peak of TNMD expression, which is due to the role of SCX as a transcription factor of TNMD [112]. Additionally, higher deposition of TNMD in constructs under magneto-mechanical stimulation may be due to SCX being activated earlier and/or more efficiently under this condition. High expression of both SCX and TNMD is indicative of commitment of cells towards the tenogenic lineage, as previously discussed [113,114]. Thus, these results further highlight the synergistic effect of aligned topography and magneto-mechanical stimulus on the promotion of the tenogenic differentiation of hASCs seeded onto PCL/DT-NP5 yarns.

For optimization and characterization purposes, the performance of the developed magnetic responsive material, in terms of both mechanic and biologic behaviour, was evaluated on the yarns as representative units of the 3D scaffolds. Although the yarns might be useful as a miniaturized 3D model substrate for *in vitro* studies, when envisioning practical applications higher hierarchical 3D scaffolds are needed for implantation. For this reason, the developed yarns were assembled into higher hierarchical structures (Figure 3.11A) that mimic the biomechanical behaviour of native tendons following the reports of Laranjeira *et al.*, 2017 [35]. In order to evaluate whether the scaffolds could perform similarly to their yarn units and induce the tenogenic commitment of stem cells while promoting the production of tendon-like ECM, hASCs were cultured on these scaffolds under magnetic stimulation for 21 days. For this purpose, immunocytochemistry analysis was performed to investigate the deposition of COL1A1 and TNMD (Figure 3.11B and C). The results indicate high deposition of TNMD protein, similarly to previously observed for cells cultured on PCL/DT-NP5 yarns under the same condition (Figure 3.10). Additionally, there is also deposition of considerable amounts of COL1A1 which show some signs of fibrillation and follow the cell aligned patterns at 21 days. Even though only the expression of TNMD and COL1A1 was assessed through immunocytochemistry, as key representative markers of tenocytes and tendon ECM, other characteristic markers of these native tissues should also likely be present, following the same trend observed for the yarns and for the hASCs cultured on similar scaffolds under static conditions [35]. These results demonstrate that the 3D tendon mimetic architecture and topography of the fabricated scaffolds in combination with their magnetic responsiveness, can boost the tenogenic commitment of stem cells, as well as promoting the deposition of aligned ECM that resembles that of native tendons. From a clinical perspective, a scaffold with these characteristics would be of great interest for both acellular and cellular tissue engineering strategies as an option for the treatment of tendon defects of variable sizes. This system will enable to extend the proposed contactless cell mechanomodulatory stimuli to *in vivo* settings after construct implantation, contributing not only to direct the fate of seeded or recruited stem cells toward the tenogenic phenotype (or its maintenance by resident tenocytes) and promoting the deposition of tendon-like ECM, but would also likely prevent chronic inflammation. Collectively, all these effects would contribute to prevent the formation of fibrotic tissue at the injury site and lead to the regeneration of functional tendon tissue.

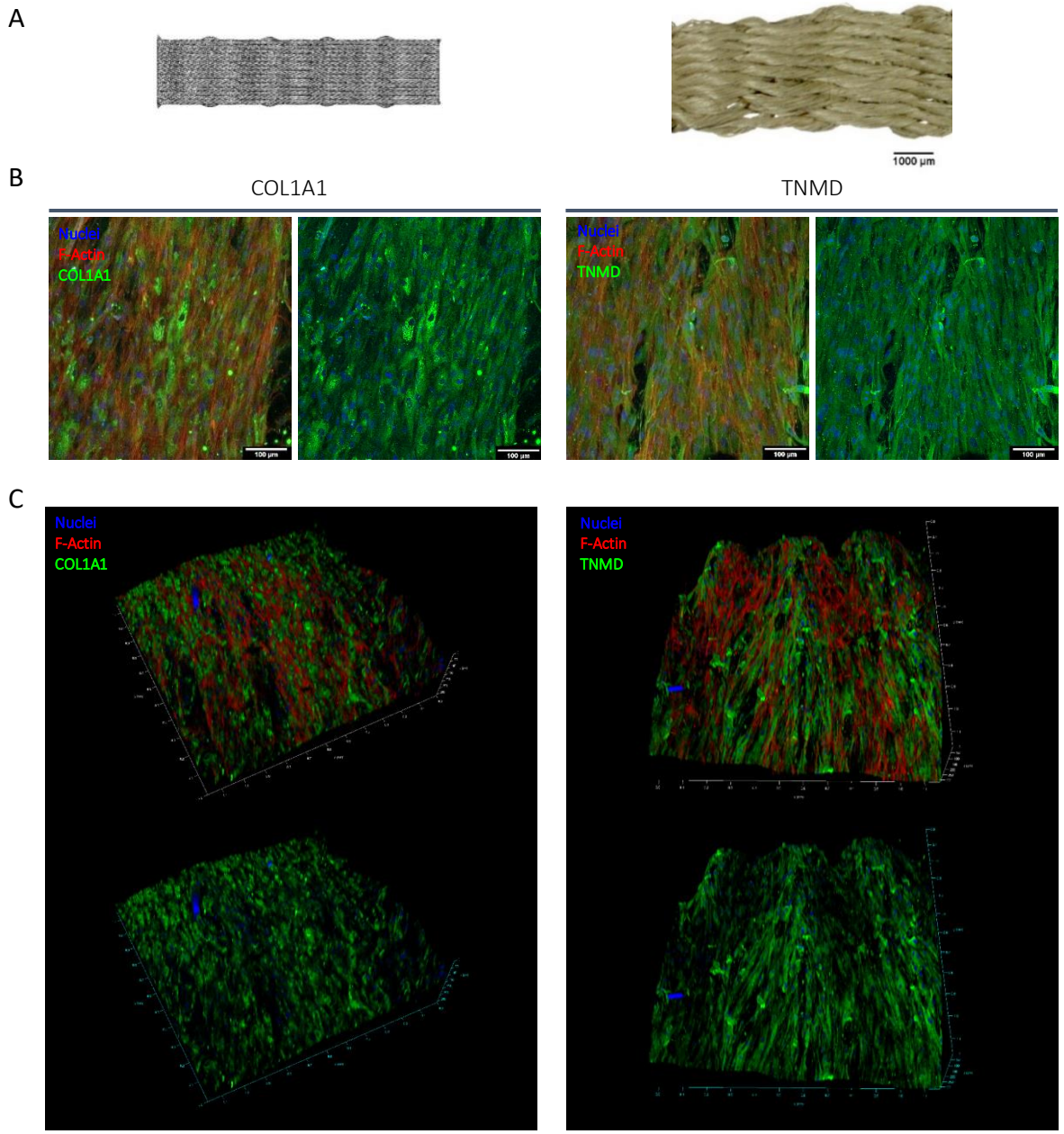

Figure 3.11. Immunocytochemistry of COL1A1 and TNMD proteins deposited by hASCs. (A) Schematic depicting the overall structure of a woven scaffold (adapted from ref [35]) and optical microscopy images of a PCL/DT-NP5 scaffold (scale bar: 1mm). (B) Confocal microscopy images of hASCs cultured on scaffolds of PCL/DT-NP5 for 21 days under magnetic stimulation conditions (scale bar 100 µm). (C) 3D reconstruction of confocal microscopy images of hASCs cultured on scaffolds of PCL/DT-NP5 for 21 days under magnetic stimulation conditions (scale 1.2mm x 1.2mm x 350µm). Nuclei are stained in blue (DAPI), actin filaments in red (phalloidin) and COL1A1/ TNMD in green.

Chapter 4. Conclusions

The role of tendons to the overall functioning of the musculoskeletal system as well as its limited healing capabilities has been extensively discussed in the medical field. In recent years, as tendon injuries have been identified as a frequent and recurrent problem affecting not only active but also sedentary individuals, several treatment options have been applied aiming at achieving full regeneration of ruptured or damaged tendons. Nevertheless, both surgical approaches and conservative treatments revealed to be relatively ineffective, since they result in just a partial recovery of the native tissue functionality. TE strategies have, thus, been proposed as a promising alternative to achieve full regeneration of tendon tissue and re-establish their functional properties prior to injury. Although many studies have proposed completely different approaches, in general they agree on the basic requirements for a tendon directed scaffold. Ideally, these should mimic the native tendon structure, specifically its ECM architecture, and possess adequate load-bearing capabilities to temporarily support the biomechanical role of the injured tissue during the regeneration process. Moreover, tendon intended scaffolds should provide cells with either physical, biological or chemical cues to prevent tenocytes phenotypic drift and to induce their tenogenic commitment of stem cells. Remarkably, all these requirements have been recently combined in a hierarchical nanocomposite fibrous scaffold with unpaired tendon biomimetic features. Through the textile assembly of CANT into hierarchical structures, from the nano to the macro scale, the tendon ECM organization and the biomechanical behaviour of native tendons was successfully replicated.

Herein, a new approach to tendon regeneration was presented, building on the key principles of these scaffolds. Intending on satisfying the mechanosensitive nature of tendons, these constructs were endowed with magnetic responsiveness to be able to mechanically stimulate cells on command, not only during the *in vitro* maturation of the constructs but also during the *in vivo* regeneration after their transplantation. For this purpose, continuous and aligned electrospun fibre threads were produced from a Poly-ε-caprolactone (PCL) reinforced with Cellulose Nanocrystals (CNCs) decorated with superparamagnetic nanoparticles of iron oxide (MNP@CNC). Moreover, MNP@CNC were coated with thin layers of polydopamine and further grafted with hydrophobic dodecanethiol (DT-NP) to assure their chemical and colloidal stability in the used solvent system as well as to improve the interfacial compatibility of the nanofiller with the polymeric matrix.

The constructs were fabricated using a customized electrospinning system in which the PCL/DT-NP solution was jetted to a support bath and the resulting fibres were taken-up by a roller, in thread form, at constant speed. By varying the fibre composition and spinning conditions, such as the concentration of nanofiller (0 – 5wt.%) in the polymeric solution or the speed at which the fibres are pulled from the support bath, the morphology of the resulting threads can be modulated to fit the desired requirements. Results showed that an increase in nanofiller content lead to an increase in fibre and, therefore, thread diameter. On the other hand, increasing the take-up speed lead to smaller fibre and thread diameters, as well as, higher anisotropic alignment of fibres within the thread. Taking advantage of this feature, the present fabrication method may be used to engineer 3D constructs with gradients of fibre alignment. Herein, randomly oriented fibre threads were produced at a lower take up speed and used as a control for the degree of fibre orientation and mechanical properties analysis. Although, the assessment of their biological performance was not included in the scope of this project, it is expected that the lack of anisotropic organization of fibre would be detrimental for tenogenic commitment. In contrast, the random topography may be useful to induce other types of cell responses, such as osteogenic commitment of stem cells or to mimic the typical organization of pathogenic tendon tissues. As such, constructs encompassing gradients of fibre alignment would be of interest for the regeneration of tissue interfaces, such as the tendon to bone interface, and threads with varying degrees of fibre

alignment might be used as building blocks to engineer *in vitro* 3D models of healthy and diseased tendon tissues. Another advantage of this fabrication method is the continuous production of material that allows the scalable production of fibre threads. Consequently, the dimensions of the projected scaffolds can be adapted to fit the demands of the target tissue. From a clinical standpoint, this feature is of considerable interest to engineer personalised scaffolds fulfilling the requirements of specific injuries and patients. Furthermore, the production of woven scaffolds may be automatized by using automated textile *jacquard* machines, standardizing their assembly while increasing productivity.

The mechanic, magnetic and biological performance of the materials were assessed using yarns as representative miniaturized 3D units of the hierarchical structure and organization of the final 3D scaffolds, which facilitated the realization of the numerous assays herein proposed to perform. The incorporation of small amounts of nanofiller (2.5 or 5 wt.%) lead to an increase in the mechanical properties of the constructs, in comparison to bare PCL ones. In particular, incorporating 5 wt.% DT-NP increased the Young's modulus and ultimate tensile strength of bare PCL yarns in 98 % and 49 %, respectively, raising them to the lower range of native tendons tensile properties. Although, the complete range of the native tendon tensile properties could not be mimicked, these yarns should be able to handle the physiological demands of a healing tissue given that, in a post injury setting, the tissue will unlikely be overloaded. Moreover, as expected the PCL/DT-NP yarns were not able to replicate the full biomechanical behaviour of native tissues, failing to mimic the toe region that corresponds to the behaviour at low strains (0 – 2 %). Interestingly, this region could only be replicated in woven scaffolds, as was shown in a previous study. Though the mechanical behaviour of the scaffolds herein produced was not evaluated, an increase in the tensile properties of the material and the full replication of the tendons biomechanical behaviour is expected. Therefore, the stress-strain profile of woven scaffolds of PCL/DT-NP should be the focus of future studies in order to complete the detailed characterization of the proposed system.

Regarding the magnetic properties of the material, results revealed an increase in Ms with the increase in nanofiller content. Most importantly, they presented a superparamagnetic behaviour, meaning that the yarns are only actuated in the presence of a magnetic field. From a clinical point of view, superparamagnetism is a crucial feature for the design of personalized treatments encompassing such constructs, given that cells would not be magneto-mechanically stimulated in the absence of a magnetic field. Thus, different regimes of stimulation could be adapted to the needs of the healing tissue.

Biological performance of the constructs, namely their capacity to induce tenogenic differentiation of stem cells, was assessed on PCL yarns reinforced with 5 wt.% DT-NP, given they exhibited the best mechanical and magnetic properties for the intended goal. Results indicated that the physical cues provided by the yarns topography was itself sufficient to induce the tenogenic commitment of stem cells, confirming the previous results obtained with similar scaffolds systems. Nonetheless, cells under magneto-mechanical stimulation showed a higher degree of alignment along the direction of the fibres, as well as higher expression of genetic markers related with the tenogenic commitment of stem cells, while inhibiting expression of osteogenic and chondrogenic markers. To demonstrate that the proposed remote magnetic actuation can indeed provide mechanical stimuli to the seeded cells, the expression of transcription regulators (YAP/TAZ) that have been linked to the process of mechanotransduction was investigated. Results indicated that activation of YAP/TAZ signalling pathway was significantly superior in magneto-mechanically stimulated cells in comparison to those in static culture. Altogether, these results suggest that there was an effective transmission of the mechanical stimulus to the cells in response to the external magnetic field and that this mechanical stimulus was beneficial to boost tenogenic commitment of hASCs.

Given that the implantation of any scaffold into an injured tissue will inevitably lead to an inflammatory response (foreign body response), it would be of clinical interest if the implanted

construct could contribute to direct immune cells towards the reparative phase of the healing process and divert it from chronic inflammation or fibroses. One potential way of achieving such outcome is by modulating the secretome of the seeded hASCs, promoting the secretion of pro-healing cytokines and chemokines. Therefore, the modulatory effects of the magneto-mechanical stimuli on the hASCs inflammatory response was also assessed by evaluating the gene expression of pro and anti-inflammatory factors by hASCs cultured under both stimulation conditions. Results suggest that the yarns topography may once again be sufficient to direct the tendon healing process towards the reparative phase. However, cells under magneto-mechanical stimulation showed higher upregulation of anti-inflammatory factors as well as significantly lower expression of pro-inflammatory factors. Therefore, it is suspected that the scaffolds developed herein and the magnetic stimuli synergistically contribute to influence the polarization of macrophages from M1 to M2 phenotype, that is from the inflammatory to the pro-healing state. As such, the effect of the magnetic actuation of these scaffolds on the modulation of the inflammatory response of mono (hASCs) and co-cultures (hASCs and monocytes) should be further investigated due to its importance in the management of tendon pathologies and to achieve the regeneration of these tissues.

Finally, PCL yarns reinforced with 5 wt.% DT-NP were woven into 3D scaffolds as proof of concept for the application of these constructs in a clinical setting. Results regarding hASCs cultured on woven scaffolds under magnetic stimulation for 21 days, showed expression of tenomodulin, suggesting tenogenic differentiation, and type I collagen deposition following the scaffold topography, confirming the positive results obtained with the yarns as representative miniaturized 3D units of the scaffolds.

In summary, the results demonstrate that composite magnetic nanoparticles were successfully incorporated in electrospun fibres, thereby allowing their remote actuation while improving their mechanical properties up to the lower limits of tendon tissues. Magnetic actuation of the constructs boosted the tenogenic differentiation of stem cells and promoted the expression of anti-inflammatory factors, thus suggesting a positive influence over the inflammatory process after construct implantation. In the future, *in vivo* studies could be performed to complement the work herein developed, shedding light on the influence of magneto-mechanical stimulation on the healing process of a critical rupture or semi-functional tissue.

Overall, the present work highlights the synergistic role of mechanical stimulation and tendon biomimetic scaffolds to promote steady tenogenic differentiation of stem cells without additional biological factors supplementation. Importantly, it proposes a new approach to deliver the referred mechanical stimuli through remote magnetic systems, which can be applied not only during *in vitro* construct maturation, but can continue to be delivery after *in vivo* transplantation, thus potentially contributing to promote the regeneration and restoration of the tendons functionality.

References

1. Robi, K., Jakob, N., Matevz, K. & Matjaz, V. The Physiology of Sports Injuries and Repair Processes. in *Current Issues in Sports and Exercise Medicine* (eds. Hamlin, M., Draper, N. & Kathiravel, Y.) 43–86 (InTech, 2013).

2. Wu, F., Nerlich, M. & Docheva, D. Tendon injuries: basic science and new repair proposals. *EFORT Open Rev.* **2,** 332–342 (2017).

3. Snedeker, J. G. & Foolen, J. Tendon injury and repair - A perspective on the basic mechanisms of tendon disease and future clinical therapy. *Acta Biomater.* **63,** 18–36 (2017).

4. Santos, M. L., Rodrigues, M. T. & Domingues, R. M. A. Biomaterials as Tendon and Ligament Substitutes: Current Developments. in *Regenerative Strategies for the Treatment of Knee Joint Disabilities* (eds. Oliveira, M. & Reis, R. L.) **21,** 349–371 (Springer International Publishing, 2017).

5. Costa-Almeida, R. *et al.* Tendon Stem Cell Niche. in *Tissue-Specific Stem Cell Niche* (ed. Turksen, K.) 221–244 (Springer International Publishing, 2015).

6. Kannus, P. & Kannus, P. Structure of the tendon connective tissue. *Scand J Med Sci Sport. Copyr. C MUNKSGAARD* **10,** 312–320 (2000).

7. Schneider, M., Angele, P., Järvinen, T. A. H. & Docheva, D. Rescue plan for Achilles: Therapeutics steering the fate and functions of stem cells in tendon wound healing. *Adv. Drug Deliv. Rev.* **129,** 352–375 (2018).

8. Wang, J. H. C. Mechanobiology of tendon. *J. Biomech.* **39,** 1563–1582 (2006).

9. LaCroix, A. S., Duenwald-Kuehl, S. E., Lakes, R. S. & Vanderby, R. Relationship between tendon stiffness and failure: a metaanalysis. *J. Appl. Physiol.* **115,** 43–51 (2013).

10. Lomas, A. J. *et al.* The past, present and future in scaffold-based tendon treatments. *Adv. Drug Deliv. Rev.* **84,** 257–277 (2015).

11. Walden, G. *et al.* A Clinical, Biological, and Biomaterials Perspective into Tendon Injuries and Regeneration. *Tissue Eng. Part B Rev.* **23,** 44–58 (2017).

12. Sahoo, S. Biologic- and Synthetic-Based Scaffolds for Tendon Regeneration. in *Tendon Regeneration Understanding tissue physiology and development to engineer functional substitutes* (eds. Gomes, M. E., Reis, R. L. & Rodrigues, M. T.) 243–255 (Academic Press, 2015).

13. Galloway, M. T., Lalley, A. L. & Shearn, J. T. The Role of Mechanical Loading in Tendon Development, Maintenance, Injury, and Repair. *J. Bone Jt. Surgery-American Vol.* **95,** 1620–1628 (2013).

14. Ackermann, P. W. Tendinopathy I: Understanding Epidemiology, Pathology, Healing, and Treatment. in *Tendon Regeneration Understanding tissue physiology and development to engineer functional substitutes* (eds. Gomes, M. E., Reis, R. L. & Rodrigues, M. T.) 113–147 (Academic Press, 2015).

15. Spanoudes, K., Gaspar, D., Pandit, A. & Zeugolis, D. I. The biophysical, biochemical, and biological toolbox for tenogenic phenotype maintenance in vitro. *Trends Biotechnol.* **32,** 474–482 (2014).

16. Halder, G., Dupont, S. & Piccolo, S. Transduction of mechanical and cytoskeletal cues by YAP and TAZ. *Nat. Rev. Mol. Cell Biol.* **13,** 591–600 (2012).

17. Totaro, A., Panciera, T. & Piccolo, S. YAP/TAZ upstream signals and downstream responses.

Nat. Cell Biol. **20,** 888–899 (2018).

18. Gonçalves, A. I., Rodrigues, M. T., Reis, R. L. & Gomes, M. E. Bioengineered Strategies for Tendon Regeneration. in *In Situ Tissue Regeneration: Host Cell Recruitment and Biomaterial Design* (eds. Lee, S. J., Yoo, J. J. & Atala, A.) 275–293 (Elsevier Inc., 2016).

19. Riggin, C. N., Morris, T. R. & Soslowsky, L. J. Tendinopathy II: Etiology, Pathology, and Healing of Tendon Injury and Disease. in *Tendon Regeneration Understanding tissue physiology and development to engineer functional substitutes* (eds. Gomes, M. E., Reis, R. L. & Rodrigues, M. T.) 149–183 (Academic Press, 2015).

20. Gonçalves, A. I. *et al.* Cell-Based Approaches for Tendon Regeneration. in *Tendon Regeneration Understanding tissue physiology and development to engineer functional substitutes* (eds. Gomes, M. E., Reis, R. L. & Rodrigues, M. T.) 187–203 (Academic Press, 2015).

21. Liu, W., Wang, B. & Cao, Y. Engineered Tendon Repair and Regeneration. in *Tendon Regeneration Understanding tissue physiology and development to engineer functional substitutes* (eds. Gomes, M. E., Reis, R. L. & Rodrigues, M. T.) 381–412 (Academic Press, 2015).

22. Gonçalves, A. I. *et al.* Understanding the Role of Growth Factors in Modulating Stem Cell Tenogenesis. *PLoS One* **8,** e83734 (2013).

23. Liu, Y., Suen, C. W., Zhang, J. fang & Li, G. Current concepts on tenogenic differentiation and clinical applications. *J. Orthop. Transl.* **9,** 28–42 (2017).

24. Qiu, Y. *et al.* Development of a refined tenocyte expansion culture technique for tendon tissue engineering. *J. Tissue Eng. Regen. Med.* **8,** 955–962 (2014).

25. Mortimer, C. J. & Wright, C. J. The fabrication of iron oxide nanoparticle-nanofiber composites by electrospinning and their applications in tissue engineering. *Biotechnol. J.* **12,** 1–10 (2017).

26. Wang, X., Ding, B. & Li, B. Biomimetic electrospun nanofibrous structures for tissue engineering. *Mater. Today* **16,** 229–241 (2013).

27. Rodrigues, M. T., Reis, R. L. & Gomes, M. E. Engineering tendon and ligament tissues: present developments towards successful clinical products. *J. Tissue Eng. Regen. Med.* **7,** 673–686 (2012).

28. Agarwal, S., Wendorff, J. H. & Greiner, A. Use of electrospinning technique for biomedical applications. *Polymer (Guildf).* **49,** 5603–5621 (2008).

29. Bhardwaj, N. & Kundu, S. C. Electrospinning: A fascinating fiber fabrication technique. *Biotechnol. Adv.* **28,** 325–347 (2010).

30. Domingues, R. M. A. *et al.* Fabrication of Hierarchical and Biomimetic Fibrous Structures to Support the Regeneration of Tendon Tissues. in *Tendon Regeneration Understanding tissue physiology and development to engineer functional substitutes* (eds. Gomes, M. E., Reis, R. L. & Rodrigues, M. T.) 259–280 (Academic Press, 2015).

31. Sallach, R. & Chaikof, E. Electrospun elastin and collagen nanofibers and their application as biomaterials. in *Natural-Based Polymers for Biomedical Applications* (eds. Reis, R. L. et al.) 315–336 (Woodhead Publishing, 2008).

32. Yin, Z. *et al.* The regulation of tendon stem cell differentiation by the alignment of nanofibers. *Biomaterials* **31,** 2163–2175 (2010).

33. Domingues, R. M. A. *et al.* Enhancing the Biomechanical Performance of Anisotropic Nanofibrous Scaffolds in Tendon Tissue Engineering: Reinforcement with Cellulose Nanocrystals. *Adv. Healthc. Mater.* **5,** 1364–1375 (2016).

34. Domingues, R. M. A., Gomes, M. E. & Reis, R. L. The Potential of Cellulose Nanocrystals in Tissue Engineering Strategies. *Biomacromolecules* **15,** 2327–2346 (2014).

35. Laranjeira, M., Domingues, R. M. A., Costa-Almeida, R., Reis, R. L. & Gomes, M. E. 3D Mimicry of Native-Tissue-Fiber Architecture Guides Tendon-Derived Cells and Adipose Stem Cells into Artificial Tendon Constructs. *Small* **13,** 1–13 (2017).

36. Benhardt, H. A. & Cosgriff-Hernandez, E. M. The Role of Mechanical Loading in Ligament Tissue Engineering. *Tissue Eng. Part B Rev.* **15,** 467–475 (2009).

37. Jiang, Y. *et al.* A proteomic analysis of engineered tendon formation under dynamic mechanical loading in vitro. *Biomaterials* **32,** 4085–4095 (2011).

38. Riehl, B. D., Park, J.-H., Kwon, I. K. & Lim, J. Y. Mechanical Stretching for Tissue Engineering: Two-Dimensional and Three-Dimensional Constructs. *Tissue Eng. Part B Rev.* **18,** 288–300 (2012).

39. Kuo, C. K. & Tuan, R. S. Mechanoactive Tenogenic Differentiation of Human Mesenchymal Stem Cells. *Tissue Eng. Part A* **14,** 1615–1627 (2008).

40. Lee, K. Il *et al.* Mechanical properties of decellularized tendon cultured by cyclic straining bioreactor. *J. Biomed. Mater. Res. - Part A* **101,** 3152–3158 (2013).

41. Dupont, S. Role of YAP/TAZ in cell-matrix adhesion-mediated signalling and mechanotransduction. *Exp. Cell Res.* **343,** 42–53 (2016).

42. Sapir-Lekhovitser, Y. *et al.* Magnetically actuated tissue engineered scaffold: insights into mechanism of physical stimulation. *Nanoscale* **8,** 3386–3399 (2016).

43. Santos, L. J., Reis, R. L. & Gomes, M. E. Harnessing magnetic-mechano actuation in regenerative medicine and tissue engineering. *Trends Biotechnol.* **33,** 471–479 (2015).

44. Gonçalves, A. I., Miranda, M. S., Rodrigues, M. T., Reis, R. L. & Gomes, M. E. Magnetic responsive cell based strategies for diagnostic and therapeutics. *Biomed. Mater.* **13,** 0–39 (2018).

45. Singh, R. K. *et al.* Potential of magnetic nanofiber scaffolds with mechanical and biological properties applicable for bone regeneration. *PLoS One* **9,** (2014).

46. Meng, J. *et al.* Super-paramagnetic responsive nanofibrous scaffolds under static magnetic field enhance osteogenesis for bone repair in vivo. *Sci. Rep.* **3,** 1–7 (2013).

47. Hao, S. *et al.* Macrophage phenotypic mechanomodulation of enhancing bone regeneration by superparamagnetic scaffold upon magnetization. *Biomaterials* **140,** 16–25 (2017).

48. Gonçalves, A. I. *et al.* Exploring the Potential of Starch/Polycaprolactone Aligned Magnetic Responsive Scaffolds for Tendon Regeneration. *Adv. Healthc. Mater.* **5,** 213–222 (2016).

49. Pesqueira, T., Costa-Almeida, R. & Gomes, M. E. Uncovering the effect of low-frequency static magnetic field on tendon-derived cells: from mechanosensing to tenogenesis. *Sci. Rep.* **7,** 10948 (2017).

50. Kaushik, M. & Moores, A. Review: nanocelluloses as versatile supports for metal nanoparticles and their applications in catalysis. *Green Chem.* **18,** 622–637 (2016).

51. Sunasee, R., Hemraz, U. D. & Ckless, K. Cellulose nanocrystals: a versatile nanoplatform for emerging biomedical applications. *Expert Opin. Drug Deliv.* **13,** 1243–1256 (2016).

52. Chen, L. *et al.* Tailoring the yield and characteristics of wood cellulose nanocrystals (CNC) using concentrated acid hydrolysis. *Cellulose* **22,** 1753–1762 (2015).

53. Bondeson, D., Mathew, A. & Oksman, K. Optimization of the isolation of nanocrystals from microcrystalline cellulose by acid hydrolysis. *Cellulose* **13,** 171–180 (2006).

54. Teja, A. S. & Koh, P. Y. Synthesis, properties, and applications of magnetic iron oxide nanoparticles. *Prog. Cryst. Growth Charact. Mater.* **55,** 22–45 (2009).

55. Mahdavi, M. *et al.* Synthesis, surface modification and characterisation of biocompatible magnetic iron oxide nanoparticles for biomedical applications. *Molecules* **18,** 7533–7548 (2013).

56. Dhar, P., Kumar, A. & Katiyar, V. Magnetic Cellulose Nanocrystal Based Anisotropic Polylactic Acid Nanocomposite Films: Influence on Electrical, Magnetic, Thermal, and Mechanical Properties. *ACS Appl. Mater. Interfaces* **8,** 18393–18409 (2016).

57. Barclay, T. G., Hegab, H. M., Clarke, S. R. & Ginic-Markovic, M. Versatile Surface Modification Using Polydopamine and Related Polycatecholamines: Chemistry, Structure, and Applications. *Adv. Mater. Interfaces* **4,** 1–38 (2017).

58. Lee, H., Dellatore, S. M., Miller, W. M. & Messersmith, P. B. Mussel-inspired surface chemistry for multifunctional coatings. *Science (80-.).* **318,** 426–430 (2007).

59. Batul, R., Tamanna, T., Khaliq, A. & Yu, A. Recent progress in the biomedical applications of polydopamine nanostructures. *Biomater. Sci.* **5,** 1204–1229 (2017).

60. Lee, H., Rho, J. & Messersmith, P. B. Facile conjugation of biomolecules onto surfaces via mussel adhesive protein inspired coatings. *Adv. Mater.* **21,** 431–434 (2009).

61. Shi, Z. *et al.* Enhanced colloidal stability and antibacterial performance of silver nanoparticles/cellulose nanocrystal hybrids. *J. Mater. Chem. B* **3,** 603–611 (2015).

62. Mazur, M. *et al.* Iron oxide magnetic nanoparticles with versatile surface functions based on dopamine anchors. *Nanoscale* **5,** 2692 (2013).

63. Zhu, Q. & Pan, Q. Mussel-inspired direct immobilization of nanoparticles and application for oil-water separation. *ACS Nano* **8,** 1402–1409 (2014).

64. Zhang, H. *et al.* Magnetic nanoparticle-loaded electrospun polymeric nanofibers for tissue engineering. *Mater. Sci. Eng. C* **73,** 537–543 (2017).

65. Zhang, X. *et al.* Combining mussel-inspired chemistry and the Michael addition reaction to disperse carbon nanotubes. *RSC Adv.* **2,** 12153 (2012).

66. Cipitria, A., Skelton, A., Dargaville, T. R., Dalton, P. D. & Hutmacher, D. W. Design, fabrication and characterization of PCL electrospun scaffolds - A review. *J. Mater. Chem.* **21,** 9419–9453 (2011).

67. Binnig, G. & Quate, C. F. Atomic Force Microscope. *Phys. Rev. Lett.* **56,** 930–933 (1986).

68. MacArthur, K. E. The Use of Annular Dark-Field Scanning Transmission Electron Microscopy for Quantitative Characterisation. *Johnson Matthey Technol. Rev.* **60,** 117–131 (2016).

69. Ismail, A. A. & van de Voort, Frederick R. Sedman, J. Fourier Transform Infrared Spectroscopy: Principles and Applications. in *Techniques and instrumentation in analytical chemistry* (eds. Paré, J. R. J. & Bélanger, J. M. R.) 93–139 (Elsevier, B. V., 1997).

70. Drenth, J. X-ray Diffraction: Principles. *Encyclopedia of Life Sciences* 1–8 (2003).

71. Scherrer, P. Bestimmung der Grosse und der Inneren Struktur von Kolloidteilchen Mittels Rontgenstrahlen. *Nachrichten von der Gesellschaft der Wissenschaften - Math. Klasse* **2,** 98–100 (1918).

72. Coats, A. W. & Redfern, J. P. Thermogravimetric Analysis. *Analyst* **88,** 906–924 (1963).

73. Foner, S. Versatile and sensitive vibrating-sample magnetometer. *Rev. Sci. Instrum.* **30,** 548–557 (1959).

74. Duarte, A. R. C., Correlo, V. M., Oliveira, J. M. & Reis, R. L. Recent developments on chitosan applications in regenerative medicine. in *Biomaterials from Nature for Advanced Devices and Therapies* (eds. Neves, N. M. & Reis, R. L.) 223–243 (John Wiley & Sons, 2016).

75. Labet, M. & Thielemans, W. Synthesis of polycaprolactone: A review. *Chem. Soc. Rev.* **38,** 3484–3504 (2009).

76. Woodruff, M. A. & Hutmacher, D. W. The return of a forgotten polymer - Polycaprolactone in the 21st century. *Prog. Polym. Sci.* **35,** 1217–1256 (2010).

77. Mondal, D., Griffith, M. & Venkatraman, S. S. Polycaprolactone-based biomaterials for tissue engineering and drug delivery: Current scenario and challenges. *Int. J. Polym. Mater. Polym. Biomater.* **65,** 255–265 (2016).

78. Stokes, D. J. Principles of SEM. *Princ. Pract. Var. Press. Scanning Electron Microsc.* 17–62 (2008).

79. Rada, T., Reis, R. L. & Gomes, M. E. Novel method for the isolation of adipose stem cells (ASCs). *J. Tissue Eng. Regen. Med.* **3,** 158–159 (2009).

80. Carvalho, P. P. *et al.* The effect of storage time on adipose-derived stem cell recovery from human lipoaspirates. *Cells Tissues Organs* **194,** 494–500 (2011).

81. Patel, M. I., Tuckerman, R. & Dong, Q. A pitfall of the 3-(4,5-dimethylthiazol-2-yl)-5(3-carboxymethonyphenol)-2- (4-sulfophenyl)-2H-tetrazolium (MTS) assay due to evaporation in wells on the edge of a 96 well plate. *Biotechnol. Lett.* **27,** 805–808 (2005).

82. Life Technologies. *Real-time PCR handbook.*

83. Erlich, H. A. Polymerase chain reaction. *J. Clin. Immunol.* **9,** 437–447 (1989).

84. Livak, K. J. & Schmittgen, T. D. Analysis of relative gene expression data using real-time quantitative PCR and the 2-ΔΔCT method. *Methods* **25,** 402–408 (2001).

85. Fritschy, J.-M. & Hartig, W. Immunofluorescence. *Encyclopedia of Life Sciences* 1–7 (1999).

86. Wei, N. *et al.* Facile construction of a polydopamine-based hydrophobic surface for protection of metals against corrosion. *RSC Adv.* **7,** 11528–11536 (2017).

87. Fang, M., Ström, V., Olsson, R. T., Belova, L. & Rao, K. V. Particle size and magnetic properties dependence on growth temperature for rapid mixed co-precipitated magnetite nanoparticles. *Nanotechnology* **23,** (2012).

88. Lai, K. *et al.* Superparamagnetic nano-composite scaffolds for promoting bone cell proliferation and defect reparation without a magnetic field. *RSC Adv.* **2,** 13007–13017 (2012).

89. Nypelö, T., Rodriguez-Abreu, C., Rivas, J., Dickey, M. D. & Rojas, O. J. Magneto-responsive hybrid materials based on cellulose nanocrystals. *Cellulose* **21,** 2557–2566 (2014).

90. Guo, J. *et al.* Complexes of Magnetic Nanoparticles with Cellulose Nanocrystals as Regenerable, Highly Efficient, and Selective Platform for Protein Separation. *Biomacromolecules* **18,** 898–905 (2017).

91. Orr, S. B. *et al.* Aligned multilayered electrospun scaffolds for rotator cuff tendon tissue engineering. *Acta Biomater.* **24,** 117–126 (2015).

92. Rothrauff, B. B. *et al.* Braided and Stacked Electrospun Nanofibrous Scaffolds for Tendon and Ligament Tissue Engineering. *Tissue Eng. Part A* **23,** 378–389 (2017).

93. Bosworth, L. A., Alam, N., Wong, J. K. & Downes, S. Investigation of 2D and 3D electrospun scaffolds intended for tendon repair. *J. Mater. Sci. Mater. Med.* **24,** 1605–1614 (2013).

94. Czaplewski, S. K., Tsai, T., Duenwald-kuehl, S. E., Vanderby, R. & Li, W. Biomaterials Tenogenic differentiation of human induced pluripotent stem cell-derived mesenchymal stem cells dictated by properties of braided submicron fibrous scaffolds. *Biomaterials* **35,** 6907–6917 (2014).

95. Wu, S., Wang, Y., Streubel, P. N. & Duan, B. Living nanofiber yarn-based woven biotextiles for tendon tissue engineering using cell tri-culture and mechanical stimulation. *Acta Biomater.* **62,** 102–115 (2017).

96. Bosworth, L. A., Rathbone, S. R., Bradley, R. S. & Cartmell, S. H. Dynamic loading of electrospun yarns guides mesenchymal stem cells towards a tendon lineage. *J. Mech. Behav. Biomed. Mater.* **39,** 175–183 (2014).

97. Erisken, C., Zhang, X., Moffat, K. L., Levine, W. N. & Lu, H. H. Scaffold Fiber Diameter Regulates Human Tendon Fibroblast Growth and Differentiation. *Tissue Eng. Part A* **19,** 519–528 (2013).

98. Lee, N. M. *et al.* Polymer fiber-based models of connective tissue repair and healing. *Biomaterials* **112,** 303–312 (2017).

99. Rossetti, L. *et al.* The microstructure and micromechanics of the tendon-bone insertion. *Nat. Mater.* **16,** 664–670 (2017).

100. Santos, L. *et al.* In vitro and in vivo assessment of magnetically actuated biomaterials and prospects in tendon healing. *Nanomedicine (Lond).* **11,** 1107–1122 (2016).

101. Barber, J. G., Handorf, A. M., Allee, T. J. & Li, W.-J. Braided Nanofibrous Scaffold for Tendon and Ligament Tissue Engineering. *Tissue Eng. Part A* **19,** 1265–1274 (2013).

102. Pauly, H. M. *et al.* Mechanical properties and cellular response of novel electrospun nanofibers for ligament tissue engineering: Effects of orientation and geometry. *J. Mech. Behav. Biomed. Mater.* **61,** 258–270 (2016).

103. Zhang, C. *et al.* Well-aligned chitosan-based ultrafine fibers committed teno-lineage differentiation of human induced pluripotent stem cells for Achilles tendon regeneration. *Biomaterials* **53,** 716–730 (2015).

104. Wang, J. H. C., Guo, Q. & Li, B. Tendon biomechanics and mechanobiology - A minireview of basic concepts and recent advancements. *J. Hand Ther.* **25,** 133–141 (2012).

105. Lavagnino, M. *et al.* Tendon mechanobiology: Current knowledge and future research opportunities. *J. Orthop. Res.* **33,** 813–822 (2015).

106. Driscoll, T. P., Cosgrove, B. D., Heo, S. J., Shurden, Z. E. & Mauck, R. L. Cytoskeletal to Nuclear Strain Transfer Regulates YAP Signaling in Mesenchymal Stem Cells. *Biophys. J.* **108,** 2783–2793 (2015).

107. Wan, S. *et al.* FAK- and YAP/TAZ dependent mechanotransduction pathways are required for enhanced immunomodulatory properties of adipose-derived mesenchymal stem cells induced by aligned fibrous scaffolds. *Biomaterials* **171,** 107–117 (2018).

108. Aragona, M. *et al.* A mechanical checkpoint controls multicellular growth through YAP/TAZ regulation by actin-processing factors. *Cell* **154,** 1047–1059 (2013).

109. Codelia, V. A., Sun, G. & Irvine, K. D. Regulation of YAP by mechanical strain through Jnk and Hippo signaling. *Curr. Biol.* **24,** 2012–2017 (2014).

110. Dupont, S. *et al.* Role of YAP/TAZ in mechanotransduction. *Nature* **474,** 179–184 (2011).

111. Gaut, L. & Duprez, D. Tendon development and diseases. *Wiley Interdiscip. Rev. Dev. Biol.* **5,** 5–23 (2016).

112. Shukunami, C. *et al.* Scleraxis is a transcriptional activator that regulates the expression of Tenomodulin, a marker of mature tenocytes and ligamentocytes. *Sci. Rep.* **8,** 1–17 (2018).

113. Li, Y. *et al.* The Role of Scleraxis in Fate Determination of Mesenchymal Stem Cells for Tenocyte Differentiation. *Sci. Rep.* **5,** 1–12 (2015).

114. Docheva, D., Hunziker, E. B., Fassler, R. & Brandau, O. Tenomodulin Is Necessary for Tenocyte Proliferation and Tendon Maturation. *Mol. Cell. Biol.* **25,** 699–705 (2005).

115. Liu, X., Wu, H., Byrne, M., Krane, S. & Jaenisch, R. Type III collagen is crucial for collagen I fibrillogenesis and for normal cardiovascular development. *Proc. Natl. Acad. Sci.* **94,** 1852–1856 (1997).

116. Komori, T. Regulation of bone development and extracellular matrix protein genes by RUNX2. *Cell Tissue Res.* **339,** 189–195 (2010).

117. Ogle, M. E., Segar, C. E., Sridhar, S. & Botchwey, E. A. Monocytes and macrophages in tissue repair: Implications for immunoregenerative biomaterial design. *Exp. Biol. Med.* **241,** 1084–1097 (2016).

118. Lin, J. *et al.* Cell-material interactions in tendon tissue engineering. *Acta Biomater.* **70,** 1–11 (2018).

119. Tsuzaki, M. *et al.* IL-1β induces COX2, MMP-1, -3 and -13, ADAMTS-4, IL-1β and IL-6 in human tendon cells. *J. Orthop. Res.* **21,** 256–264 (2003).

120. Stein, M. Interleukin 4 potently enhances murine macrophage mannose receptor activity: a marker of alternative immunologic macrophage activation. *J. Exp. Med.* **176,** 287–292 (1992).

121. Fiorentino, D. F., Zlotnik, A., Mosmann, T. R., Howard, M. & O'Garra, A. IL-10 inhibits cytokine production by activated macrophages. *J. Immunol.* **147,** 3815–3822 (1991).

122. Luu, T. U., Gott, S. C., Woo, B. W. K., Rao, M. P. & Liu, W. F. Micro and Nano-patterned Topographical Cues for Regulating Macrophage Cell Shape and Phenotype. *ACS Appl Mater Interfaces* **7,** 28665–28672 (2016).

123. McWhorter, F. Y., Wang, T., Nguyen, P., Chung, T. & Liu, W. F. Modulation of macrophage phenotype by cell shape. *Proc. Natl. Acad. Sci.* **110,** 17253–17258 (2013).

124. Mather, B. D., Viswanathan, K., Miller, K. M. & Long, T. E. Michael addition reactions in macromolecular design for emerging technologies. *Prog. Polym. Sci.* **31,** 487–531 (2006).

Appendix

```
% Determination of the mechanical properties based of the material based
% on stress-strain curves
% Ana Rita Tomás
% July 2018

clearvars, close all;
%%
file = '17PCL_5MNP.xlsx';
sample = '17PCL + 5MNP';
specnumber = 11; % total number of specimens

E = zeros(specnumber,1); % Young's Modulus
YieldStrength = zeros(specnumber,1); % Yield Strength
YieldStrain = zeros(specnumber,1); % Yield Strain
MaxStrength = zeros(specnumber,1); % Ultimate Tensile Strength
BreakStrain = zeros(specnumber,1); % Strain at Break

%% Calculate stress-strain curve of each specimen

for i=1:specnumber

    % Load data from Excel files
    sheet = ['Specimen ' num2str(i)];

    TStrain = xlsread(file,sheet,'S28:S1018'); % Tensile Strain
    TStress = xlsread(file,sheet,'T28:T1018'); % Tensile Stress

    % Find Breaking Point - where the specimen breaks
    bpoint = zeros(length(TStress),1);
    for j=2:length(TStress)
        bpoint(j-1) = TStress(j-1)-TStress(j);
    end

    if any(bpoint>0.35)
        breakpoint = find(bpoint>0.35,1,'first');
        % Breaking point here considered when the tensile stress drops 0.35
        % MPa
        if (breakpoint + 70) < length(TStress)
            % Limit arrays to the breaking point for representation
            TStress = TStress(1:breakpoint+10);
            TStrain = TStrain(1:breakpoint+10);
        else
            TStress = TStress(1:breakpoint);
            TStrain = TStrain(1:breakpoint);
        end
    else
        % In case there is no 0.35 MPa drop in Stress when the sample
        % breaks, find the index of the maximum stress and estimate the
        % limit
        [~,breakpoint] = max(TStress(:));
        TStress = TStress(1:breakpoint+300);
        TStrain = TStrain(1:breakpoint+300);
    end

    % Calculate Ultimate Tensile Strain and Strain at Break
    MaxStrength(i)= max(TStress(:)); % Ultimate Tensile Strain
    BreakStrain(i) = TStrain(breakpoint); % Strain at Break

    % Draw stress-strain curve
    figure
    plot(TStrain,TStress)
    title({sample; sheet})
    xlabel('Strain (mm/mm)')
    ylabel('Stress (MPa)')
```

```
    % Calculate Young's Modulus - Slope of the curve's linear region
    % 0.025-0.065 mm/mm strain for the linear region of PCL and
    % PCL/DT-NP2.5 yarns (row 15-39)
    % 0.01-0.065 mm/mm strain for the linear region of PCL/DT-NP5 yarns
    % both random and aligned(row 6-39)

    YMod = polyfit(TStrain(6:39),TStress(6:39),1);
    YModLine = YMod(1).*TStrain(:) + YMod(2);
    E(i) = YMod(1); % Young's Modulus

    % Find Yield Stress and Strain- Intersection of the line parallel to
    % the linear region offsetted to cross 5% strain
    b = -0.05*E(i); % Line offset
    YieldLine = E(i).*TStrain(:) + b;

    dif = TStress - YieldLine; % Curve and YieldLine intersect when dif=0
    YieldPoint2 = find(dif < 0, 1, 'first'); % First value after intersection
    YieldPoint1 = YieldPoint2 - 1;

    YieldStrength(i) = (TStress(YieldPoint1)+ TStress(YieldPoint2))/2;
    YieldStrain(i) = (TStrain(YieldPoint1)+ TStrain(YieldPoint2))/2;

    % Draw stress-strain curve and intersection with the YieldLine
    figure
    plot(TStrain,TStress, TStrain, YieldLine, TStrain, YModLine)
    hold on
    plot(TStrain(YieldPoint1),TStress(YieldPoint1),'+r')
    plot(TStrain(YieldPoint2),TStress(YieldPoint2),'+r')
    hold off
    title({sample; sheet})
    xlabel('Strain (mm/mm)')
    ylabel('Stress (MPa)')
    xlim([0 0.7])
    ylim([0 2.5])

end
```

Figure A.1. MATAB script to determine the mechanical properties of the material based on stress-strain curves.

```
% Determination of the YAP/TAZ nuclear/cytoplasmatic ratio from
% immunofluorescence images
% Ana Rita Tomás
% September 2018

% The original image is a composite of 3 channels, each corresponding to a
% different staining:
% Red - F-actin cytoskeleton
% Green - YAP/TAZ
% Blue - Nuclei (stained with DAPI)

clearvars, close all;
%% Load Image
original = imread('YAP_Bioreact_D11.lif_Series005_Processed001.tif');
blue = original(:,:,3);
green = imread('YAP_Bioreact_D11.lif_Series005_Processed001.tif (green)_1out.tif');

%% Convert to double
yap = im2double(green);
dapi = im2double(blue);

% Hide the scale in the bottom right corner
for l = 999:1019
    for c = 877: 1016
        if yap(l,c)==1
            yap(l,c)=0;
        end
        if dapi(l,c)==1
            dapi(l,c)=0;
        end
    end
end

%% Mask
% Creates a mask based on the blue channel (nuclei)
lvl = graythresh(dapi);
bwdapi = im2bw(dapi,lvl);

se = strel('disk',1);
bwdapi2 = imclose(bwdapi,se);
bwdapi3 = imfill(bwdapi2,'holes');

%% Segment the nuclei from the green channel
% The mask created in the previous section is used to segment the nuclei
% and the cytoplasm in the green channel (YAP/TAZ)

invbwdapi = ~bwdapi3; %invert mask
nuclei = yap.* bwdapi3;
cytoplasm = yap.*invbwdapi;

figure
subplot(1,2,1), imshow(nuclei)
title('Nuclei')
subplot(1,2,2), imshow(cytoplasm)
title ('Cytoplasm')

%% Measure intensity
% Find the nonzero elements
[~,~,nuc]= find(nuclei);
[~,~,cyt]= find(cytoplasm);

% Calculate the mean grey value of each image
YAPnuclei = mean(nuc);
YAPcytoplasm = mean(cyt);
YAPRatio = YAPnuclei/YAPcytoplasm;
```

Figure A.2. MATAB script to determine the YAP/TAZ nuclear/cytoplasmatic ratio from immunofluorescent images.